ABSTRACT

MATTHEWS, SUZANNE RODDEN. Plasma Aided Finishing of Textile Materials. (Under the direction of Marian G. McCord.)

Surface modification of textile materials extends over a wide range of alterations to provide desired single or multi-features for various applications. It is a highly focused area of research in which alterations to physical and/or chemical properties lead to new textile products that provide new applications or satisfy specific needs. These processes, however, can involve numerous chemicals, some of which are toxic to humans and hazardous to the environment. In an effort to eliminate these harmful chemicals and waste products, surface modification and finishing via plasma treatment has become an attractive alternative, and is the focus of this work. Through analyzing and understanding plasma-substrate interactions, new and novel finishing applications have been developed. These processes include plasma-aided desizing of polyvinyl alcohol, and plasma-aided grafting of antimicrobial agents onto polypropylene nonwoven fabrics. Plasma treatment of PVA films has shown a significant amount of size removal through sputtering mechanisms, as well as increased solubility via chain scission, which further aids in ease of removal. Plasma treatment of PP fabrics has shown a viable pretreatment for free radical grafting of antimicrobial agents without the use of chemical etchants. In addition to new processing methods, this work has also provided an investigation into the development of a generalized solubility model for plasma exposed materials.

PLASMA AIDED FINISHING OF TEXTILE MATERIALS

by
SUZANNE RODDEN MATTHEWS

A dissertation submitted to the Graduate Faculty of
North Carolina State University
in partial fulfillment of the requirements for the Degree of
Doctor of Philosophy

FIBER AND POLYMER SCIENCE

Raleigh
2005

APPROVED BY:

_____ _____

_____ _____

Chair of Advisory Committee

DEDICATION

I would like to dedicate this dissertation and all the work involved in its completion to my loving husband, Brad, and to my supportive family. I could not have done it without the love and support of you all!

BIOGRAPHY

Suzanne Rodden Matthews was born on September 6, 1977 in Gaston County to Karen H. Kale and David F. Rodden. She graduated with honors from East Gaston High School in 1995, and received her B.S. degree from NC State University in Textile Chemistry in May of 1999.

Continuing in her academic pursuits, she completed her Master of Science degree in December of 2001 in Textile Chemistry under the instruction of Marian G. McCord and Samuel Hudson. This degree was completed as part of the five year BS/MS program and concentrated on the study of nylon 6/montmorillonite clay nanocomposite fibers.

Following her M.S. degree, Suzanne married her husband, Robert B. Matthews, on May 26, 2001. In June of 2001, she returned to NC State to begin work on her Ph.D. in Fiber and Polymer Science under the instruction of Marian G. McCord. Her work focused on plasma applications, and she received her minor in Nuclear Engineering.

ACKNOWLEDGEMENTS

I would first like to express my appreciation to my advisor, Dr. Marian G. McCord for her support throughout my years in graduate school. I would also like to thank my minor advisor, Dr. Mohamed Bourham, for his encouragement and guidance. To Dr. Peter Hauser and Dr. Sam Hudson, I would like to express my thanks for their continued help and guidance throughout my graduate career.

I wish to thank Dr. Keith Beck for his tireless efforts in helping me with the GPC, and to Birgit Anderson for all her assistance in the analytical lab. I would also like to acknowledge Drs. Samiha Gawish, Yoon J. Hwang, and Zaisheng Cai, for their contributions to my research. An additional thanks to Brian Bures for his help with plasma treatments and for his work on the plasma chamber.

The author greatly acknowledges the support of the National Textile Center (NTC) and the National Science Foundation (NSF), without their support this work could not have been completed. This project received partial support from the National Textile Center Project C99-S09 (2000-2002)"A Novel Non-Aqueous Fabric Finishing Process"; and partial support from the National Science Foundation contract NSF INT-0318758 (2003-2005) "Production and Application of Novel Insecticidal and Antimicrobial Textiles Using Atmospheric Plasmas and Irradiation Techniques".

Lastly, and most importantly, I would like to extend special appreciation to my husband, my parents, and my grandparents for their endless support and love.

TABLE OF CONTENTS

LIST OF FIGURES

LIST OF TABLES

I. INTRODUCTION

The importance of surface modification of textile materials extends over a wide range of alterations or embedded selective additions, to provide desired single or multi-features for various applications. It is a highly focused area of research in which alterations to physical and/or chemical properties lead to new textile products that provide new applications or satisfy specific needs. These processes, however, can involve numerous chemicals, some of which are toxic to humans and hazardous to the environment. Additional problems also arise due to degradation and/or weakening of the treated material [1]. Alternative techniques have been investigated over the past two decades to decrease or eliminate dependency on chemical treatments. One recent alternative, involving non-aqueous processing, is plasma treatment of textile materials.

Surface modification via plasma treatment not only eliminates the need for wet processing, but also yields unique surface characteristics. Several modifications include, but are not limited to: hydrophilicity/ hydrophobicity alterations, surface roughening, grafting, flame retardant, antimicrobial, insect repellant, stain resistant, and single or multiple surface functionalization [2]. Research on plasma treatment alterations of textile materials has been widely investigated using vacuum plasma systems, which create a gaseous discharge at low pressure. Many novel changes using vacuum plasmas have been thoroughly analyzed and well documented. Vacuum plasma provides an excellent way to study surface modifications, and is reasonable for batch processing of small product quantities. It is not, however, feasible for on-line processing in a textile mill. An ideal plasma treatment for textile applications is a plasma system that can be introduced into the production line without major changes or system interruption, allowing for high

speed and continuous processing. The ideal plasma system for such application requires that the plasma be generated at atmospheric conditions and not under vacuum. Numerous atmospheric plasma devices have been developed for a wide range of applications, including textile materials, but atmospheric plasma technology lacks appropriate plasma models, correct plasma diagnostics, and an understanding of the mechanisms by which such plasma interacts with surfaces.

The aim of this work is to better characterize atmospheric plasmas, fully understand the mechanism(s) of surface interaction, and to develop a model for the effects of atmospheric pressure plasma on various substrates. In addition to modeling, two different plasma-aided finishing techniques will be examined. These modifications will be compared to current techniques including vacuum plasma systems. A review of these techniques and other textile modification processes are discussed below. This review also includes an in-depth look at plasma surface modification.

II. LITERATURE REVIEW

2.1 Conventional Modifications of Textile Materials

Property modification, often referred to as "finishing," is the final step in the manufacturing of textile materials. This is the process by which the final properties of the material are developed. Property modification is achieved through various techniques, both chemical and physicochemical, which alter the appearance, aesthetics, and surface characteristics for improved product performance. Figure 1 illustrates an example process for surface modification of polymers. Examples of property modification include, but are not limited to, resistance to wrinkling, fire, soils and stains,

water, microorganisms and insects, light, heat and cold, shrinkage, air pollutants and chemical agents, weathering, and build up of static charges [1]. Various processing methods for surface and bulk property modification are shown below.

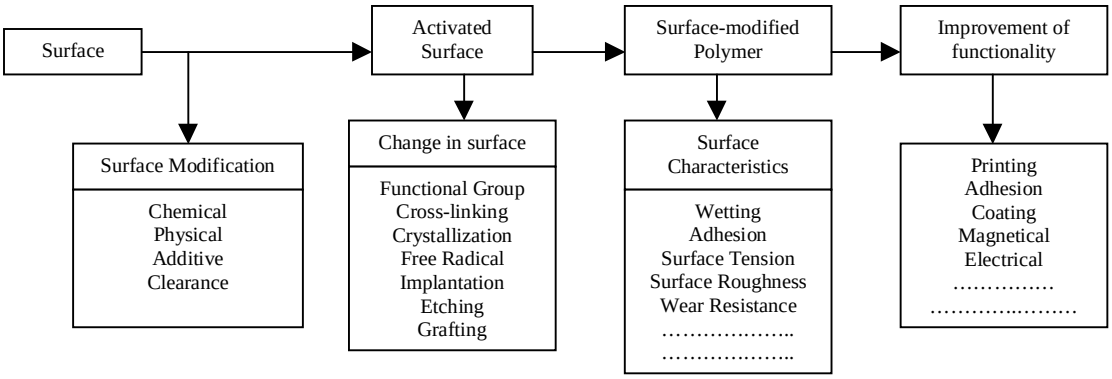

Figure 1 Effect of Surface Modification on Polymers

2.1.1 Chemical Processes

Chemical modification is defined by direct chemical reaction with a given solvent or by the covalent bonding of suitable macromolecular chains to the substrate surface. This process involves the development of specified solutions, which exploit specific liquid-polymer interactions, thereby modifying the surface functionality [3]. The depth of modification is controlled by the ratio between the diffusion and reaction rates, as well as the reaction time [4]. Control of these parameters is essential to the level of modification and the optimization of the resulting surface treatment. Over-exposure to chemical agents may result in discoloration, irreversible fiber damage, and deterioration of mechanical properties.

In addition to the use of wet chemicals, heat treatments are employed at various points in the modification process. This not only includes drying, but also the use of high temperatures to activate the chemicals and cure the finish. Once again, a delicate balance involving exposure time is required to prevent discoloration and loss of mechanical properties [1]. Two examples of property modification that employ both chemical processing and heat treatments are wrinkle-resistant and flame-retardant finishes.

2.1.1.1 Examples of Chemical Finishing

2.1.1.1.1 Wrinkle Resistant Finishes

Wrinkle resistant finishes are defined as chemicals used to improve the properties and performance of washable fabrics. When cotton is exposed to water, the hydrogen bonds between adjacent cellulose chains will be disrupted and new hydrogen bonds will be formed between the water molecules and the cellulose hydroxyls. Water then acts as a lubricant between the chains causing slippage, and in effect, "wrinkling" [5]. To overcome this problem, modification techniques involving a pad/dry/cure process are employed to cross-link the cellulose chains. This process is acid catalyzed, and involves the application of formaldehyde or di- or polyfunctional linear and cyclic ureas (such as DMDHEU), carbamates, amides or melamines to the fabric [1]. The final step involves heat curing at temperatures above 100°C to cross-link the finish to the cellulose [6]. Although the modification imparts notable wrinkle-resistance, the finish causes sizable losses in tensile strength and other mechanical properties, as well as discoloration during laundering, and the possibility of free formaldehyde release [7].

2.1.1.1.2 Flame Retardant Finishes

Flame-retardant finishes are defined as chemicals used to impart resistance to burning. A fiber is considered flame-retardant when it self-extinguishes upon removal of the flame source [8]. Modifications can be made to alter the material's flammability in the various stages of the burning process, which include heating, degradation and decomposition, volatilization, and oxidation [9]. Most flame-retardants decrease flammability by increasing the formation of char and/or reducing the formation of volatiles in the solid/condensed phase, or by inhibiting oxidation in the gas/vapor phase [10]. The simplest methods of modification involve the addition of water-soluble acid ammonium phosphates and borates. More sophisticated and more durable finishes use phosphorus compounds in conjunction with urea and melamine resins to create a cross-linked finish with the cellulose [6]. This type of finish is applied via a pad/dry/cure method [11]. Problems occurring from these finishes include yellowing from heat curing and acid damage, alteration of fabric hand, as well as degradation or total loss of mechanical properties [1,12].

2.1.1.2 Disadvantages of Chemically-Modified Textiles

In addition to alterations in the aesthetics and mechanical properties of chemically modified textiles, there are other disadvantages to this form of processing. These disadvantages include the use of large amounts of chemicals, high temperature treatments, increased cost, and environmental concerns. Environmental problems arise from both air-born particulate emission during processing, and water pollution caused by the discharge of untreated effluents. Figure 2 illustrates areas in processing of woven

fabric finishing where these pollutants occur. These effluents are sometimes toxic and can lower the oxygen content of the receiving waters as well as threaten aquatic life [13]. Increased public concern on this issue has led to very strict EPA guidelines requiring industrial discharges to maintain specified effluent quality. These restrictions create further expense by adding the cost for clean-up processes, not to mention the administering of steep fines for violations. These concerns and limitations have led to the further development of alternative physicochemical processing methods.

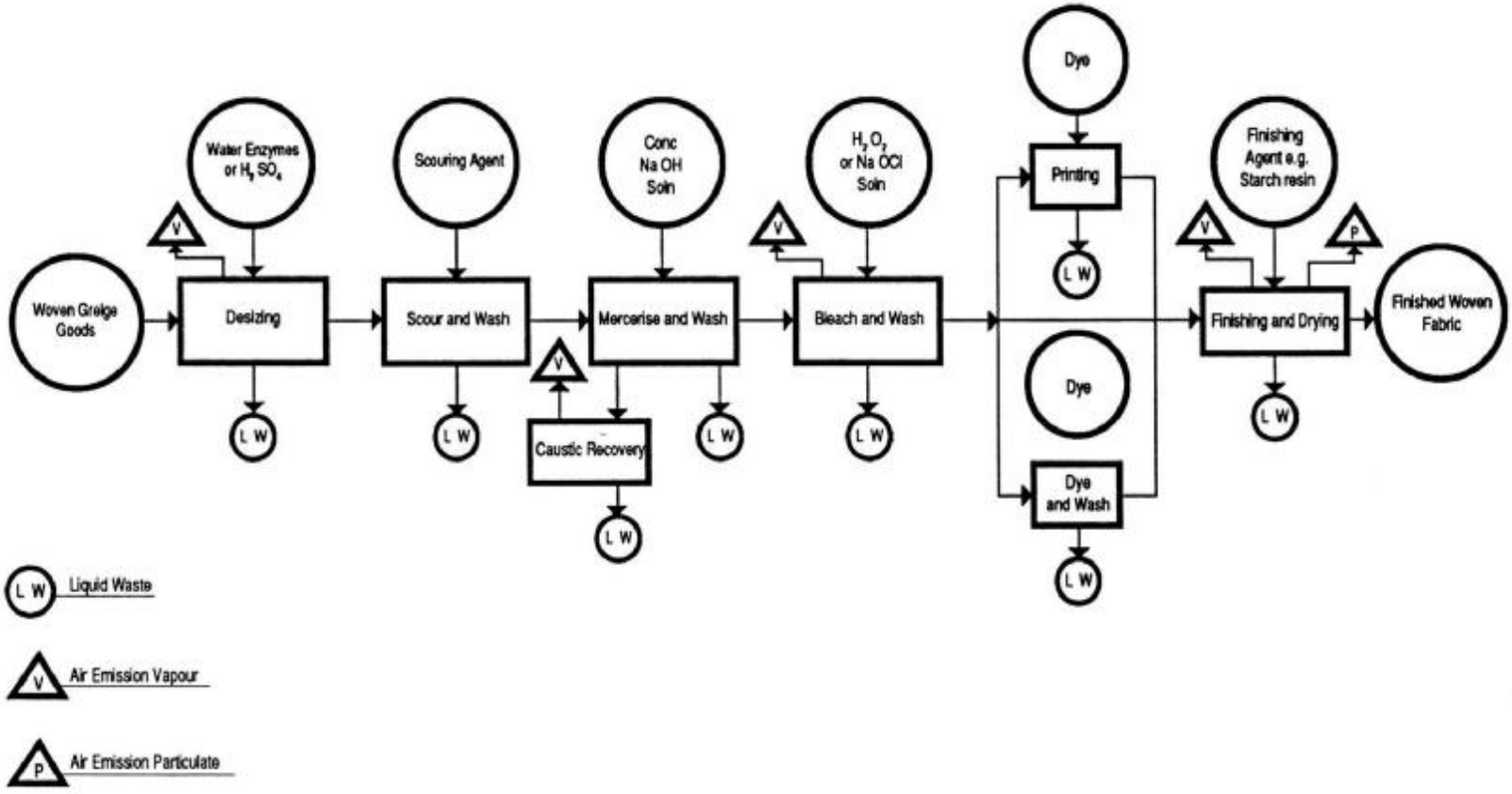

Figure 2 Emission Sources in Woven Fabric Finishing [13]

2.1.2 Physicochemical Processes

Over recent years, physicochemical techniques have become more commercially attractive and have begun to supercede conventional wet chemical methods for property modification. These techniques involve the alteration of the fiber/fabric surface by high energy, coating, insolubilization or deposition, and microencapsulation [1]. Fabric coating processes are direct, indirect, or transfer coating which form a composite material consisting of fiber and matrix phases [14]. This technique provides a fabric with a construction that combines the beneficial properties of a textile material with those of a polymer [15]. Insolubilization involves deposition of active chemical agents on or in the fabrics via padding. Microencapsulation processes affix finishing agent microcapsules to fibrous substrates followed by controlled release diffusion [16]. High-energy treatments are much more diverse in application, and include corona discharge, flame treatments, hot or cold gaseous plasmas, UV irradiation, γ–ray exposure, as well as electron or ion beam treatments. In the following sections, the difference in each of these application methods and resulting property modifications will be further explored.

2.1.2.1 **Corona Discharge**

An electrical-corona discharge is the formation of high-energy electromagnetic fields close to charged thin wires, or points, with consequent ionization in their proximity [3].

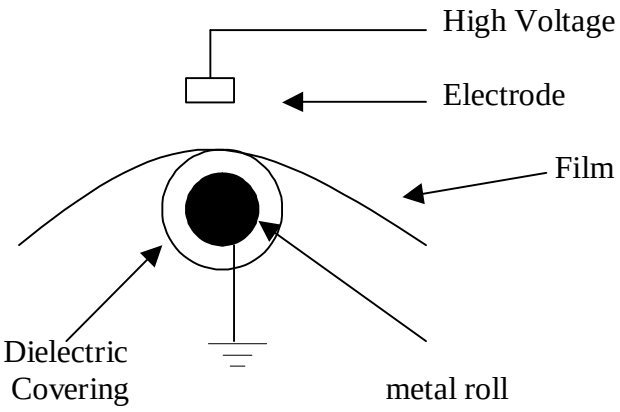

Figure 3 Schematic Diagram of a Corona Discharge. A polymeric film moves between a trip or filament held at high electric potential (thousands of volts) and a grounded roll. The discharge induces the formation of excited species, which modify the surface.

The corona discharge, which is not exactly plasma, generates electrons and ions via ionization. Additionally, the discharge energy is sufficient to excite atoms and molecules if not ionized. Electrons, ions, excited neutrals, and photons formed by the discharge react with the polymer surface to create surface radicals. These surface free radicals then rearrange to form functional groups, which create a pronounced physicochemical modification of the surface [18,19]. Surface modification, typically oxidation, lead to enhanced wettability and adhesion. Problems occurring with this treatment include non-uniformity, the creation of "pinholes," and difficulty in property control [17]. The variations in electron and ion energies, and their respective randomization, are the main reasons for non-uniformity of treated surfaces. Pinholes are essentially due to the impact of corona , i.e. small arcs, on the surface causing localized heat and penetration into the surface. Corona discharges have been widely used for

surface modification of textile materials, especially since corona discharges can be generated at atmospheric pressure.

2.1.2.2 Flame Treatment

Flame treatments impart oxidation to the polymer/fabric surface, a process much similar to corona discharge in providing oxidation. This is accomplished by high heat activation of radicals, ions, and molecules in excited states [3]. Figure 4 illustrates a simplified diagram of the treatment apparatus.

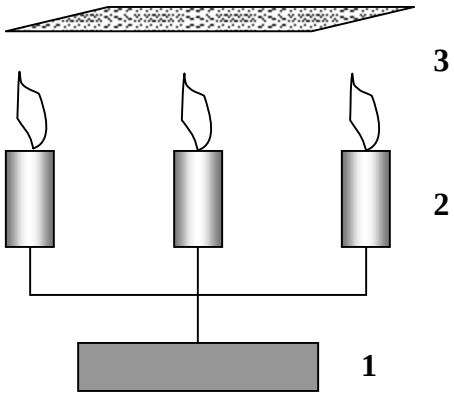

Figure 4 Schematic of Flame Treatment Process. A driving system (1) scans the flames produced by the burners (2) on the substrate (3).

This form of modification is commonly used for enhanced adhesion. Variables that must be controlled for property optimization include air-to-gas ratio, flow rate, distance of the flame from the sample, and exposure time [17].

2.1.2.3 Gaseous Plasmas

Plasma processing occurs via the bombardment of energetic particles from a discharge in a cold background gas [20]. Typical plasma chamber set-ups are shown in section 2.2 in Figures 8, 10 and 11. Plasmas may be classified as "hot" or "cold". Plasma temperature is expressed in units of electronvolts "eV' (1eV = 11600K). Cold, or non-thermal, plasmas contain very hot free electrons of several eV, which generate high chemical reactivity while neutrals and ions remain near room temperature (0.025eV). Cold plasmas are also partially-ionized with a low fractional ionization. On the other hand, hot, or thermal equilibrium plasmas contain constituents, which are all at approximately the same temperature so that the heat content, and therefore overall temperature, is high (>10000K, close to 1eV) [21]. Such hot plasmas may still be partially-ionized but may be at local thermodynamic equilibrium (LTE). Other plasma forms, such as fusion plasmas at several keV tempertaures, are at LTE and almost fully-ionized. Cold or hot plasmas may be used for surface treatment, but fusion plasmas are only for energy production from fusion reactors.

Due to the low heat resistance of most textile/polymeric materials, hot plasma treatment has little to no applicability in surface modification. Cold plasma treatments, however, offer a wide range of modifications. Materials can undergo surface activation through the introduction of oxygen-containing functions, etching by formation of gaseous species, or coating deposition by plasma polymerization [3]. This diversity, coupled with the elimination of wet chemicals has increased the research and use of plasma for industrial applications. This form of treatment and resulting surface modifications will be the main focus of this work in later sections.

2.1.2.4 UV Irradiation

UV exposure to polymeric surfaces has been used to promote photon-activated cross-links (negative resists) and fragmentation of coatings (positive resist) [3]. UV irradiation in the presence of oxygen promotes enhanced wettability and adhesion, as well as antistatic characteristics resulting from photo-oxidation of the surface. By conducting UV irradiation in the presence of polymerizable organic vapors, surface polymerization is also possible by creating a thin polymeric film layer on the surface [22]. Like most high-energy sources, UV exposure may result in the deterioration of physical properties and promotes photo-degradation [23].

2.1.2.5 Electron Beam Bombardment

Electron beam processing uses high-energy electrons from an accelerator to initiate polymerization and cross-link reactions, thereby curing polymer coatings and enhancing the specific physical and chemical properties of coated substrates [24]. This is achieved using an accelerator, which produces a beam of electrons that are accelerated to high energies, and thus high speeds, and directed onto a substrate. Electron beam systems vary in energy from as low as 60 keV to as high as 300keV. Figure 5 illustrates an electron beam processing system [25], where the beam is initially generated from a hot filament by thermionic emission, then accelerated by a high-intensity electric field developed by the high-voltage between the metal window (anode) and the filament (cathode).

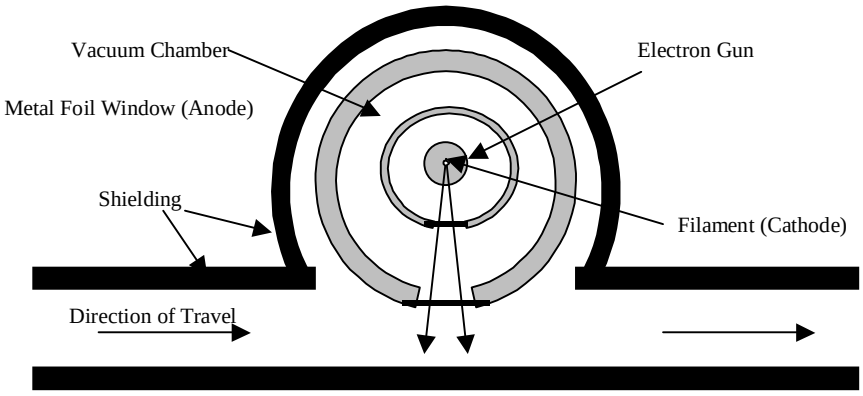

Figure 5 Electrocurtain® Processor

The degree of radiation is controlled by either varying the speed of the material passing through the processor, which means changing the fabric residence time and/or time of exposure, or by altering the amount of beam current being transmitted [26]. Unlike UV treatments, which require a photo-initiator, electron beams generate radicals by direct interaction with the substrate or coating mixture thereon. Since electrons are lightweight, negative-charged particles, they can directly initiate radical polymerization and promote cross-linking. Electron processing offers many advantages such as curing at ambient temperature, short cure times, reduction in produced volatiles, and most importantly, reduced operating costs [27]. One major disadvantage, however, is degradation of polymer surfaces due to over exposure, and the change in bulk property due to high-energy electrons impacting on and penetrating through the bulk. Another disadvantage is the unfeasibility to employ a high-energy electron beam irradiation system on-line in a fabric production mill and the safety requirements associated with operation of an accelerator.

2.1.2.6 g-ray Treatment

In a similar manner as the electron beam accelerator, γ-radiation can be used to induce cross-linking and grafting onto polymers. In the presence of oxygen, high-energy photons induce the formation of radical sites on the substrate surface, which then react with atmospheric oxygen to form new functional groups necessary for grafting [3]. This process has already proven effective in the grafting of butyl acrylate and cyclohexyl methacrylate to ultrahigh-molecular weight-polyethylene (UHMW-PE) [4,27]. Due to the penetrating depth and high energy of this treatment, however, the effects appear in the bulk as well. This is due to the fact that the linear attenuation coefficient of γ-rays is highly dependent on the specific density of the material and the energy of incident γ-rays. To restrict grafting to the surface, a small radiation dose must be used, as well as limiting the time of diffusion of the grafted monomer [4]. Dosing should also be limited to prevent degradation of the polymer substrate [27]. This degradation is due to the high penetrability of γ-rays into matter, and the radiation effects on the material property. Irradiation using γ-rays can cause severe bond-breakage, swelling and embitterment.

2.1.2.6 Ion Beam Bombardment

Due to their mass, ions are energetic species with high momentum and low mean free path. As a result, they greatly alter the surface composition of target materials and lead to extensive physicochemical modification. Ion beam modification could be performed using two different exposure methods. The first process involves direct ion implantation onto the substrate, while the second involves ion-assisted deposition of a target species onto the substrate surface through sputtering [3]. Figure 6 shows a

schematic of ion treatment using direct impact (top drawing) and ion-assisted deposition (bottom drawing) [3]. As ions collide with the substrate surface, chain-scission occur causing free radical sites to form. These sites then react with oxygen, if present, to create hydrophilic groups, or form cross-links with adjacent molecules [28]. Through this and other mechanisms including carbonization, chemical reactions, and surface roughness induced by ion bombardment, polymer properties can be notably enhanced. One specific modification involving chain-scission results in improved wettability and adhesion. Extensive exposure and chain-scission, however, can lead to polymer damage and degradation [29]. A disadvantage, similar to electron beams, is the necessity to employ an ion accelerator to acquire the necessary ion energy needed for the treatment.

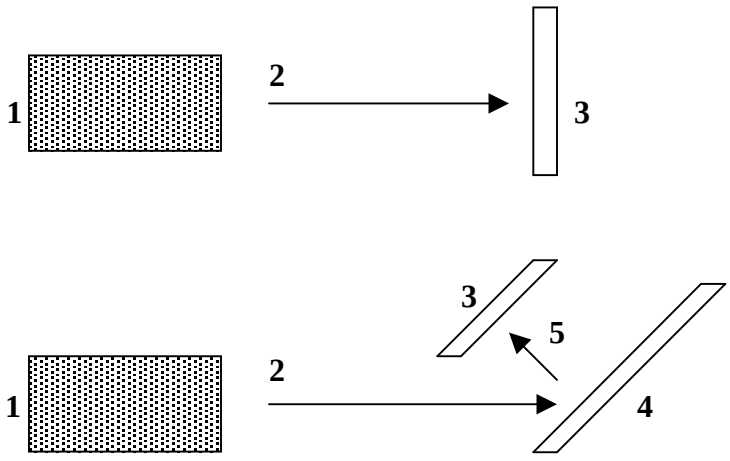

Figure 6 Schematic of Ion Treatment. The top drawing shows direct ion implantation in which ions are directed to the substrate and implanted into it. The bottom drawing shows ion activated deposition. In this process, the ion gun (1) emits a beam (2), which hits a target (4) with particular composition, exciting the emission of neutral particulates (5) which form a coating on the substrate (3).

2.2 Modification Techniques Using Plasma Treatments

Plasma may be defined as an ionized gas containing both charged and neutral species, including free electrons, positive and/or negative ions, atoms, and molecules. Ions and radical formation results from electron and ion impact [17]. Electron impact, defined as collisional processes in plasmas, is the impact of electrons on other plasma species, including non-ionized neutrals (atoms and molecules). Effectiveness of a certain collision is determined by the collision cross section σ, the velocities of interacting species v_1 and v_2, and their respective population n_1 and n_2. Each reaction rate R is given by $n_1\ n_2 <\sigma\ v_r>$, where v_r is the relative velocity between the two interacting species. The reaction rate coefficient is taken as the average $<\sigma\ v_r>$ over a Maxwellian distribution. Reaction rates may be ionization, dissociation, recombination or photo-ionization depending on the plasma nature and its parameters. The overall state of the plasma is considered neutral with the density of electrons and negative ions being equal to the density of the positively charged ions, known as plasma quasi-neutrality. In order to form and sustain plasma, an energy source capable of producing the required degree of ionization must be used. Either direct current (dc) or alternating current (ac) power supplies may be used to generate the electric field required for plasma generation [30]. For many industrial types of plasmas, radio-frequency (RF) power supplies are used, usually at a standard frequency of 13.56MHz. Plasma generation may also be performed at various pressures including low (vacuum), atmospheric, or high pressure. This chapter will deal with the various types, their set-ups and processing abilities, as well as their advantages and disadvantages.

2.2.1 Low Pressure (Vacuum) Plasma Devices

Low pressure plasmas are proven methods for surface modification. Vacuum devices provide a microscopically thorough, chemically mild, and mechanically non-destructive means for the removal of adsorbates such as dust, grease, and fatty acids or bacteria [20]. Improved adhesion and wettability have also been reported. For vacuum plasma devices the typical operating pressure range is between 10mTorr and 10Torr [31]. Low pressure plasmas may be generated using a dc power supply thus providing a glow discharge, or RF power supply to produce a quasi-glow discharge or more specifically a quasi-neutral plasma bulk formed between two sheaths. A description of each is in the following sections.

2.2.1.1 DC Glow Discharge

A glow discharge is defined as a partially ionized gas containing equal volume concentrations of positive and negative charged species with different concentrations of ground-state and excited species. This partially ionized gas may be generated by subjecting the gas to very high temperatures, or to a strong electric field, or excited by a radioactive source or strong photoemission. The electric field is induced by a direct current. Direct current (DC) discharge, as illustrated in Figure 7, is comprised of a self-consistent combination of a cathode surface, cathode dark space, negative glow region, Faraday dark region, and a positive column. Most of the applied voltage appears across the space between the cathode and the negative glow, known as the sheath.

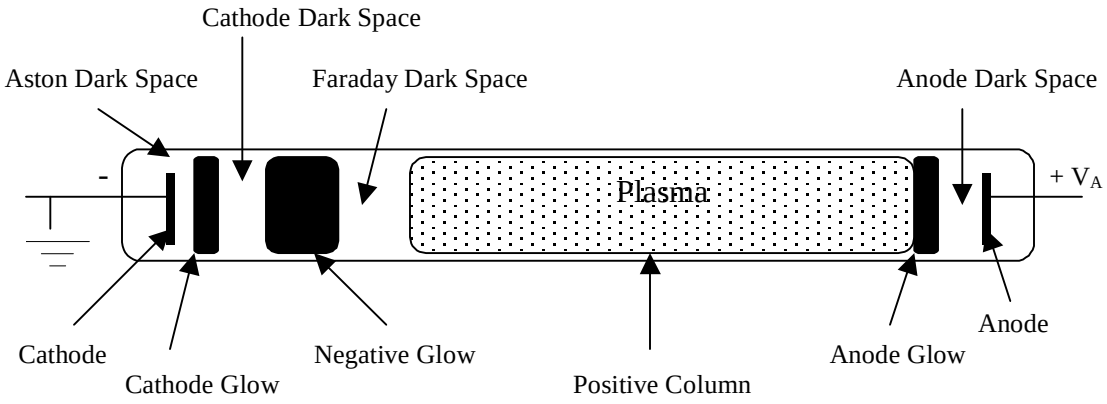

Figure 7 Visible Regions of a Normal Glow Discharge

Ions formed in the dark space and negative glow regions are accelerated into the cathode surface, where they cause secondary electron emission and sputtering. The emitted electrons are then propelled back across the dark space and cause ionization directly or by transferring their energy to electrons in the plasma. Here electrons equilibrate with the electric field and create the positive column [30]. This process creates a steady state discharge by keeping an equal ion-electron pair generation rate. The discharge is self-sustained by the secondary electron emission from the surface of the cathode. The striking voltage is a function of the pressure, electrode separation, and the coefficient of secondary electron emission. The breakdown voltage V_b has the following equation:

$$V_b = \frac{Bpd}{\ln(Apd) - \ln\left[\ln\left(1+\frac{1}{\gamma_{se}}\right)\right]}$$

where pd represents the multiplication of the pressure, p, by the separation distance d. γ_{se} is the secondary electron emission coefficient, and A and B are constants depending on the electrode material and working gas.

A typical DC glow discharge is used as a sputtering source for metallic materials, but is limited in use for many industrial applications as it has a narrow range of pressure applicability for sputtering. Most DC glow discharges for sputter deposition operate in what is known as the abnormal regime, which has a narrow range of pressure. The limitation of applicability is also due, in part, to the continuous need to conduct a net current to sustain the discharge [33]. Another important limiting factor is the inability to use insulating materials over the electrodes, which will inhibit current conduction. By eliminating the contact between the electrode and the plasma, both reliability and reproducibility are improved. The lifetime of the plasma is also enhanced and the chance of impurities is dramatically lowered [32]. For these reasons, more practical plasma processes are typically RF excited, however, DC glow discharges are commonly used for sputter deposition of metallic materials such as sputter deposition of gold on non-metallic surface for the purpose of scanning electron microscopy (SEM) to eliminate static charges and glaring under SEM.

2.2.2 RF (AC) Discharges

Radio frequency power is the most common alternating current (AC) discharge used in plasma technology. RF discharges embody many of the same qualitative features of the DC glow discharge, including sheath formation, which creates a strong electric field resulting in the acceleration of ions and electrons. At low frequencies both DC and

RF discharges behave similarly, but as frequency is increased, they substantially differ from each other and a new phenomenon is observed [30].

When the applied frequency becomes high enough (approximately 13.56 MHz, which is the standard industrial frequency), the period of oscillation will become comparable to the time it takes electrons and ions to traverse the sheath between the plasma and the electrodes. Electrons will instantaneously respond to changes in electric field as it oscillates, while ions respond to time-average changes due to their heavy mass and inertia. In addition, the power supply begins to interact with the plasma almost exclusively by displacement current $\varepsilon_o \frac{\partial E}{\partial t}$, rather than a real conduction current (*J*), and new physical processes will occur [32].

Energetic ions striking the electrode will cause the formation of secondary electrons, which can then be accelerated through the sheath and cause ionization. In addition, the oscillating electric fields in the plasma bulk can input energy directly into the electrons, similar to the positive column of the dc discharge. Finally, the oscillating sheath electric field will accelerate electrons in the glow, known as a "surf-riding" mechanism, unique to the RF discharge [30].

Radio frequency discharges can be subdivided into inductive and capacitive discharges, differing in the way the RF field is induced in the discharge space. Inductive methods are based on electromagnetic induction so that the created electric field is a vortex field with closed lines. In capacitive methods, the voltage from the RF generator is applied across the electrodes, where the lines of force strike them, and the resultant field is essentially a potential field [34]. RF discharges can also take the form of a

microwave discharge, known as wave-heated discharge using higher frequency (~2.45 GHz), but only the previous two will be discussed in this work.

2.2.2.1 Inductively Coupled RF Discharge

Inductively coupled plasma sources (ICP) have been researched for over a century, with the first "electrodeless ring discharge" reported in 1884 [31]. The simplest form of an inductive discharge is a quartz tube placed inside a solenoid (the primary coil), through which a current is applied to generate the plasma [35]. A circular electric field is induced in the coil, which can then initiate and maintain the discharge. The RF power, which is transferred by Ohmic dissipation (joule heating) of induced RF currents, causes flow in the plasma by high frequency transformer action [32]. Most of the RF power is dissipated in the skin depth layer, which is the layer between the plasma bulk and the containing chamber. This means the interaction of the electromagnetic field with electrons is governed by electron thermal motion rather than electron-atom collisions. Depending on the operational regime, and the pressure, the skin depth is either collisional or collisionless. The power absorbed in Ohmic heating in the skin layer, in a cylindrical geometry inductively coupled discharge is given by:

$$P_{absorbed} = \frac{1}{2}\left|\tilde{I}_{RF}\right|^2 \frac{2\pi R m_e \nu_{en}}{n_e e^2 l \delta_p}$$

where $\tilde{I}_{RF}$ is the amplitude of the RF current, R is the radius of the chamber, m_e is the electron mass, n_e is the electron number density, e is the unit charge, ν_{en} is the electron-neutral collision frequency, and δ_p is the skin depth.

ICP's have been studied in both high and low-pressure regimes. At high gas pressures (atmospheric) a near-equilibrium plasma is generated, whereas at low-pressure (vacuum) regimes, a non-equilibrium plasma is created. Low pressure ICP's have been used as ion sources for particle accelerators and ion thrusters for space propulsion. Due to the high density of the low-pressure plasma, more research has been conducted using this regime. The main interaction between an electromagnetic field and the plasma, and thus the RF power dissipation, takes place in the skin layer near the plasma boundary. Depending on the plasma size, gas pressure, and driving frequency, various interactions between the electromagnetic field and the plasma may occur. Under such conditions, ICP's manifest a variety of plasma physics effects typical for both low temperature collisional gas discharge plasmas and for hot fusion and space plasmas [36].

The two forms of inductive-source configuration, cylindrical and planar geometries, are shown in Figure 8 (a) and (b).

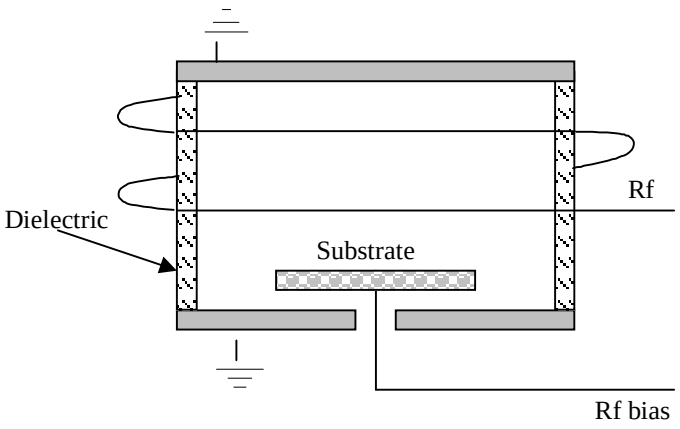

(a)

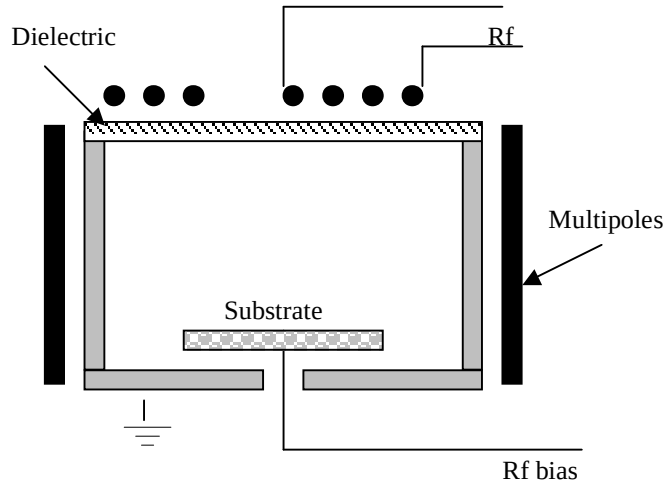

(b)

Figure 8 Schematic of inductively driven sources in (a) cylindrical and (b) planar configurations.

The inductive discharge in the cylindrical configuration is the closest in resemblance to the earliest form of ICP. This form of discharge is either maintained by the axial electrostatic field or by azimuthal electromagnetic field of the primary coil [35]. In contrast, the planar coil consists of a flat helix, wound from the axis to the outer radius of the discharge chamber. In this configuration, multipole magnets can be added around the circumference of the chamber to increase radial plasma uniformity. This can also be achieved in the cylindrical configuration by wrapping the coil in a nonuniform manner [35]. It is important to mention that increased number of turns of the RF coupling solenoid increases the ion energy loss across the sheath, and thus a one-turn solenoid would be favorable. Inductively-coupled discharges require matching of impedances between the power supply and the load (plasma) to maximize forward power transfer and minimize reflected power.

2.2.2.2 Capacitively Coupled RF Discharge

Capacitively coupled devices are the most widely used plasma source for materials processing. A schematic representation for a conventional device is shown in Figure 9. Two parallel electrodes are placed in a vessel filled with gas at a certain pressure, and an RF voltage is applied across the electrodes. These electrodes may be identical (symmetric geometry) or vary (asymmetric geometry) in diameter. They may also be insulated from the conducting discharge with a dielectric material, creating an "electrodeless" discharge [34].

Typical devices carry an alternatively driven applied RF frequency across the electrodes in the range of 1-150 MHz, with an RF voltage of 100 to 1000V [37]. The RF power is transferred to the plasma by the randomization of kinetic energy imparted to the electron population by RF electric fields [32].

The total power absorbed in a capacitively coupled discharge is the total of electron and ion heating, the addition of electron random heating in the sheaths, and the total power averaged over one cycle is given by:

$$< p_{Total} > = \frac{1}{2}\left[\frac{m_e}{n_e e^2}\left(\nu_{en}\delta + 2v_e\right) + 3\frac{v_{Bohm}}{\varepsilon_o \omega^2} \right] \frac{\left|\tilde{I}_{RF}\right|^2}{A^2}$$

where $\tilde{I}_{RF}$ is the amplitude of the RF current, v_e is the electron thermal speed, v_{Bohm} is the ion acoustic velocity, m_e is the electron mass, n_e is the electron number density, e is the unit charge, ν_{en} is the electron-neutral collision frequency, ε_o is the permittivity of free space, δ is the plasma length, A is the plasma cross-sectional area, and ω is the RF

frequency. Although the voltage across each sheath is nonlinear and has second harmonics, the overall voltage across the discharge is linear with the RF current.

Although capacitive sources work well for many processing applications, there are several drawbacks to note. Due to their configuration, capacitive devices are limited to plasma densities of $10^{16}m^{-3}$. Higher densities may be obtained by increasing the RF power, but this will increase the corresponding voltage across the electrodes. Electrons are then accelerated by a higher sheath voltage, resulting in less efficient heating of the plasma bulk. This leads to overall inefficiency of the device. Capacitive sources also offer no independent control of the plasma density. Despite these drawbacks, however, the use of capacitive devices for commercial applications has continually increased [38].

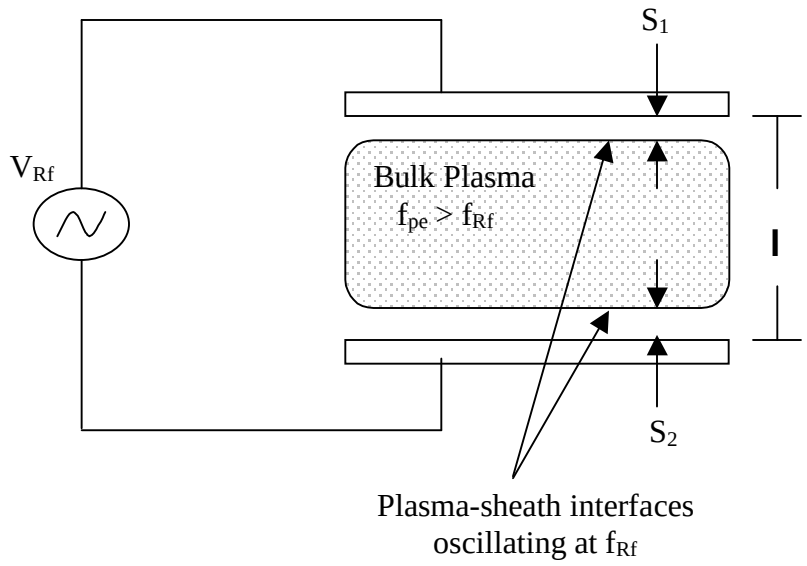

Figure 9 Schematic of a Parallel Plate Capacitive Plasma Reactor

2.2.3 Atmospheric Pressure Plasma

Although most previous research has focused on vacuum systems, their high cost and production limitations have led to the development of higher-pressure (atmospheric) devices. To create a more economical, continuous, or high-speed process, a working pressure at or near 1 atm is a necessity. Atmospheric pressure plasmas offer industry open perimeter, on-line, continuous, large area processing, unlike closed perimeter vacuum systems [21].

Current atmospheric devices include corona/dielectric barrier discharges (DBD), atmospheric pressure glow discharge (APGD), atmospheric pressure non-equilibrium plasma (APNEP), and atmospheric pressure plasma jets (APPJ). Like their vacuum counterparts, corona discharge/DBD systems induce surface modification through oxidation and radical formation. These processes have shown improvement in polymer adhesion, shrink-resistance, dyeability, printability, and sterilization [39,40,20,41]. Although offering the same treatment at lower cost and faster production, these systems still suffer from some of the disadvantages previously mentioned for vacuum and corona systems; specifically pinhole formation and non-uniformity of treatment.

Following the development of an atmospheric pressure corona discharge, the APGD was developed and reported by Kanazawa in 1988 [42]. This system, shown in Figure 10, employed a similar parallel plate discharge design. Unlike the inhomogeneous plasma formed via the previous corona discharge/DBD atmospheric systems, the APGD provided a homogeneous and streamer-free discharge [21]. This discharge is maintained by controlling the following three conditions:

(1) inclusion of a helium seed/dilution gas

(2) a high-frequency source, kilohertz to megahertz.

(3) an insulating plate/dielectric covering the electrodes

The first and foremost in importance is the inclusion of helium as the seed gas. This system requires the presence of metastable helium, which will dissociate other atoms/molecules such as oxygen, resulting in ionization of the mixed molecules:

$$He^m + O_2 \rightarrow He + O^* + O^+ + e$$

$$He^+ + O_2 \rightarrow He^+ + O + O^*$$

$$He^+ + O_2 \rightarrow He + O^+ + O^*$$

A high frequency source such as kilohertz (kHz) or radio frequency (MHz), and the dielectric plates are necessary to form a uniform discharge and prevent arc formation [43,44]. However, it is common in such discharges to have streamers in the plasma, which may cause localized effects on the treated substrate.

Dielectric Barrier Discharge

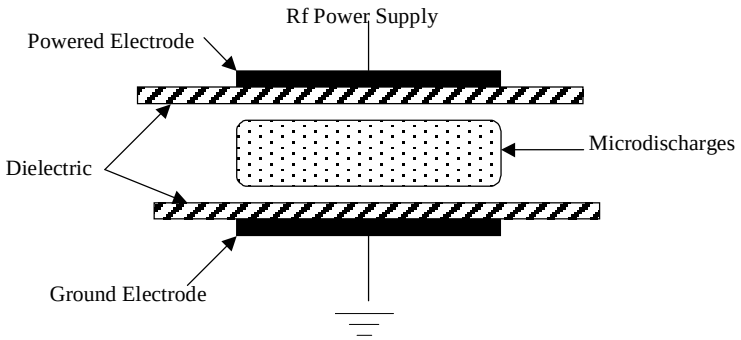

(a)

Atmospheric Pressure Glow Discharge

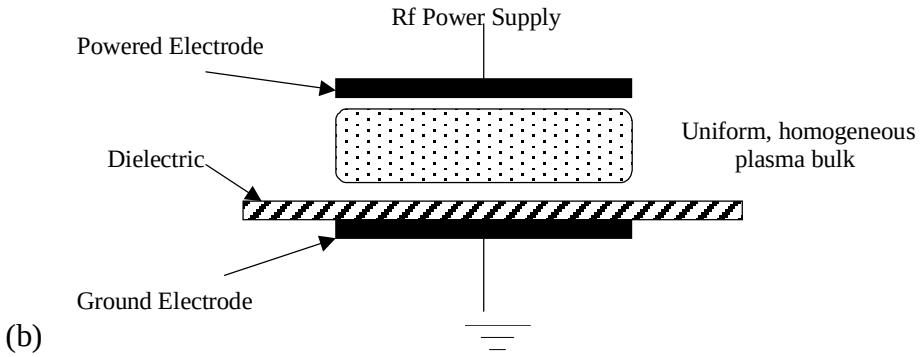

(b)

Figure 10 Non-thermal Equilibrium Plasma Systems, (a) DBD and (b) APGD

Another independently developed APGD device was created at North Carolina State University called PArallel pLate Atmospheric plasma Device for INdustry (PALADIN) [45]. This device, shown schematically in Figure 11, is a capacitively coupled device designed with an audio frequency (AF) power supply. This device was the precursor to the chamber developed in the College of Textiles, NCSU, which was used in this body of research.

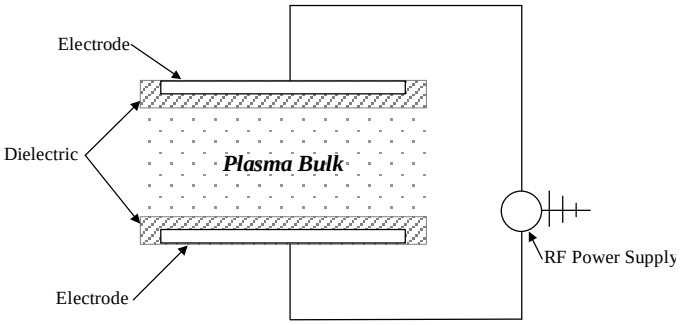

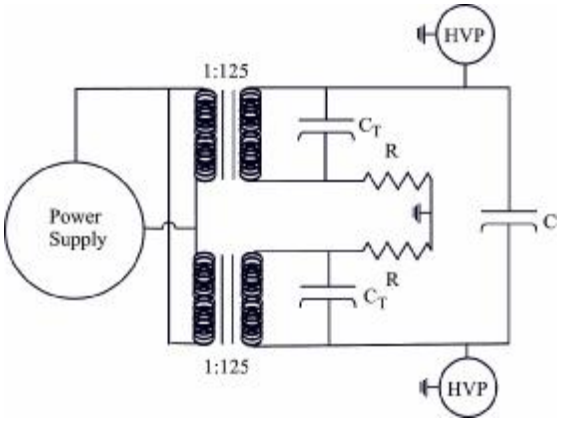

Figure 11 Schematic and Circuit Diagram of PALADIN [46]

Since their inception, APGD devices have shown a wide range of surface modification capabilities. Dai and Kviz found that APGD systems promote significant surface oxidation and chemical changes on both natural and synthetic fibers [47]. They also noted that the APGD was more uniform and stable compared to DBD, and that the treatment caused less physical damage to the surface. Researchers at NC State found surface chemistry changes in polypropylene and nylon 6,6 using the same form of APGD system [46]. Changes in wettability, adhesion, biocompatibility, and flame-retardancy have also been reported using these devices [21].

More recently, newer atmospheric devices have been developed. This includes the APNEP, developed by EA Technology Ltd. in conjunction with the University of Surrey, and the APPJ developed by researchers at Los Alamos National Laboratory [48,49]. Although neither system is available for industrial application, they have already demonstrated great potential and a wide range of applications. According to several studies conducted by Shenton et al., the APNEP treatments result in near-identical surface-chemical modification as seen by vacuum systems. The researchers concluded

that APNEP was a viable system for surface cleaning, altering surface energy, surface oxidation and cross-linking. Comparisons between vacuum and atmospheric pressure revealed similar reactions occur despite differences in pressure, gas throughput, and plasma thermal properties. With this realization, the authors felt that current vacuum plasma treatment of textile materials may be pertinent to atmospheric plasma treatments of the same materials [48,50]. However, it is important to indicate that the physics of vacuum plasmas differ from those of atmospheric plasmas due to the high collisionality of the latter. Also, the fractional ionization of atmospheric plasmas is much lower than vacuum discharges, and most standard plasma diagnostic techniques are not applicable to atmospheric discharges.

2.3 Plasma-Substrate Interaction

In the plasma bulk, reactive species (positive and negative ions, atoms, neutrals, metastables and free radicals) are generated by ionization, fragmentation, and excitation. These species lead to chemical and physical interactions between the plasma and the substrate surface depending on plasma conditions such as gas, power, pressure, frequency, and exposure time. The depth of interaction and modification, however, is independent of gas type and is limited to 5μm [51]. Figure 12 illustrates possible mechanisms for plasma-substrate interaction. The following sections will discuss the effects of plasma on surfaces based on the phenomena illustrated in this schematic.

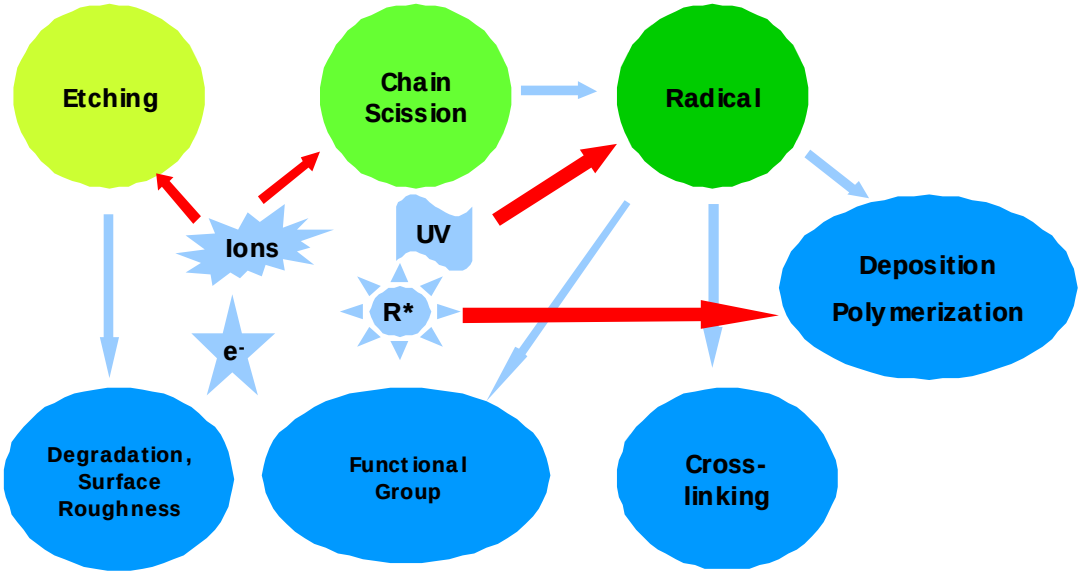

Figure 12 Mechanisms of Plasma-Substrate Interaction

2.3.1 Physical Phenomena in Plasma-Assisted Surface Modifications

2.3.1.1 Etching/Re-Deposition

Plasma etching is the key process for the removal of surface material from a given substrate. This process relies on the chemical combination of the solid surface being etched and the active gaseous species produced in the discharge. The resulting etched material will have a lower molecular weight and the topmost layer will be stripped. In previous methods, such as chemical wet processing, plasma has shown much more controllability and a much finer resolution [33].

Etching can proceed by physical sputtering or chemical reaction and ion-assisted mechanisms. The four basic plasma processes commonly used for surface removal are shown in Figure 13. Although four distinctive processes are described, often, parallel or serial combinations are employed for specific substrate modification.

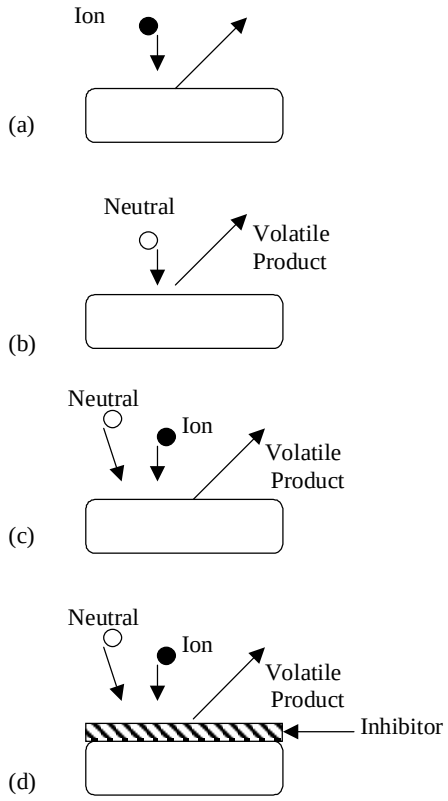

Figure 13 The Four Basic Plasma Etching Processes: (a) sputtering, (b) pure chemical etching, (c) reactive ion etching, and (d) ion inhibitor etching.

The first process, sputtering, is a purely physical, unselective process. Energetic ions crossing the sheath transfer large amounts of energy to the substrate, resulting in the ejection of surface material. This mechanical process is sensitive only to the magnitude of bonding forces and structure of the surface, rather than its chemical nature [52]. Since sputtering requires high amounts of energy, the rates are generally low and the yield is typically on the order of one atom per incident ion [31].

Unlike sputtering, chemical etching is a highly selective process due to its inherent sensitivity to the differences in bond type and chemical consistency of the

substrate. This chemically selective process involves gas-phase etchant atoms or molecules formed through collisions between energetic free electrons and gas molecules, which stimulate dissociation and reaction of the feed gas. These etchants chemically react with the surface to form volatile products [52]. This process is invariably isotropic or non-directional, since the gas-phase etchants arrive at the substrate with near uniform angular distribution. The etch rate for pure chemical etching can be quite large due to a high flux of etchants to the substrate [31].

The third technique, reactive ion etching, is characterized by a combination of physical sputtering and chemical activity of reactive species. In most situations, the chemistry in this process is provided by the neutral species. A basic reactive ion etch system proceeds by (1) generation active species in the plasma, (2) transport of reactive intermediates from the plasma bulk to the substrate surface, (3) absorption of reactive radicals and "active site" formation, concluding with (4) chemical reaction and desorption of volatile reaction products [30]. Due to this combined process, a greater amount of etched products will be produced than with sputtering or chemical etching alone. Both chemically selective and anisotropic etching will occur, and their ratio can be controlled.

In a similar method, ion-enhanced inhibitor etching can also be an effective method for surface removal. This system shares most features of reactive ion etching, but with the inclusion of inhibitor precursor molecules that absorb or deposit on the substrate. The polymer-forming inhibitor species may originate from the feed gas, feed gas additives, sputtered reactor material, or a resist mask. During this process, the plasma chemistry initiates the formation of a thin film on the sidewalls of the etched feature,

which prevents chemical attacks. The bombarding vertical ion flux keeps horizontal surfaces clear of this inhibitor film. A highly anisotropic etch with vertical side walls is formed, and a volatile etch product is released [38, 53, 54]. This process is not as selective as pure chemical etching, and contamination of the substrate and final removal of the protective inhibitor film can be a disadvantage.

In addition to the etching methods described above, it should also be noted that volatile and non-volatile etched material may return to the substrate surface, further effecting the overall surface modification. This is known as redeposition and backscattering, which depends on the volatility of the etched material.

If etching takes place at the bottom of a small feature, non-volatile etch products will tend to deposit on the sidewalls of the feature. This phenomenon is referred to as "redeposition." If all etched material is volatile, it will not condense on the sidewalls and it will eventually escape from the feature even after colliding many times with the sidewalls of the feature. In regard to etching on a flat surface, the non-volatile species can be returned to the etched surface, after undergoing numerous collisions with species in the gas phase, where they will most likely redeposit. This is known as "backscattering". Backscattering can lead to severe microroughness on the substrate. Volatile products may also be returned to the surface by this process, but, in general, they will condense on the surface due to their high vapor pressure [38].

2.3.1.1.1 Effects of Plasma Parameters on Etching

As previously mentioned, plasma-surface interactions are dependent on plasma parameters. This is especially true for etching. Depending on the gas, frequency,

pressure, and exposure time, the etching rate, uniformity, and selectivity of the substrate will vary [31]. By altering these parameters, system optimization can be achieved and controlled. This section will elaborate on these parameters and their consequent influence. Although other plasma parameters are very important, specifically plasma composition, number density, temperature, distribution function and particle diffusions, the study of these parameters are outside the scope of this research.

The effect of the working gas on the etching process includes both the gas type and its flow rate. By altering either parameter, dramatically different forms and degrees of etching will occur. Specifically, the gas type can determine whether the treatment will induce a higher or lower degree of etching, as well as promote etching in favor of deposition/polymerization. This can be seen through various works comparing inert helium, versus reactive gases such as oxygen, nitrogen, and fluorocarbons [55,56]. Due to helium's large amount of energy available to transfer to the polymer surface via ion neutralization, Auger de-excitation, and Penning ionization in the polymer, it is much more effective as a cross-linking gas than an etchant [44]. In contrast, reactive gases such as O_2 and CF_4, can have a much greater etching effect. The composition of these reactive gases must be balanced, however, in order to optimize the etching and/or polymerization balance [57].

In addition to the effect of the gas type, the influence of the flow rate must also be considered. In general, the rate of etching will rise rapidly with increasing flow rate to a maximum value, followed by a decrease at higher flow rates. Initially, in the low flow region, there is an inadequate supply of reactant gas, creating a high utilization rate. This is steadily overcome and etching is maximized at the optimum flow rate. As the flow

rate is further increased, however, the accompanying raise in pumping speed causes active species to be pumped away before having the opportunity to react, thereby decreasing the etch rate for the high flow region [33].

Pressure can also play an important role in the etching mechanism by directly affecting the major phenomena that control plasma etching. These phenomena include: (1) the sheath potentials and energy of ions bombarding the surface, (2) the electron energy, (3) the ion-to-neutral abundance ratio and fluxes to these species to the surface, (4) the relative rate of higher to lower order chemical kinetics, (5) surface coverage by physisorption, and (6) the relative rates of mass transport processes [52]. As pressure is lowered below 0.1 Torr, as in most vacuum plasma systems, the sheath potential is dramatically increased. Given that the pressure is inversely proportional to the mean-free path, this rise in potential translates into a higher energy ion flux [55]. As a result, the ion bombardment promotes etching by physical sputtering or damage-induced mechanisms versus those of chemical etching [52].

Much like pressure effects, the RF excitation frequency can alter key discharge characteristics that influence etching. Flamm has shown that in low-pressure systems, these characteristics include altering the spatial distributions of species and electrical fields across the discharge, the energy and concentration of species as a function of time, the energy of ions impinging on the surface, and the electron energy distribution function. These characteristics then limit the ability or inability of physical and chemical processes to occur, thereby regulating the rate and degree of etching [58].

Weight changes and micrographs have illustrated the effect of exposure time on plasma treated surfaces. As exposure time is lengthened, weight loss and changes in the

surface morphology are notably increased [59]. AFM analysis performed by Gupta et al showed progressively rougher surfaces with increasing exposure time for PET films treated in argon [60]. Specifically, the RMS amplitude of the modules showed a linear increase with exposure time.

Similar results were obtained by Beake, who observed exposure time dependence on the etching effect of Mylar films embedded with silicate additives. On plasma treatment, the heights of the silicate additives above the surface increased greatly as a function of exposure time [61].

2.3.1.2 Surface Morphology and Roughness Changes

Due to the etching mechanism on polymer surfaces, morphological and topographical changes will occur. These changes are visible through atomic force microscopy (AFM) or scanning electron microscopy (SEM). Since most polymers are semi-crystalline, that is, they contain both crystalline and amorphous regions; they produce very distinctive morphology changes due to selective etching.

Padhye et al observed that both PET and nylon 6,6 filaments showed selective etching patterns when exposed to nitrogen plasma. For the PET treated samples, they reported "seashore" like structure, with an average separation of $600\,\text{Å}$ between adjacent elongated units. These long periods are consistent with amorphous regions within the polymer. Due to the loosely bound structure of the amorphous regions, it is concluded that these areas are much more susceptible to etching. Similar results were observed for the nylon 6,6 samples, but due to their spherulitic crystal structure versus that of the

folded chain structure of PET, the etch pattern varied. It consisted of fibrillar branches expanding from the center [62].

Okuno et al obtained identical results for both PET and nylon when comparing weight loss from plasma exposure to the degree of crystallinity. Their research showed that the weight loss decreased with increasing percent crystallinity [63]. In another study, the etching rate was also shown to be a decreasing function of crystallinity [64].

2.3.1.3 Chain-scission

Chain-scission is defined as any event that results in the breakage of one polymer molecule into two or more parts. This can occur through a direct rearrangement of the backbone into two separate entities, or by the loss of side groups and consequent rearrangement, which inherently results in molecular division [27]. Both processes can occur as the result of etching via plasma exposure. The first interaction involves ion bombardment, in which ion energy is transferred to the polymer molecules comprising the substrate. Bond scission and radical formation then occurs, causing weight loss and a reduction in molecular weight [65].

2.3.2 Chemical Phenomena in Plasma-Assisted Surface Modifications

2.3.2.1 Radical Formation

In addition to physical modifications, plasma exposure leads to changes in the elemental composition of the polymer surface. This includes the formation of free radicals. These radicals enable reactions such as cross-linking by activated species of inert gas (CASING), surface graft polymerization, as well as the incorporation of functional groups.

Electron spin resonance (ESR) signals of polymeric materials exposed to plasma, even in short durations show new radical formations. These sites include not just terminating radicals, but mid-chain and stable monomer-derived radicals as well. ESR also has indicated dangling-bond sites, which are suitable to CASING [66].

The formation of radical sites occurs through ionization or excitation of the polymers through electrostatic interaction between fast moving electrons and the orbital electrons in the polymers. The consequent ionization leads to molecular fragmentation and the formation of a free radical. Similarly, excitation leads to dissociation of the excited polymers, also forming free radicals.

$$e^- + AB \xrightarrow{\text{radiation}} AB^+ + e^- \qquad \text{(Ionization)}$$

$$e^- + AB \xrightarrow{\text{radiation}} A^+ + B + e^-$$

$$AB \xrightarrow{\text{radiation}} AB^* \qquad \text{(Excitation)}$$

$$AB^* \longrightarrow A\cdot + B\cdot \qquad \text{(Dissociation)}$$

If the free radicals formed are unstable, they will rapidly undergo recombination. Stable radicals, however, will remain in the polymer as living radicals. These radical sites can then "catalyze" the next steps for further chemical processing such as initiation of grafting, cross-linking, or functional group attachment [65].

As with most surface modifications induced by plasma, the free radical intensity is also dependent on plasma parameters including gas, pressure, and exposure time. The substrate composition will also play an important role in radical formation and stability. Chen examined these parameters using various gases, substrates, and exposure times [67]. ESR analysis has shown that there was a distinctive increase in radical intensity for increased durations of exposure. There was also a notable difference in radical intensity

for the various substrates and gases, specifically in the order of: linen > cotton > polynosic rayon > standard rayon > nylon6 ≈ PET and CF_4 > CO > A r> N_2 > O_2. These results are summarized in Table 1.

Table 1 Relative Free Radical Intensities of Fibers Treated with Low Temperature Plasma of Various Gases with Constant Exposure Time (180 s) [67]

	Relative Free-Radical Intensity					
Plasma Gas	Linen	Cotton	Polynosic Rayon	Standard Rayon	Nylon 6	PET
CF_4	4.5	2.9	1.2	0.9	0	0
CO	3.2	2.9	0.8	0.4	0	0
Ar	1.9	1.4	0.7	0.3	0	0
N_2	0.5	0.4	0.3	0.1	0	0
O_2	0.1	0.3	1.0	0.1	0	0

*Plasma treatment was carried out for 180s

Due to the relatively low radical intensities measured for O_2 in comparison to those measured for CF_4, it is concluded that the O_2 plasma generated free radicals are unstable with a short lifetime, which will rapidly recombine. In contrast, CF_4 plasma appears to generate stable free radicals in the polymer matrix [67].

2.3.2.2 Grafting

Plasma grafting, often referred to as plasma graft-copolymerization, can occur through either of the following two mechanisms [68]:

(1) The creation of active species on the polymer surface, followed by contact with the monomer:

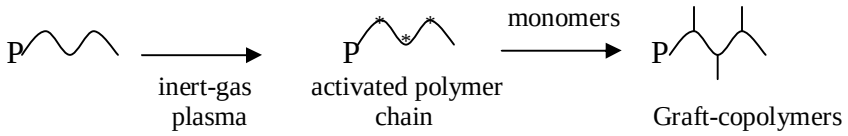

In this mechanism, free radicals are formed on the polymer surface as a result of inert gas plasma treatment. These radicals can either directly initiate grafting or be converted into peroxide or hydroperoxides by the inclusion of an oxidative gas. These activated peroxides will also initiate grafting in the presence of the monomer species [4].

(2) Direct grafting of the polymer with common or unconventional monomers under "monomer"-plasma conditions:

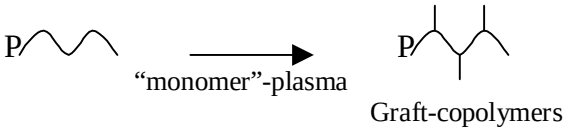

Unlike the previous method, this involves a combined plasma and monomer exposure in one step by the use of gaseous monomers in the working gas mixture [68]. Both of these techniques have shown great advantages over conventional grafting by offering a large range of chemical compounds to be used as monomers, varying thickness of monomer layers, and limited destruction [69].

Zubaidi and Hirotsu have modeled the grafting of various hydrophilic monomers, including HEMA, NiPAAm, and acrylic acid onto various natural and synthetic fibers. This study models the gas, substrate, and exposure time effects on the graft yield. In their study, the percent grafting for most substrates increased with exposure time. The inclusion of oxygen, however, reduced the extent of grafting due to its deactivation of polymer radicals. The authors also noted an increase in breaking strength for yarns that were plasma-grafted with NiPAAm, due to the binding of fibrils by graft polymers [70].

In a similar study conducted by Simionescu, the plasma grafting of cotton, polyester, and wool fibers was examined. It was shown that after plasma treatment and grafting there was altered surface roughness, increased compatibility between natural and

synthetic materials, improved surface properties by removal of outer fiber shell, water absorption and rejection properties, adhesive properties, reduced shrinkage, and improved dyeing and printing properties [69].

2.3.2.3 Polymerization

Plasma-induced polymerization can be defined as a film-forming process by which thin films are deposited directly onto the surface of a given substrate without any fabrication. The elemental reactions occurring during this process include fragmentation of monomer molecules, the formation of reactive sites (radicals), and recombination of the activated fragments. This mechanism follows similar steps to that of traditional radical polymerization with the inclusion of a possible re-initiation step [65]:

Step 1: Initiation - Radicals are formed in the gas phase and at the substrate which initiate polymerization.

$M_{(g)} + e \rightarrow 2R\bullet_{(g)} + e$
$S\text{-}X + e \rightarrow S\text{-}R_n\bullet + H\bullet$

$M_{(g)}$ = gaseous monomer
R• = radical
S = surface site
X = monomer or polymer segment

Step 2: Propagation – Continual growth of the polymer chain through the successive addition of monomer molecules and the shifting of the active center.

$R_n\bullet + M_{(g)} \rightarrow R_{n+1}\bullet$
$S\text{-}R_n\bullet + M_{(g)} \rightarrow S\text{-}R_{n+1}\bullet$

Step 3: Termination – The terminal radical on a growing chain is destroyed or rendered inactive through bonding with another chain.

$R_n\bullet + R_m\bullet \rightarrow X_{n+m}$
$S\text{-}R_n\bullet + R_m\bullet \rightarrow S\text{-}X_{n+m}$
$S\text{-}R_n\bullet + S\text{-}R_m\bullet \rightarrow S\text{-}X_{n+m} + S$

Step 4: Reinitiation – Radical formation in the deposited polymers by activation of electrons, ions, and radicals.

$$X_n + e \rightarrow R_n\bullet + H\bullet + e$$
$$X_{n+m} + e \rightarrow R_n\bullet + R_m\bullet + e$$
$$S\text{-}X_n + e \rightarrow S\text{-}R_n\bullet + H\bullet + e$$

Although the plasma initiated mechanism follows conventional processing steps, there are distinct differences when the two are compared. First and foremost is the simplicity of the plasma process. Since fewer steps are involved in the fabrication, it is a very attractive alternative. In contrast, however, the resulting polymer is distinctly different from that formed through conventional methods. The properties of the plasma-generated film are strongly dependent on the deposition parameters, including power input and pressure, which directly affect the fragmentation of the monomer species [27].

Numerous studies have been conducted using hydrocarbon and fluorocarbon gas plasmas for film deposition with successful results [57, 71, 72]. At present, however, the development of a technologically advanced plasma-polymerization reaction is limited by the generation of side reactions, which occur simultaneously with the main process. Due to the constant bombardment of active species by the plasma, active centers are generated on the polymer backbone which can initiate destruction mechanisms, cross-linking processes, secondary grafting reactions, as well as free radical trapping [68].

2.3.2.4 Cross-linking

Cross-linking occurs when two polymer molecules join to form one large molecule/network. This occurs when radical sites are created in the polymer, resulting in the formation of H or Y-links. Figure 14 illustrates this mechanism for PET. Cross-

linking can result in improved mechanical properties, decreased solubility, elimination of the melting point, and increased resistance to corrosive attack, all of which are desirable properties [27].

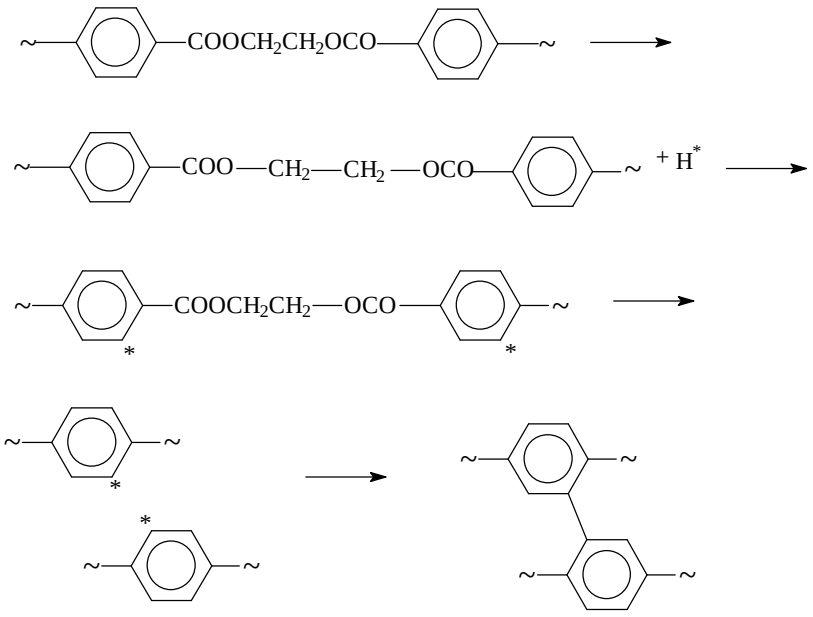

Figure 14 PET Cross-linking Mechanism via Recombination of Aryl Radicals Formed through Hydrogen Abstraction From the Benzene Ring

For plasma processing, this technique is referred to as CASING (previously mentioned in section 3.2.1), which consists of creating a cross-linked layer with a high cohesive energy as the result of an inert gas discharge action [44]. During plasma exposure of polymeric materials, both chain-scission and cross-linking occur randomly and simultaneously. The predominance of one process over the other will depend on the polymer structure and crystallinity, temperature, and gas composition. If scission/etching is the dominating process, then degradation of the physical properties will occur, and the

polymer may become unusable. For this reason, an exact balance must be obtained to control the competing processes [27].

Placinta's study on the cross-linking of PET in helium/oxygen plasma best illustrates the effect. As the concentration of oxygen is increased, cross-linking is diminished. The presence of oxygen clearly induces chain-breaking reactions, which counteracts the cross-linking process. Optical emission spectroscopy also revealed a decrease in metastable helium as a result of the increase in oxygen, which will diminish the cross-linking ability of the helium. In order to prevent this shift, the oxygen concentration in the working gas must be limited to only a few percent. The small addition of oxygen, however, can help prevent the ageing process due to its surface functionalization capability [44].

2.3.2.5 Surface Functionalization

Surface functionalization by plasma exposure occurs via the chemical interactions between gas phase species and activated radicals on the substrate surface. For this reason, functionalization is directly dependent on the type of working gas. By using an inert gas such as helium or argon, functionalization and modification of the surface will occur by the chemically reactive species created on the polymer surface by the irradiation effect of the plasma. Although helium has drastic morphological effects due to sputtering, there is no direct reaction with the surface. As a result, the broken polymer chains of the surface will recombine to form new structures, limiting the amount of new functional groups [56]. In the case of reactive gases such as oxygen, carbon dioxide, and fluorcarbons, however, atoms or molecular portions are added to the polymer surface.

For most polymer substrates treated in an oxygen plasma regime, there will be a visible increase in the O:C ratio as new oxygen-containing functional groups are introduced. These groups include, but are not limited to –OH and –COOH, which dramatically increase the surface energy of the substrate [73]. In a similar manner, polymers treated in a fluorine gas such as CF_4 will show an increase in the F:C ratio as surface fluorination occurs [71]. In both cases, the added functional groups are directly related to the working gas and its dissociated species. By the inclusion of these functional groups, new and novel surface properties can be achieved. Several of these applications will be discussed in the next section.

2.4 Plasma Finishing Applications

2.4.1 Hydrophilicity/Hydrophobicity Alterations

For most textile finishing applications, wettability is a crucial function. Not only is it a desirable property for end use products, but it also aids in the dyeing and finishing process. By introducing polar groups such as –OH, –OOH, and -COOH through oxygen plasma treatment, the wettability of hydrophobic polymers such as PET can be greatly enhanced. The surface roughness caused by etching can also increase surface area and aid in wetting. Contact angle analysis has shown that PET films were wetted thoroughly following oxygen plasma exposure. In contrast, films treated in fluorocarbon gases resulted in strongly hydrophobic surfaces that did not wet [74].

Although plasma exposure can dramatically alter wettability, an ageing effect is observed. Gupta reported that the contact angle of PET films showed a gradual increase with storage times up to 10 days [60]. This suggests that the polar functionalities undergo considerable changes over time. Popular consensus is that the polar groups

undergo migration into the polymer bulk in order to reduce the interfacial tension. However, it is always possible that a fraction of the functional groups are transformed into stable structures, thereby diminishing the surface hydrophilicity [60, 75].

2.4.2 Adhesion Enhancement

The first attempt at improving adhesion through plasma modification was conducted by Schonhorn and Hensen in 1966. Numerous studies have followed with satisfactory results. Through these studies, it was concluded that plasma treatment increases adhesive properties through the following mechanisms [3]:

(1) Removal of a low surface energy layer through cleaning and etching

(2) Strengthening of the top layer through cross-linking

(3) Introduction of new functional groups by reaction of the activated surface with plasma species

(4) The creation of a high-energy coating tightly bonded to the substrate by grafting

2.4.3 Desizing

Desizing via plasma treatment is a fairly recent and novel process. Typical desizing procedures include a series of hot water baths containing detergent. The effluent/waste water must then be treated to remove all PVA. Although PVA itself is a low cost material, the removal and wastewater treatment can be costly in addition to environmental compliance requirements. These concerns and limitations have resulted in increased research to find ways to improve this process and the type of size used. One

method that has recently been explored is the use of atmospheric pressure plasma treatment as an aid in the desizing process.

In a recent study conducted by researchers at NC State University, both helium and oxygenated-helium atmospheric plasma treatments were applied to desizing PVA on woven cotton fabric. The percent desizing ratio (PDR) and tensile strengths of both the fabric and single yarns were measured. The results shown in Figure 15 conclude that the plasma treatments can both remove some PVA sizing and significantly improve PDR by washing, specifically by eliminating the need for hot water washing. Tensile data revealed no significant difference between the treated samples and the control, indicating that no fabric damage was incurred. In further research, XPS analysis of plasma treated PVA films revealed surface chemical changes such as chain scission and formation of polar groups, which promote the solubility of PVA in cold water [76].

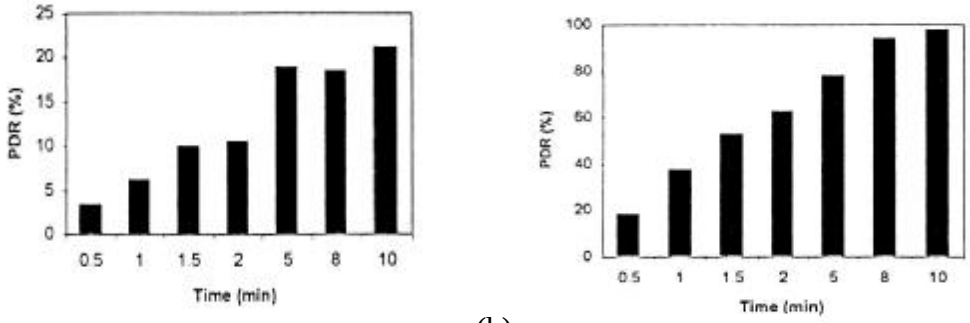

(a) (b)

Figure 15 Effect of plasma exposure time on PDR by (a) plasma treatment only and (b) plasma treatment followed by cold-water wash [77]

In a similar study presented by Rakowski, oxygen plasma was utilized to determine its effect on the removal of sizes and finishes from greige cotton and cotton/polyester blends. Results demonstrated the plasma's ability to etch and volatilize both sizes and finishes off of the fabric. The decomposed material was converted into

ecologically harmless products such as carbon dioxide and water [51]. This clearly demonstrates the viability and ecological benefits of a plasma-aided size removal system.

2.4.4 Sterilization/Antimicrobial Properties

Sterilization is defined as "any process or procedure designed to entirely eliminate microorganisms from a material or medium" [78]. Conventional techniques for sterilization include the use of autoclaves, ovens, and chemicals such as ethylene oxide (EtO), methyl bromide or hydrogen peroxide. These methods rely on irreversible metabolic inactivation or on the breakdown of vital structural components of the microorganism [79]. Although very effective, these methods are often associated with damage to the material/medium that is supporting the microorganisms. As a result, newer, more effective forms of sterilization are being researched, and have led to the discovery of plasma sterilization.

Plasma sterilization operates through the following basic mechanisms [80], which are further illustrated in Figure 16:

(1) Destruction of the genetic material of the microorganism through UV irradiation.

(2) Erosion of the microorganism, atom by atom, through *photo-induced desorption*. This occurs as a result of UV photons breaking chemical bonds in the microorganism material, leading to the release of volatile compounds that are intrinsic to the microorganism.

(3) Erosion of the microorganism, atom by atom, through *etching*. Reactive species from the plasma adsorb on the microorganism material, which subsequently causes them to undergo chemical reactions and form volatile products.

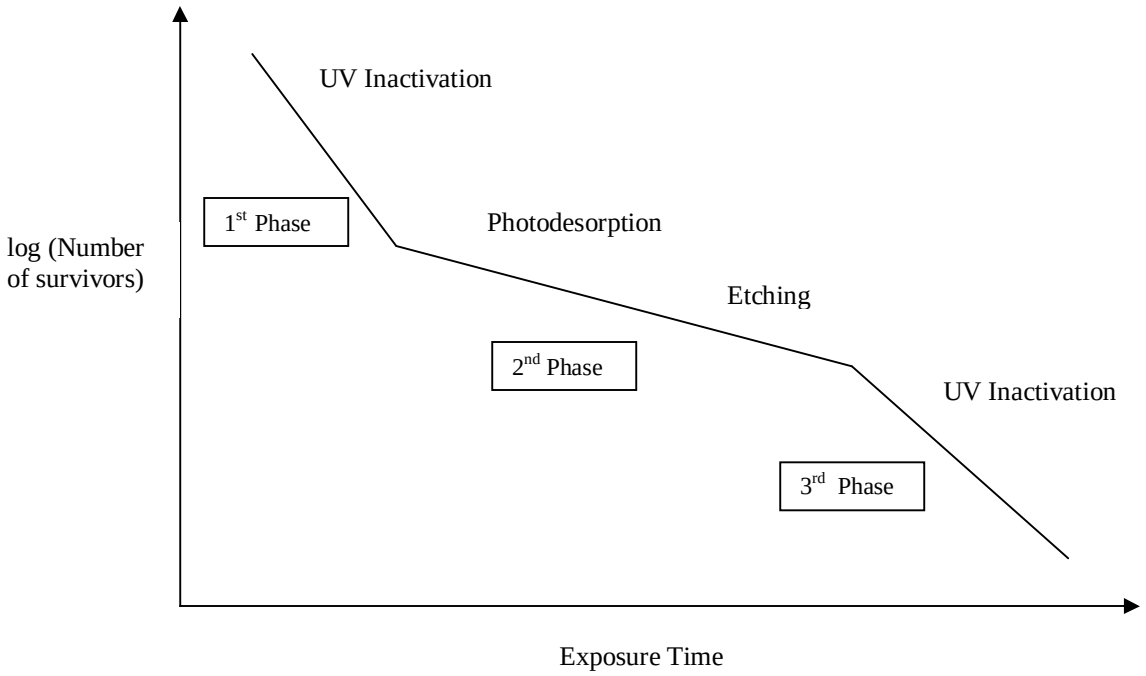

Figure 16 Schematic of the three-phase survival curve characterizing plasma sterilization, showing the mechanisms predominantly acting during each phase.

These processes not only kill microorganisms, but they have also been effective in destroying bacteria, spores, fungi, and viruses [81].

In addition to sterilization, plasma treatments can also impart antimicrobial and antibacterial functionality or aid in antimicrobial finishing. Due to the inherent properties of textile fibers, they readily support the growth of microorganisms, and must undergo preventative treatments. If infestation of microbes does occur, staining and foul odors may form, not to mention a loss of performance properties. Traditional finishing techniques involve coating, spraying, or padding of antimicrobial chemicals directly onto the fiber/fabric [82]. Recently, however, there has been growth in the area of plasma aided antibacterial finishing.

Several methods have been employed for antibacterial plasma finishing. One technique uses plasma to impart functional groups on packing materials for improved barrier characteristics and conferred antimicrobial properties [83]. Another technique involves plasma-aided deposition of polyethylene glycol (PEG). Since PEG surfaces have been shown to reduce protein absorption and bacterial attachment, it makes a perfect antimicrobial coating material. Under cold plasma environments, desired structures can be generated directly from fragmentation of the appropriate starting materials, which will recombine and deposit. This technique has proven highly affective for inhibiting microbial attachment, and can be applied to a wide range of materials including rubber and polyester [84]. Plasma treatments have also shown promise for graft co-polymerization of antimicrobial agents onto nonwovens.

III. **RESEARCH OBJECTIVES**

3.1 Objective 1: Modeling of Plasma Effects on Polymeric Materials

The modeling objective focuses on determining plasma-substrate interactions, and the effect of plasma exposure time and gas species on polymeric materials at fixed power and frequency. A developed model would allow for the prediction of a desired treatment based on the mechanisms of the plasma-substrate interaction. Although a comprehensive model including kinetics and plasma models would be optimal, this model is limited to semi-empirical modeling based on experimental results. These results may then be extended to different substrates using various plasma conditions.

3.2 Objective 2: Plasma Aided Finishing Applications

This objective focuses on finishing applications using plasma treatment, specifically plasma-aided desizing, and plasma graft copolymerization for antimicrobial finishing.

In plasma-aided desizing, it is important to determine the mechanism by which desizing is achieved, and how to optimize the treatment through plasma-substrate interactions. This optimization can further improve the process of dry desizing with plasmas.

In graft-copolymerization, the plasma initiates sites for grafting, followed by a set of chemical processes using bioactive monomers. Due to the ability of plasma to generate free radicals and –OH/-OOH sites, graft copolymerization can occur when exposed to the reacting medium. This process allows for biocidal finishing of textiles, which incorporates both antimicrobial and insect repelling finishes. Figure 17 illustrates the

basic processes for plasma-aided graft copolymerization to produce antimicrobial or antimicrobial/insect repelling finishes.

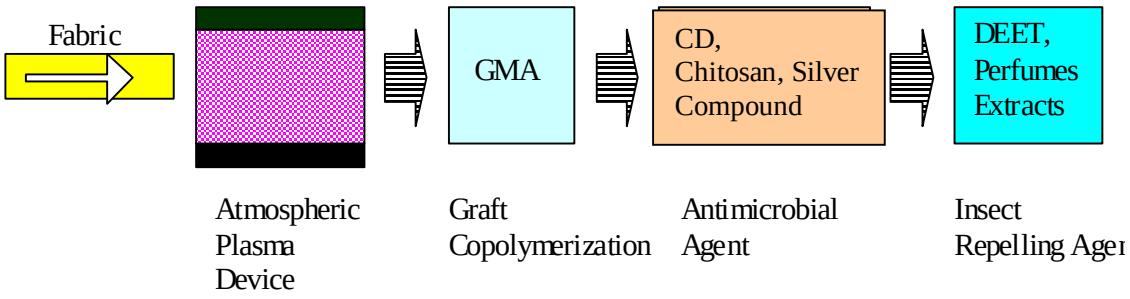

Figure 17 Illustration of the atmospheric plasma-aided antimicrobial/insecticidal finishing process

IV. EXPERIMENTAL

4.1 Atmospheric Plasma Facility

The atmospheric plasma facility located on NCSU's Centennial Campus has an active exposure area of approximately 60 x 60 cm between two copper electrodes with 5 cm gap separation. Each copper electrode is embedded in a polycarbonate dielectric barrier. The device is powered by a 4.8 kW power supply operating in the frequency range between 5-10 kHz. The device has an inner plasma chamber installed inside of an outer chamber, where the latter is equipped with a fabric rolling system for continuous fabric modification treatments. The working gas is fed into the chamber through gas flow controllers. Figure 18 shows a schematic drawing of the experimental facility. When flowing helium or oxygenated-helium into the plasma chamber, there will always be a slight amount of air due to the fact that the chamber is not pumped down and operates at

atmospheric pressure. The device is capable of batch treatment of films and fabric pieces using a test cell, as well as continuous operation using a feed roller system for large fabric rolls or continuous filaments and yarns. All samples in this study were exposed to plasma using the test cell. The test cell is a closed geometry chamber, with little to no ventilation, in which volatiles are not continuously removed. Samples are placed on a suspended nylon grid within the test cell, which allows for complete exposure to plasma on both sides of the substrate. Input power, operating voltage, frequency, and plate separations were all held constant. The helium gas flow rate was held at approximately 10 L/m. For experiments with other gas mixes, an additional flow of either 1% oxygen or 1% CF_4 was added to the chamber. The plasma discharge inside of the test cell is uniform and free from coronas, which allows for uniform treatment of the exposed samples.

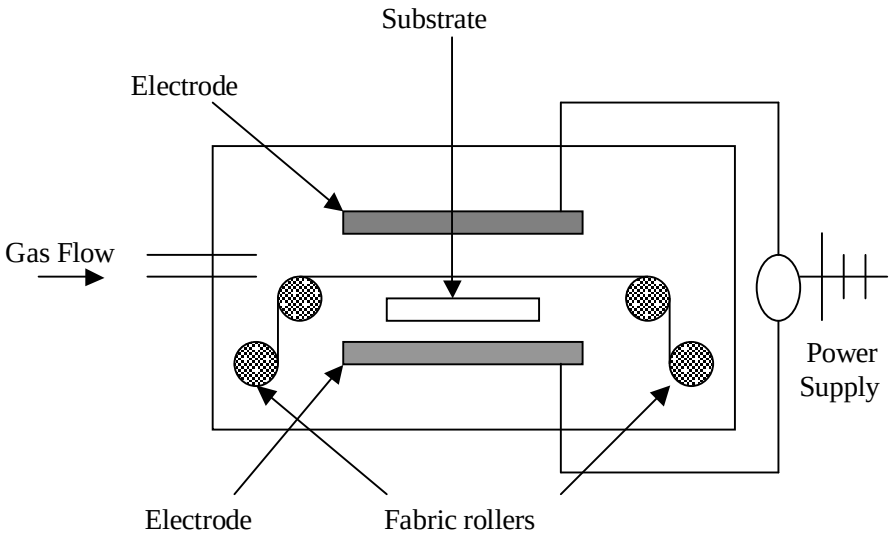

Figure 18 Schematic of the Atmospheric Plasma Chamber

4.2 Materials

4.2.1 Study 1: Polyethelyne Terephthalate (PET) Films

Melinex® polyethylene terephthalate (PET) films were obtained from DuPont Teijin Films. These films were untreated and classified as slightly hazy. Except for a difference in thickness, both films were identical in composition with a thickness of 50μm for the S/200 samples and 125 μm for the S/500 samples. Both films types were exposed to helium and oxygenated-helium plasmas. The exposure time was varied between 0.5 and 5.0 minutes in 30-second intervals.

4.2.2 Study 2: Polyvinyl Alcohol (PVA) Films

The first set of PVA films were generated using 99% hydrolyzed PVA chips. Using a heated water bath, 40.0 grams of PVA were dissolved in 200 ml of deionized water forming a viscous syrup. Two milliliters of the PVA syrup was then dissolved in a 6 cm aluminum pan using 10 ml of heated deionized water. The resulting films had an average thickness of approximately 244 μm. Once the PVA syrup was dissolved, the films were left to dry in ambient conditions for approximately four days. The second set of PVA films were supplied by MonoSol, LLC. These films are hot water soluble at 140°C and have a thickness of 40 μm (1.5 mils).

Both the lab created and commercial films were exposed to helium, oxygenated-helium, and helium/CF_4 plasmas. The exposure time was varied between 0.5 and 5.0 minutes in 30-second intervals. Two additional samples were treated at 8.0 and 10.0 minutes to view the effects of extended exposure.

4.2.3 Study 3: Polypropylene Nonwoven Fabric

Nonwoven, polypropylene (PP) fabrics were prepared in the Nonwoven Cooperative Research Center at NC State University through hydroentanglement with a fiber linear density of 1.74 dtex and a fabric basis weight of ~46.7 g/m^2. Sample strips weighing approximately two grams were prepared by washing in acetone to remove lubricants, and air dried prior to processing.

The nonwoven fabric strips were exposed to either oxygenated-helium plasma or a helium/forming gas (90% nitrogen/10% hydrogen) plasma for two and five minute intervals. All samples were immediately immersed in either a glycidyl methacrylate (GMA) or methacrylic acid solution following plasma exposure. GMA containing 50 ppm methyl hydroquinone inhibitor was purchased from Aldrich, and was used without any further purification. The methacrylic acid was also purchased from Aldrich, and contained 200 ppm methyl hydroquinone inhibitor. It was distilled before use to strip off the inhibitor.

The antimicrobial agents, including β–cyclodextrin was purchased from Aldrich, and the MCT β–cyclodextrin was purchased from Wacker, GmbH, in Munich Germany. Chitosan (type 652, viscosity 4-20 cps) was given as a gift from France Chitine, France, and the glycidyl trimethyl ammonium chloride (GTMAC) was purchased from Dow Chemicals.

Plasma Graft Copolymerization Reaction

Following plasma exposure, the samples were immediately graft copolymerized with GMA as shown by Scheme 1. The PP samples were placed in a closed conical flask containing a 50% aqueous methanolic solution of 10-20% glycidyl methacrylate (GMA): liquor ratio of 1:30. The flask was placed in a shaking water bath at 70-80°C for 30-60 minutes. After grafting, the sample was thoroughly washed with warm distilled water, ethanol, and acetone, and dried at 50°C. The weights of the dried, grafted samples (W_2) were determined and compared to the original (W_1). The graft yield was calculated as follows:

$$\%add-on = \frac{W_2 - W_1}{W_1} \times 100$$

Scheme 1: Plasma graft copolymerization reaction of polypropylene with GMA

GMA Structure

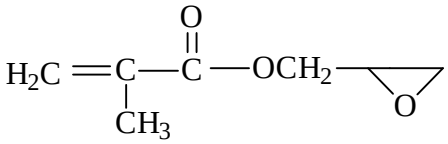

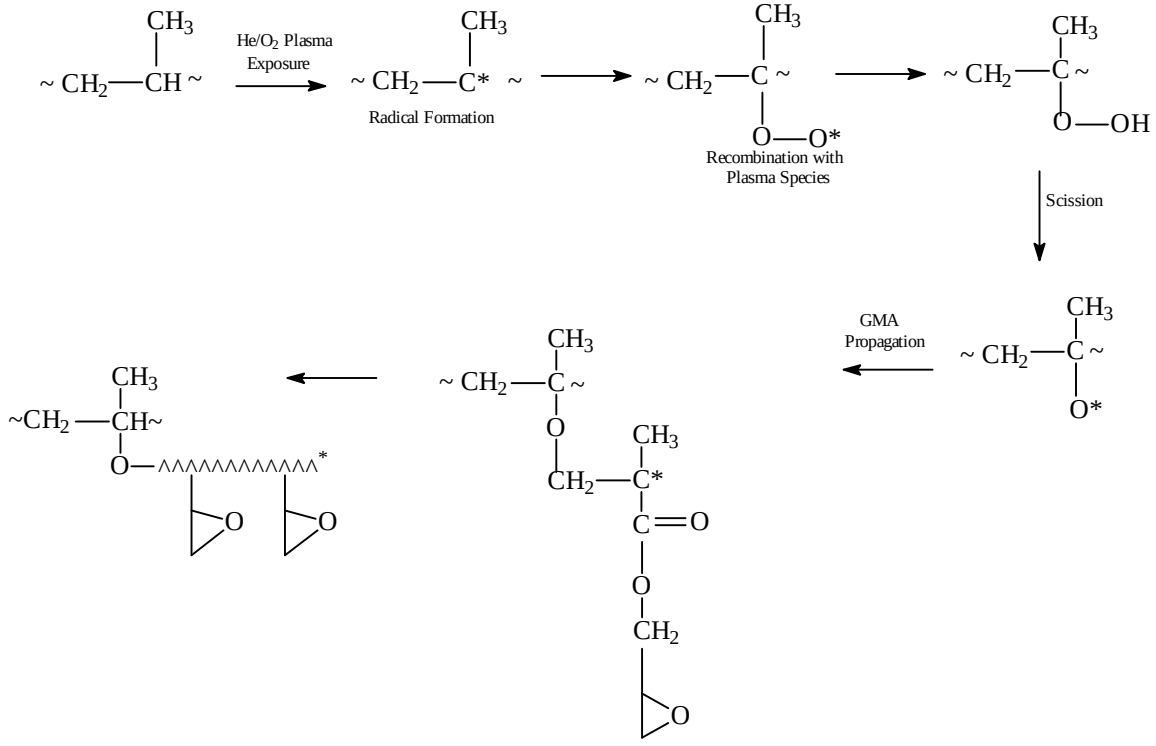

Reaction of Quaternary Ammonium Chitosan Derivative onto PP/GMA

Further grafting of the PP/GMA fabrics was affected with an antimicrobial agent, which is N-(2 hydroxy) propyl-3-trimethylammonium chitosan chloride (HTCC). HTCC was used due to its superior antimicrobial activity compared to pure chitosan. This compound not only enhances the water solubility and antimicrobial activity of chitosan, but it can also be used as antistatic finishing agent due to the presence of quaternary ammonium groups. The HTCC compound was synthesized using glycidyl trimethyl ammonium chloride (GTMAC) and chitosan as follows:

Scheme 2: Reaction for HTCC synthesis

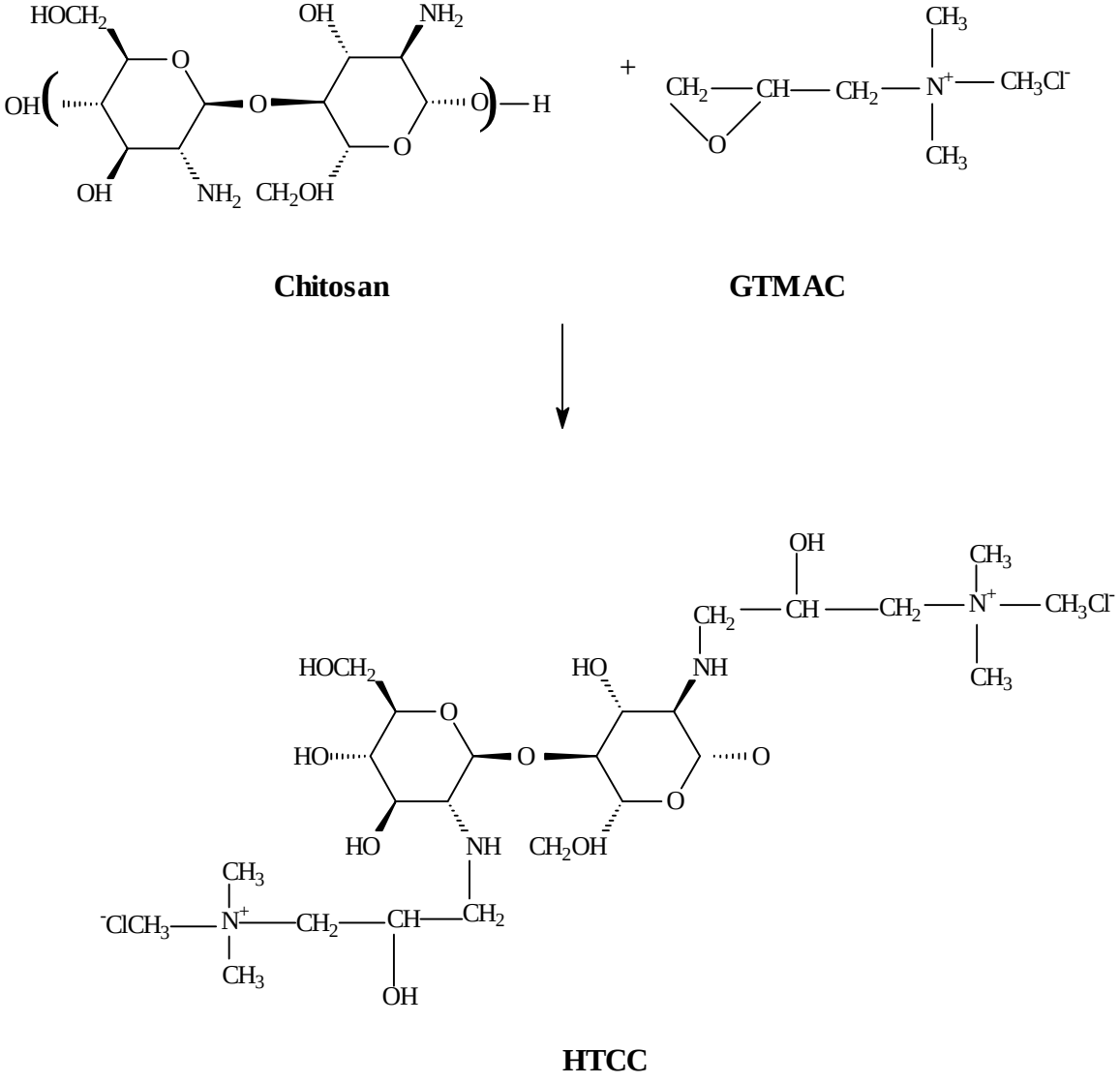

Chitosan (1%, 4-20 cps) was purified by dissolving in 1% acetic acid, and then reprecipitated with 0.1N NaOH. The precipitate was centrifuged at 0-4°C. A mixture of 2% chitosan and 8% glycigyl trimethylammonium chloride (GTMAC) were dispersed in distilled water. The solution was stirred at 80°C for 24 hours. After the reaction, the product was centrifuged at 0-4°C, which separated the insoluble chitosan from the water-

soluble fraction containing the quaternary ammonium chitosan. The quaternary ammonium chitosan was then reprecipitated with a 50% ethanol/acetone mixture, and air dried under suction.

Following the synthesis of HTCC, a PP/GMA grafted fabric was allowed to react with 2 grams of HTCC in the presence of 1% NaOH: liquor ratio 1:30. The reaction was held at 80°C for the specified time to produce the grafted PP/GMA/HTCC fabric according to the following reaction:

Scheme 3: Reaction of PP/GMA with HTCC to produce PP/GMA/HTCC grafted fabric.

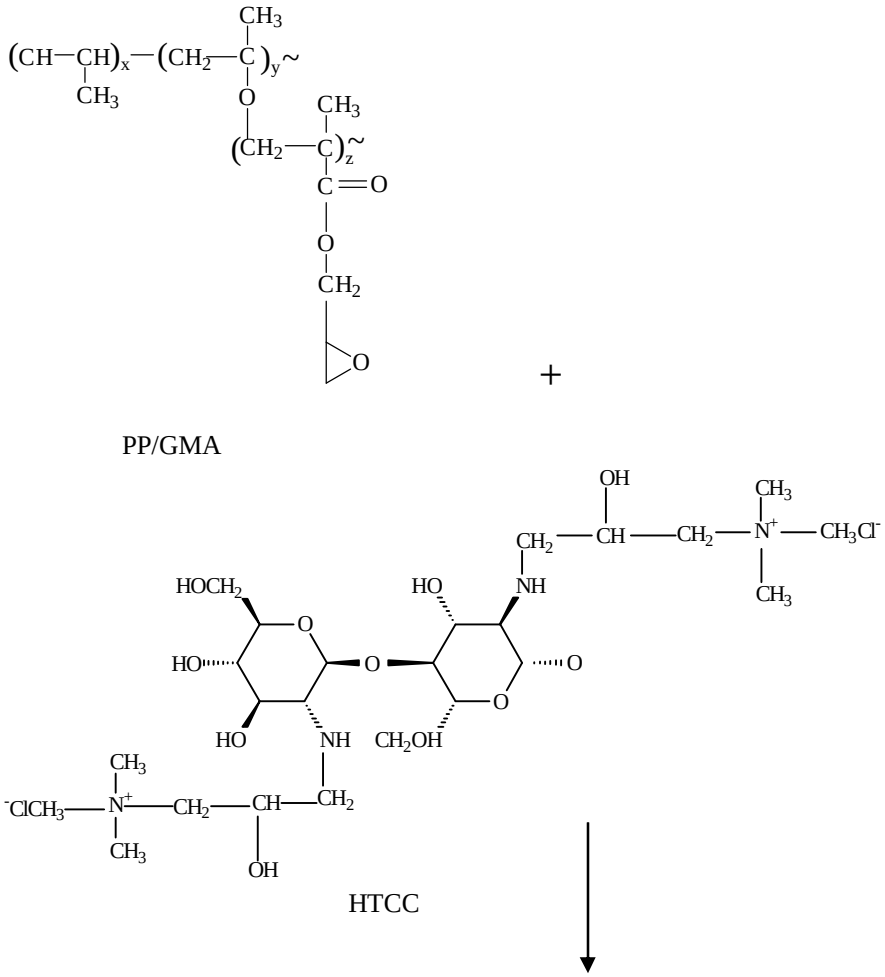

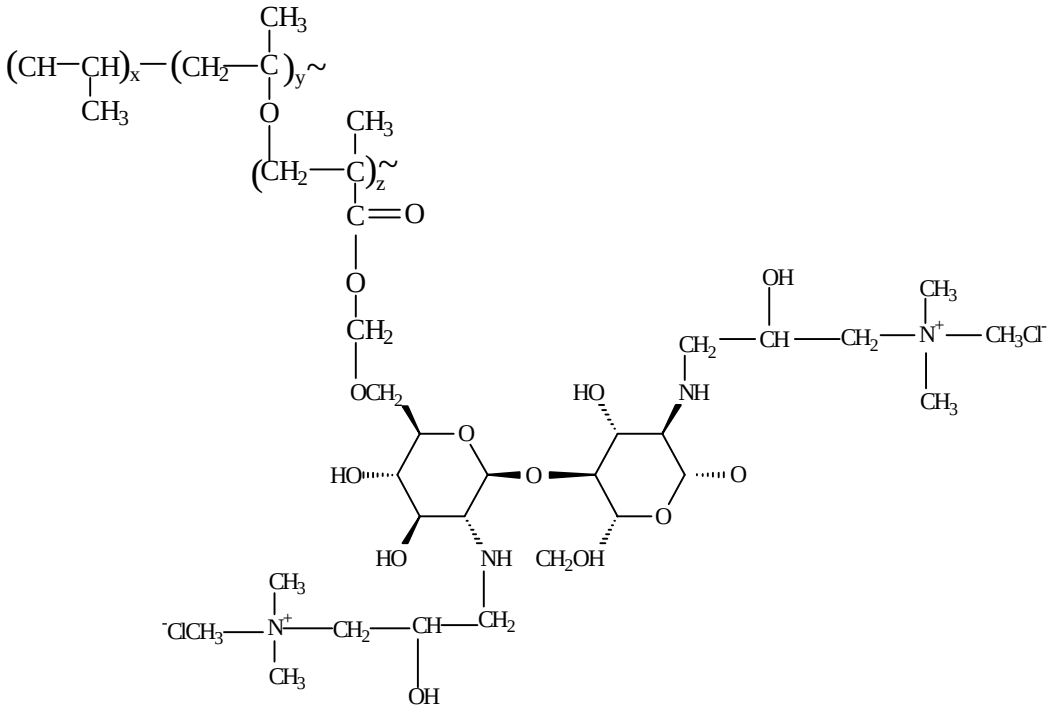

Reactions of Cyclodextrin onto PP/GMA

The PP/GMA grafted fabrics were then allowed to further react with either the β-cyclodextrin or the CMT-βCD. A 1.0 gram fabric sample was added to a solution containing 2% β–CD, 1M NaCl, and 1% NaOH. The solution was stirred at 80°C for the desired time. The grafted fabric was washed with warm distilled water and acetone. The sample was then dried and weighed. The percent graft yield was determined from the weight difference using the previous formula.

Scheme 4: Grafting of β-CD onto PP/GMA

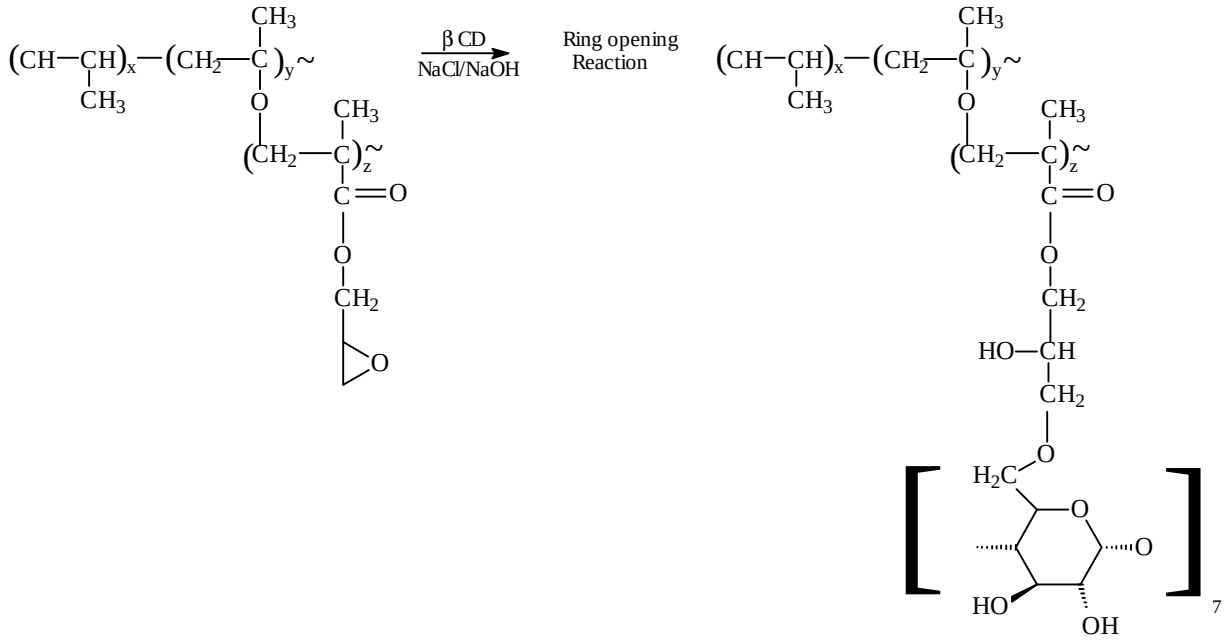

Inclusion of Insecticidal Complexes into PP/GMA/CD Fabrics

Once the β-CD compound was grafted, additional insecticidal agents were incorporated inside the inclusion compound. One gram of the PP/GMA/β-CD fabric was immersed in a 25 ml mixture (10% distilled water and 90% ethanol) containing 1-2% of a guest molecule. These guest molecules included insect repelling oils such as citronella, jasmine, sweet basil, or DEET, as well as p-benzoic acid, a $AgNO_3$-ethanolamine mixture, and iodine. The fabrics were soaked for 24 hours in this solution at room temperature to form the inclusion complexes. Samples were then washed several times with cold distilled water and ethanol. The rinsed fabrics were then air-dried.

4.3 Characterization Techniques

4.3.1 Weight Changes

Each sample was weighed before (W_0) and after plasma treatment (W_1), using an Explorer® microbalance with an accuracy of ± 100 micrograms to determine weight changes, gain or loss. The percent weight change was then plotted versus the exposure time for both PET and PVA samples. The weight changes for the PP fabric were correlated to percent graft yield, in which W_1 represented the weight of the fabric after grafting.

$$\text{Weight add on (\%)} = \frac{W_1 - W_0}{W_0} \times 100$$

4.3.1.1 Thickness Changes

The weight loss data calculated for the PVA films and previously studied PVA sized fabrics [77] were further used to calculate the thickness of PVA removed from each plasma treated sample. These values relate directly to the depth of surface ablation. Initial thickness measurements for the MonoSol and lab created films were collected using a Model II Thwing-Albert Thickness Tester, and averaged 50 μm and 244 μm respectively. The initial thickness measurements for the sized fabrics were calculated using the following equation:

$$W_{initial} = (\text{area})(2\delta_{pva})\,\rho_{pva}$$

where $W_{initial}$ is the original sample weight, δ is the sample thickness, and ρ is the PVA density. For this equation, ρ was assumed to be a uniform average, and equaled 126,930 g/m^3.

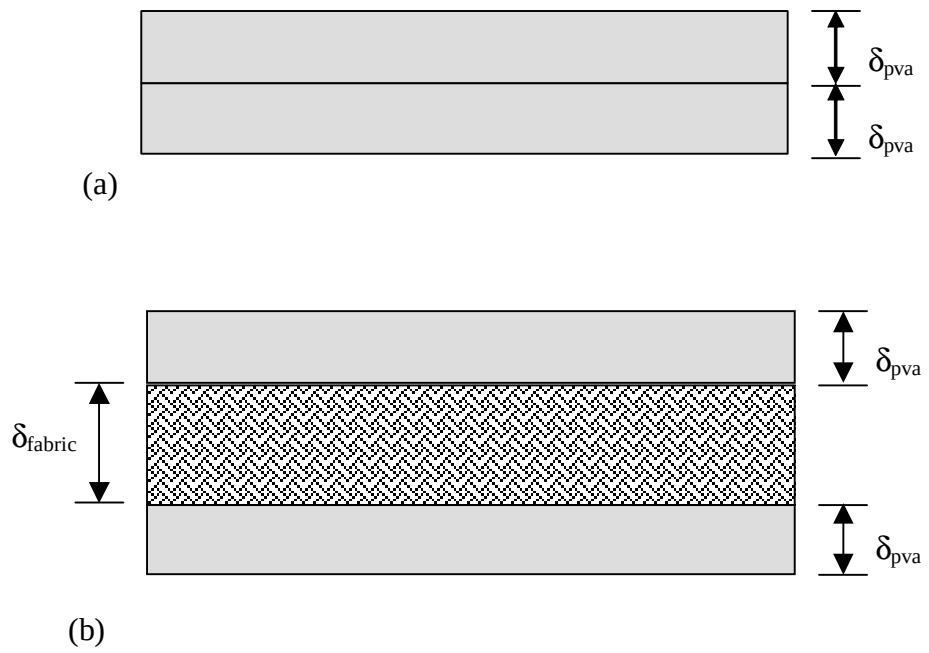

Figure 19 A Cross-sectional drawing of (a) PVA film and (b) PVA sized cotton fabric

For the sized fabric samples, $W_{initial}$ is equal to 8.9% of the total sample weight, corresponding to the amount of size added. The average thickness for these samples was calculated at an average of 37 μm. This same equation is then used to calculate the final thickness of each specimen using the weight after exposure (W_{final}). The thickness removed will then be $\delta_{initial} - \delta_{final}$.

4.3.2 Differential Scanning Calorimetry

Thermal analysis of the PET samples was conducted using a Perkin-Elmer 7 Power Compensated Differential Scanning Calorimeter (DSC). Each sample was scanned at a rate of 20°C/minute over the range of 25-300°C. The onset melting and crystallization temperatures were obtained from the intercept of the baseline and the

maximum tangent of the corresponding exothermic and endothermic peaks. Peak areas were also calculated to evaluate the changes in percent crystallinity.

PVA films were tested and examined using the above protocol, with a scan rate of 20°C/min over a range of 25-250°C. The nonwoven PP grafted samples were run at a scan rate of 30°C/min over a range of 25-190°C. Only the melt endotherm was evaluated for the PP samples.

4.3.3 X-Ray Diffraction

X-ray spectra were obtained using an Omnic Instruments® wide angle x-ray diffractometer (WAXD) at 30 kV and 20 mA. Samples were scanned from an angle (2θ) range of 5-40 degrees, with a 0.2 step size. TRXD 4.11 software was used to evaluate the peak spectra.

4.3.4 Thermal Gravimetric Analysis

Thermal analysis was further conducted on the nonwoven PP samples using a Perkin Elmer Thermal Gravimetric Analysis device. Percent weight change versus temperature was evaluated at a scan rate of 30°C/min over a range of 25-700°C.

4.3.5 Solubility

Portions of each PET film sample were soaked for 20 hours in 100% toluene. The samples were weighed before and after soaking using a Denver Instrument® M-220D microbalance with an accuracy of ± 10 micrograms. The same procedure was followed for both types of PVA films. The solubility tests were conducted in 100% methanol for

20 hours. The swelling ability/degree of solubility was determined for each film from the calculated weight difference.

4.3.6 Fourier Transform Infrared Spectroscopy (FTIR)

Polypropylene nonwoven fabric samples were evaluated using a Nexus® 470 FTIR in conjunction with a Nicolet® Omnisampler.

4.3.7 Gel Permeation Chromatography (GPC)

Samples weighing between 2 and 4 mg were dissolved in a 0.1M solution of polished water and sodium nitrate in ratio of 1mg film/ml solvent. Samples were then filtered using 0.22 micron nylon syringe filters. Gel Permeation Chromatography (GPC) was performed using a PL Aquagel 40 column, and a Waters© 2414 Refractive Index Detector with a sensitivity setting of 32. Samples were analyzed using Breeze Version 3.20 Software. All measurements were based on PEG and PEO standards.

4.4Microscopic Analysis

4.4.1 Scanning Electron Microscopy

Polypropylene nonwoven fabric samples were evaluated using a Hitachi S-3200N Variable Pressure SEM. Photos were collected at ranges from 100X to 2000X.

4.4.2 Atomic Force Microscopy

Atomic force microscopy was conducted on the PVA films using a 3000 Dimension AFM at the Engineering Graduate Research Center on Centennial Campus.

V. RESULTS AND DISCUSSION

5.1 Study 1: Etching Effects of Atmospheric Pressure Plasma on Polyethylene Terephthalate Films

5.1.1 Differential Scanning Calorimetry

Results of Differential Scanning Calorimetry (DSC) showed slight fluctuations in the melt and crystallization onset temperatures, with the average temperature values being no more than 2°C higher than the control, as shown in Tables 2-3. No conclusions could be drawn from these measurements since no significant difference was observed. Following these results, the crystallinity for each film was analyzed based on the formula [85]:

$$\% \text{ Crystallinity} = (\Delta H_{sample} / \Delta H_o^f) \times 100$$

where ΔH_o^f is the standard heat of formation, and ΔH_{sample} is the based on the measured endotherm peak.

Table 2: DSC Results for PET S/200 Films Treated in (A) Helium and (B) Oxygenated-Helium Plasma

(A)

Exposure Time (min)	Melt Onset (°C)	Peak Area (mJ)
0	244.91	166.31
0.5	245.27	167.97
1	244.44	150.85
1.5	254.67	155.04
2	246.14	178.67
2.5	248.07	174.19
3	245.34	179.4
3.5	245.3	195.75
4	244.57	172.46
4.5	248.19	175.98
5	245.61	188.81
Treated Ave.	246.76	173.91
% Change	0.76	4.57%

(B)

Exposure Time (min)	Melt Onset (°C)	Peak Area (mJ)
0	244.91	166.31
0.5	245.97	156.48
1	245.62	191.1
1.5	246.17	181.1
2	248.64	176.48
2.5	246.49	190.57
3	243.32	197.54
3.5	246.82	214.43
4	245.49	200.51
4.5	244.71	185.42
5	244.06	195.04
Treated Ave.	245.73	188.87
% Change	0.33%	13.56%

Table 3: DSC Results for PET S/500 Films Treated in (C) Helium and (D) Oxygenated-Helium Plasma

(C)

Exposure Time (min)	Melt Onset (°C)	Peak Area (mJ)
0	245.43	171.2
0.5	246.17	177.22
1	244.12	172.66
1.5	246.45	165.62
2	245.68	161.08
2.5	247.38	208.63
3	244.53	171.86
3.5	247.03	172.59
4	244.25	160.24
4.5	243.45	186.06
5	244.49	182.33
Treated Ave.	245.36	175.83
% Change	0.76%	2.70%

(D)

Exposure Time (min)	Melt Onset (°C)	Peak Area (mJ)
0	245.43	171.2
0.5	246	170.36
1	244.59	163.63
1.5	242.08	162.53
2	245.99	182.72
2.5	246.87	180.12
3	244.44	181.05
3.5	245.11	152.09
4	246.07	166.27
4.5	245.64	177.19
5	245.5	161.68
Treated Ave.	245.23	169.77
% Change	-0.08%	-0.84%

Based on the above calculation, there was a notable increase in peak area observed for both the helium and oxygenated-helium exposed S/200 films. Specifically, there was a 4.57% average increase in the helium-exposed films, and a 13.56% increase in the oxygenated-helium exposed films. This same increase was observed when analyzing the exotherm peak area. In contrast, the S/500 films exhibited little to no change in % peak area. This minimal effect is most likely due to the larger thickness of the S/500 films. With this increased bulk, the DSC may not be as sensitive to the surface treatment.

In addition to peak area increases, there was a significant increase in percent crystallinity for the S/200 film set. This data is illustrated in Figure 20. The helium exposed set showed a maximum percent increase of 11.82% at 3.5 minutes, and the helium-oxygen exposed set showed a maximum of 17.54% at the same exposure time. Following this maximum peak, there was a drop in % crystallinity. This corresponds

well with the weight loss trends shown in the following section, and is attributed to re-deposited amorphous material.

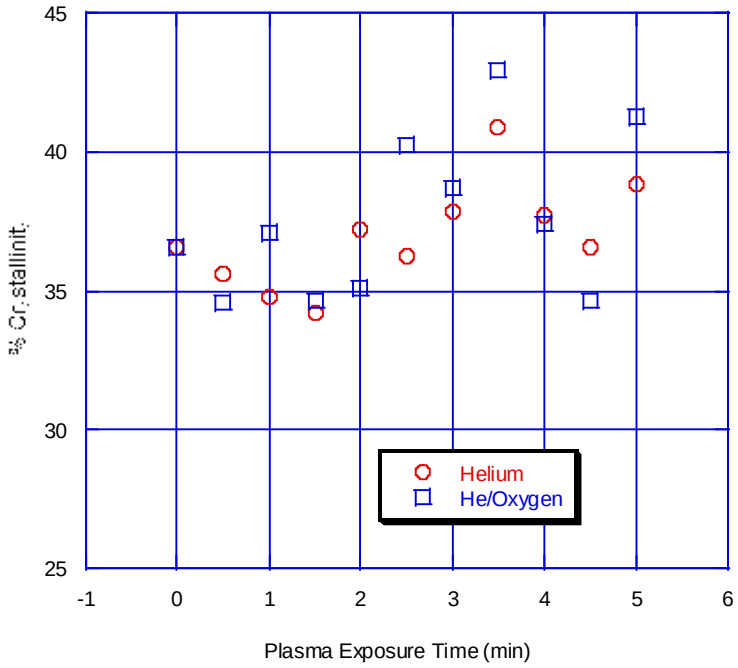

Figure 20 Percent crystallinity change for plasma exposed PET S/200 films

The S/500 films also demonstrated a similar trend in crystallinity changes, with a maximum increase of 25.6% for 2.5 minutes exposure to helium, and a near identical increase of 25.3% for 2.0 minutes oxygenated-helium exposure. For both film types, the oxygenated-helium exposed samples showed either higher maximum crystallinity values or a faster rate at which the max was achieved. This is due to the high reactivity and etching ability of the additional oxygen added to the feed gas.

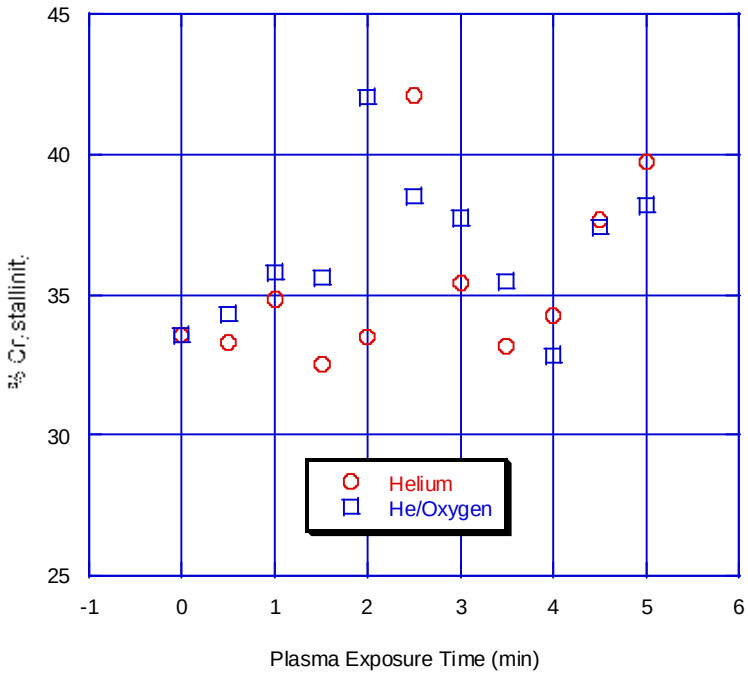

Figure 21 Percent crystallinity change for plasma exposed PET S/500 films

The increase in % crystallinity for these films may be explained by several possible mechanisms: (1) an elevation in temperature from plasma exposure creates thermal energy in the polymer chains, which then move to form new crystals or cause small crystals to grow in size, (2) etching creates spacing in the polymer network allowing for chain movement and further crystallization, (3) amorphous regions are selectively etched due to ease of removal, thereby shifting the crystalline/amorphous ratio. As amorphous content is decreased, the percent crystallinity is automatically increased. Since no change was observed for the melt and crystallization onset temperatures, which would indicate an increase in crystalline content, the most probable mechanism is a decrease in the amorphous regions by selective etching. This mechanism was previously proposed by Okuno et al when testing the dyeability of PET treated in a

vacuum plasma [63]. The following sections will further develop the validity of this mechanism.

5.1.2 Weight Loss

This experimental configuration allows for surface etching with an increased etching rate until reaching saturation inside of the test cell. As no ventilation is allowed, re-deposition of etched volatiles is possible. The rate of etching and re-deposition, could be determined from the time-to-saturation measurements of the weight change of exposed samples. Figures 22 and 23 illustrate the weight loss trend for both the S/200 and S/500 films in both plasma treatment regimes. It is obvious from the figures that surface etching immediately starts when exposing the films to the plasma. The time-to-saturation indicates the threshold to a re-deposition-dominating regime. This behavior indicates competing etching and re-deposition effects in a closed geometry exposure configuration.

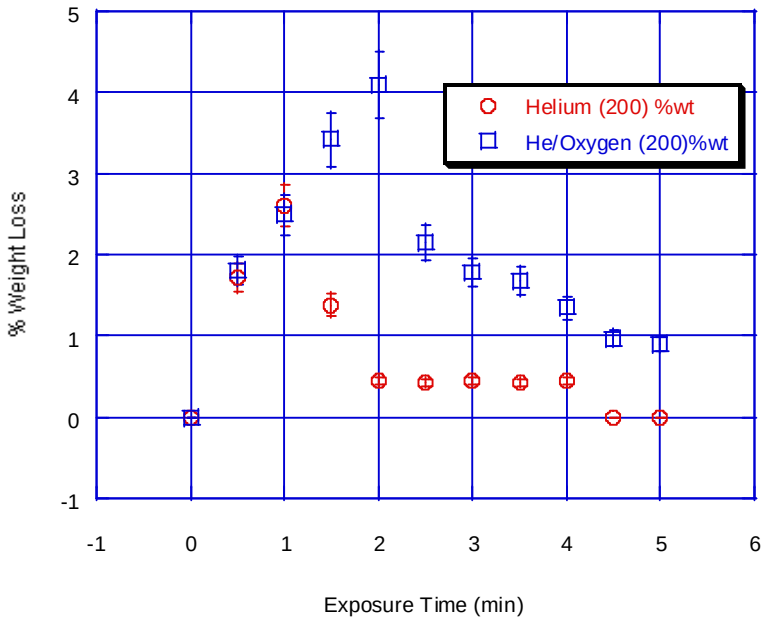

Figure 22 Percent weight loss versus exposure time for PET S/200 treated in helium and oxygenated-helium plasmas

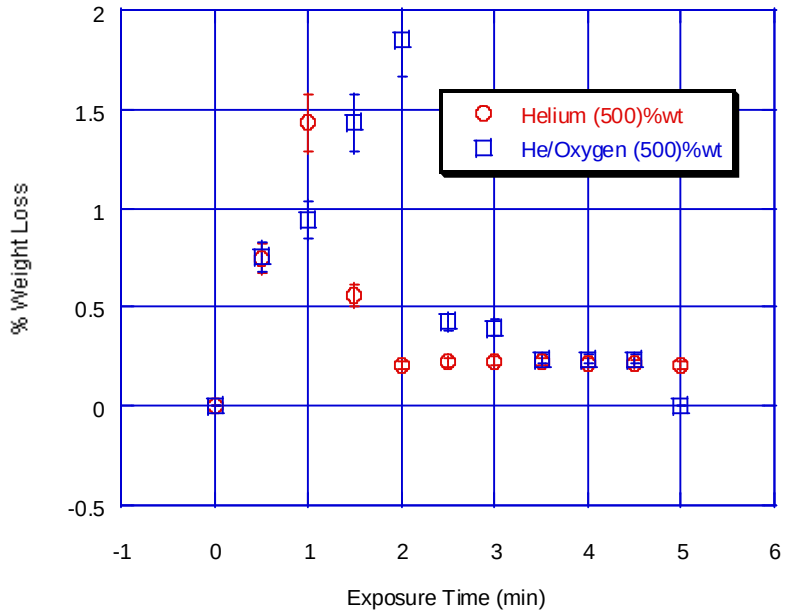

Figure 23 Percent weight loss versus exposure time for PET S/500 treated in helium and oxygenated-helium plasmas

For the helium-exposed films, the maximum weight loss is at approximately 1-minute exposure, and the oxygenated-helium treated samples reached a maximum weight loss at 2 minutes exposure. This, in correlation with the enhanced peak magnitude of the oxygenated-helium samples, shows that the presence of oxygen in the discharge provides a higher etching rate when compared to etching in helium-only plasma. Charge exchange may also be responsible for the production of oxygen ions when the test cell is operated using only helium. Typically, helium is not considered an etchant gas, however, helium ions can sputter the substrate. Additionally, a fraction of air with helium can induce etching, because of the fact that the test cell will always contain a fraction of air, which includes the presence of nitrogen and oxygen. With the presence of air, charge exchange can occur between nitrogen and oxygen [31]:

$$N^+ + O \rightarrow N + O^+$$

The result of this charge exchange causes an increase in the formation of oxygen ions, which induces etching of the substrate. Etching will be increased further by the addition of oxygen to the feed gas forming oxygenated-helium plasma.

5.1.3 Model for Etching Mechanism

For mono-phase surfaces exposed to an ion flux from non-thermal plasma, the etching is expected to be uniform over the entire surface, with a constant etching rate. When a poly-phase surface is exposed to the ion flux, the expected etching rate will be determined by the difference between the phases and their corresponding composition. Differential or selective etching of a poly-phase surface depends on the particle flux and molecules leaving the surface at different rates as determined by each phase. The time-dependent relation between the degree of solubility and surface etching may be linear or non-linear depending on the difference between these phases. The total surface etching may be expressed by the sum of all etching rates δw on the surface:

$$dw = \frac{\sum_j n_j}{\Phi} \tag{1}$$

where n_j is the etch rate of the specific phase and Φ_j is the number of phases in the substrate [89].

Relating the degree of solubility D_s to the exposure time of the film to the plasma ion flux and composition may be expressed by either a linear (Eq.2) or a non-linear (Eq.3) decay function with respect to δw:

$$D_s = G - (\delta w)\tau \tag{2}$$

$$D_s = Ge^{-(\delta w)\tau} \tag{3}$$

where τ represents plasma exposure time and G is a gas determined constant .

For PET the surface is a three-phase composition [86-88], in which 40% is crystalline, and 60% is a combination of amorphous and ordered amorphous phases. Thus, for PET, Eq.1 could be re-written as:

$$dw = \frac{n_{amorphus} + n_{ordered\ \text{amorphus}} + n_{crystalline}}{3} \tag{4}$$

Based on this equation and the contribution of each phase to the total surface etching, a mechanism could be explained as shown in Figure 24. Due to the high order and high bond energy in the crystalline phase, it is assumed that etching of the crystalline regions, $n_{crystalline}$, is almost zero. Etching of the crystalline phase may be induced with a stronger etchant gas species, however, this will be a small yield and $n_{crystalline}$ will still be negligible. This means that the ratio of $\Sigma n/\Phi$ for PET will vary between 1/3 and 2/3.

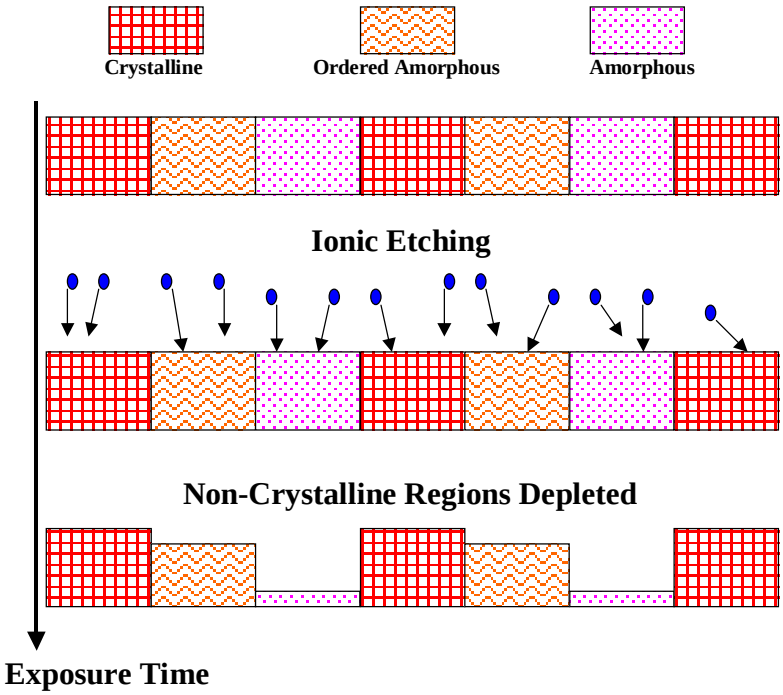

Figure 24 Schematic illustration of etching PET in atmospheric plasma treatment showing time evolution of selective etching

5.1.4 Solubility

Portions of each film were soaked in 100% toluene, a known swelling agent for PET. The effects of plasma exposure on the films' relative solubility were determined based on the weight changes of each film after soaking. Since swelling is highly dependent on the amorphous content, a decrease for the plasma-exposed film was predicted. Plots of the percent weight change in films before and after soaking revealed a notable decrease in their swelling ability in relation to plasma exposure. Since swelling is the first stage of solvation, it is directly related to the material's solubility, and is used here to determine the relative degree of solubility. In other words, as the swelling ability of the polymer is decreased, the solubility of the polymer is also decreased. As shown by the weight changes, the swelling ability of the plasma treated films decreased with

increasing plasma exposure time for both species, which supports the mechanism of selective etching. As exposure time increases, etching increases, specifically in the amorphous regions, causing an increase in percent crystallinity and a decrease in the relative solubility. The decreasing solubility trend shows the rate of change slowing after 1.5 minutes for helium exposed films, and after 2 minutes for the oxygenated-helium exposed films. This corresponds to the weight loss trend previously discussed. It should also be noted that the S/200 and S/500 measurements have an order of magnitude difference due to their difference in thickness.

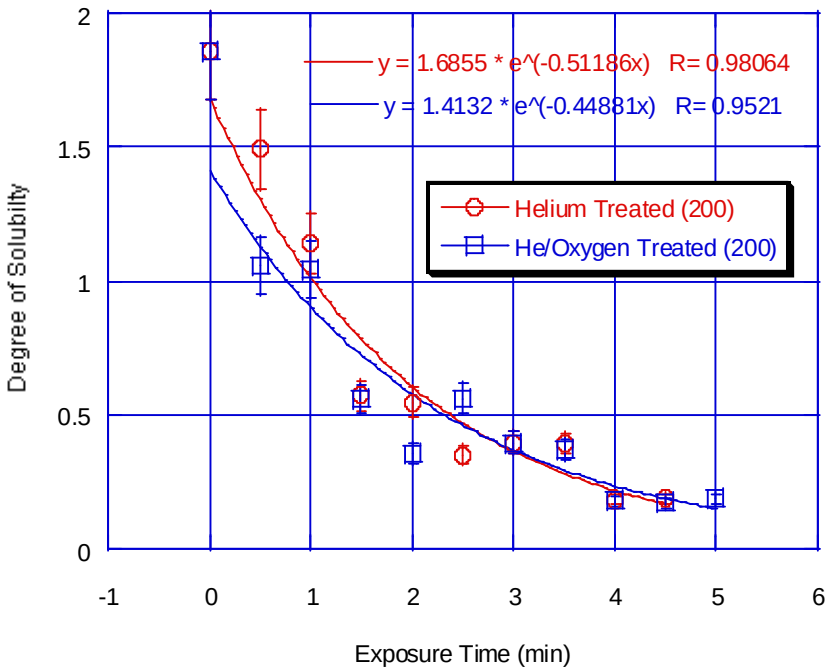

Figure 25 Degree of solubility versus exposure time for PET 200 treated in helium and oxygenated-helium plasmas, and fitted data to exponentially decaying function

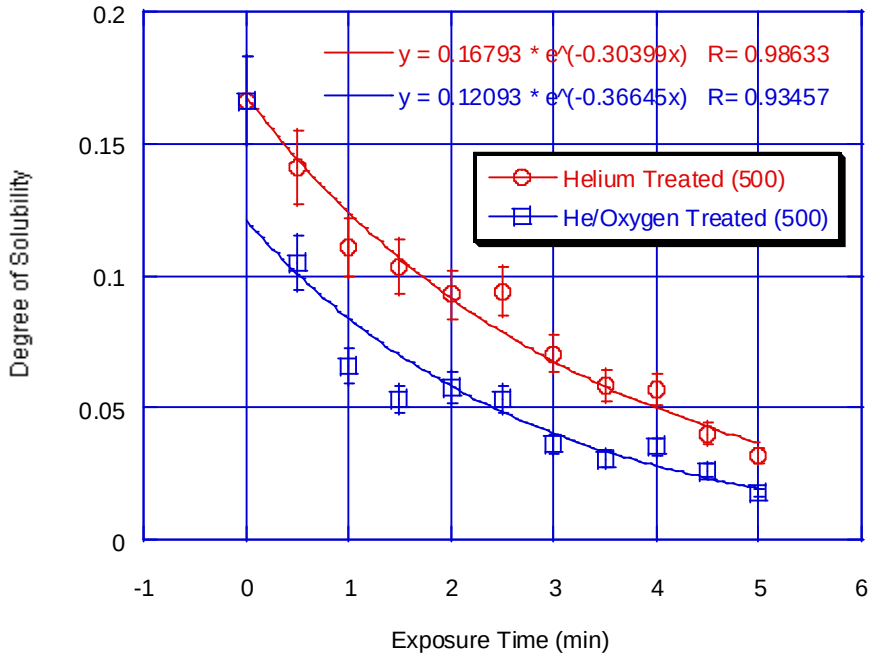

Figure 26 Degree of solubility versus exposure time for PET 500 treated in helium and oxygenated-helium plasmas, and fitted data to exponentially decaying function

Further analysis of the solubility revealed an exponentially decaying trend versus a linear trend. This is illustrated in the above Figures 25 and 26. Using Equations 3 and 4, the final model can be written as:

$$D_s = Ge^{-(n/3)\tau} \tag{5}$$

Investigation of the experimental results revealed that the $\Sigma n/\Phi$ ratio for all samples falls within the predicted range of 1/3 to 2/3. For the S/500 films treated in helium-only regime the $\Sigma n/\Phi$ ratio is 0.304, but once oxygen is added to the plasma, the $\Sigma n/\Phi$ ratio increases to 0.366. This shows a slight increase in the etching rate for the oxygenated-helium treatment due to oxygen's strong etching ability. For the helium-only treated film

n equals 0.912, and for the oxygenated-helium treated films n equals 1.099. This indicates that both films had almost 100% of the surface amorphous regions removed.

The S/200 films showed less difference between the helium treatment and the oxygenated-helium treatment. Specifically, the helium treated films had an n/Φ ratio of 0.5119 and the oxygentated-helium treated films had an $\Sigma n/\Phi$ ratio of 0.4488. This relates to Σn values equaling 1.536 and 1.346 respectively. These values are much higher than those observed with the S/500 films, and show not only a complete etching of surface amorphous regions, but additional etching of the ordered amorphous regions as well. These differences are most likely due to the difference in the film thickness. Since the S/200 films are thinner, they will therefore show a more notable etching effect. This correlates directly to the weight loss trend. Surface roughening shown through AFM analysis [59] is also in agreement with this theory.

5.2 Study 2: Plasma Desizing of Polyvinyl Alcohol (PVA) Films

Based on the etching data obtained from the PET films, it was then conceivable that this knowledge could be directly applied to the desizing of PVA. Through etching and chain-scission it should be possible to remove a significant portion of the size, as well as increase the solubility of the remaining size through surface functionalization [89, 59].

5.2.1 Weight Loss

The weight loss trends for both the lab created (LC) and commercial (MS) films are shown in Figures 27 and 28. Both graphs illustrate a steady increase in weight loss as plasma exposure time is increased, followed by a slight weight regain during the extended exposure times. This trend indicates a nearly continual surface ablation process with slight re-deposition effects. This trend is, in general, similar to observed trends in PET; however, the mechanism might be completely different. It could also be hypothesized that partial mechanisms may take place, such as etching and sputtering.

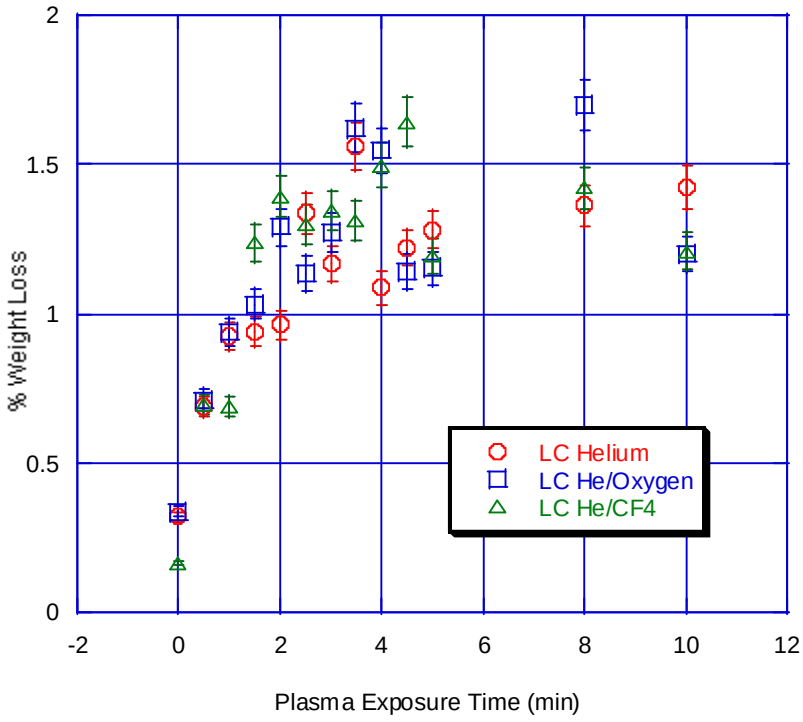

Figure 27 Weight loss vs. exposure time for lab-created (LC) PVA films

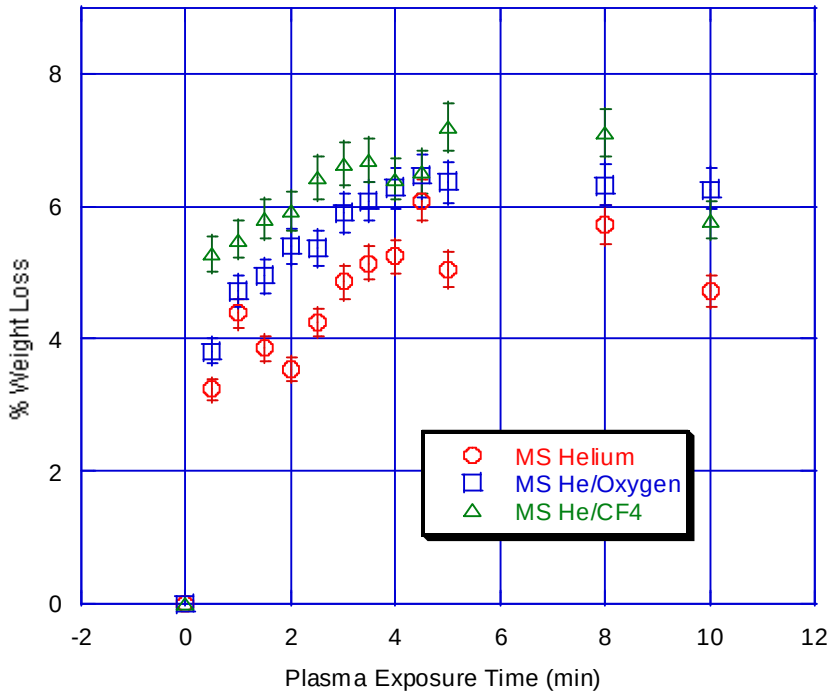

Figure 28 Weight loss vs. exposure time for commercial-grade MonoSol (MS) PVA films

Due to the high amorphous content, the poorly developed and randomly oriented crystal structure of the PVA films, and the weight loss trends observed as a result of plasma treatment, it is proposed that physical sputtering is the main mechanism of surface removal versus that of a reactive etching process [90]. This is in contrast to the chemical etching observed with PET in the previous study. It is also reasonable to consider both etching and sputtering with the latter as the dominant mechanism for this case. Figure 29 is a representation of the physical sputtering mechanism.

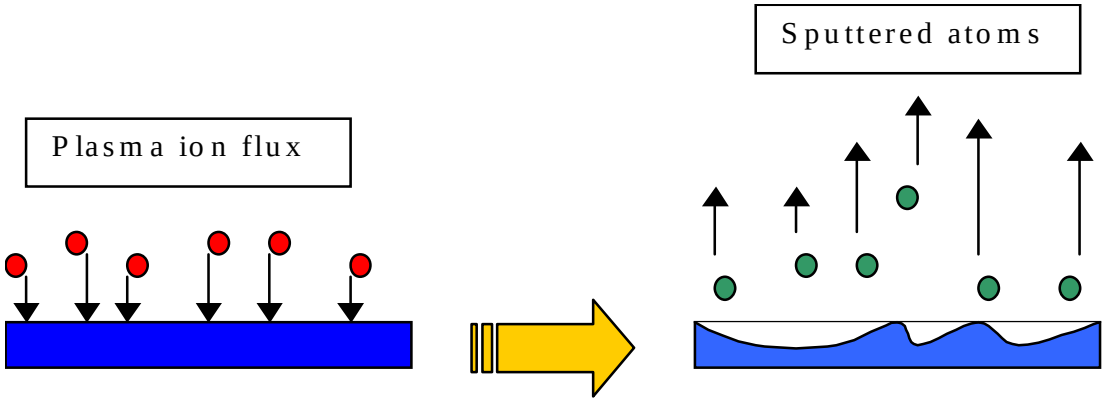

Figure 29 Physical sputtering mechanism of plasma exposed PVA films

This process is investigated by calculating the rate of sputtering for each ionic gas species using Equation 6,

$$R_{sputter} \propto \left(\frac{1}{e_t}\right)\left(\frac{m_i}{m_i + m_t}\right)\left(\frac{\Gamma_i}{n_f}\right)\left(\frac{A_t}{A_s}\right)$$

$$= C\left(\frac{1}{1+(m_t / m_i)}\right)$$

$$Total = R_{sputter} * t = C\, t\left(\frac{1}{(1+\frac{m_t}{m_i})}\right) \qquad (6)$$

where $R_{sputter}$ is the physical sputtering rate, ε_t is the surface binding energy, A_t is the area of sputtered target material, and A_s is the area of the substrate. Under the condition of unchanged ion flux (Γ_i) and particle density n_f, with equal areas A_t and A_s; the physical sputtering yield is proportional to the ratio of target and ion masses. The reaction rates determined for each gas type were as follows:

R_{He}	(100% He)	~ 8.3333 x 10^{-2} cm/sec
$R_{He/O2}$	(99% He + 1% O_2)	~ 8.5619 x 10^{-2} cm/sec
$R_{He/CF4}$	(99% He +1%CF_4)	~ 9.8360 x 10^{-2} cm/sec

The calculated values indicate that the addition of oxygen or CF_4 to the helium feed gas should increase the rate of sputtering. This increase in sputtering rates has a direct influence on the total amount of volatile species in the discharge. As oxygen and CF_4 are added to the helium feed gas, the rate of sputtering is increased and more material is removed from the film's surface. Specifically, the rate of sputtering is lowest for helium, followed by an increase with the oxygenated-helium, and further increases when CF_4 is added to the helium discharge. This trend is seen with both the LC and MS film sets.

The only noted difference between the LC and the MS films is their total percent weight loss. Although both sample sets showed similar weight loss trends, the MS films had a much higher percent weight loss, which is attributed to the difference in the thicknesses of the two film types. The MS films are much thinner than the LC films, and are therefore more affected by the surface weight loss since their bulk-to-surface ratio is smaller. Figure 30 illustrates the differing percent weight loss for both film types, with MS films about a factor of 4 higher than that of the LC films.

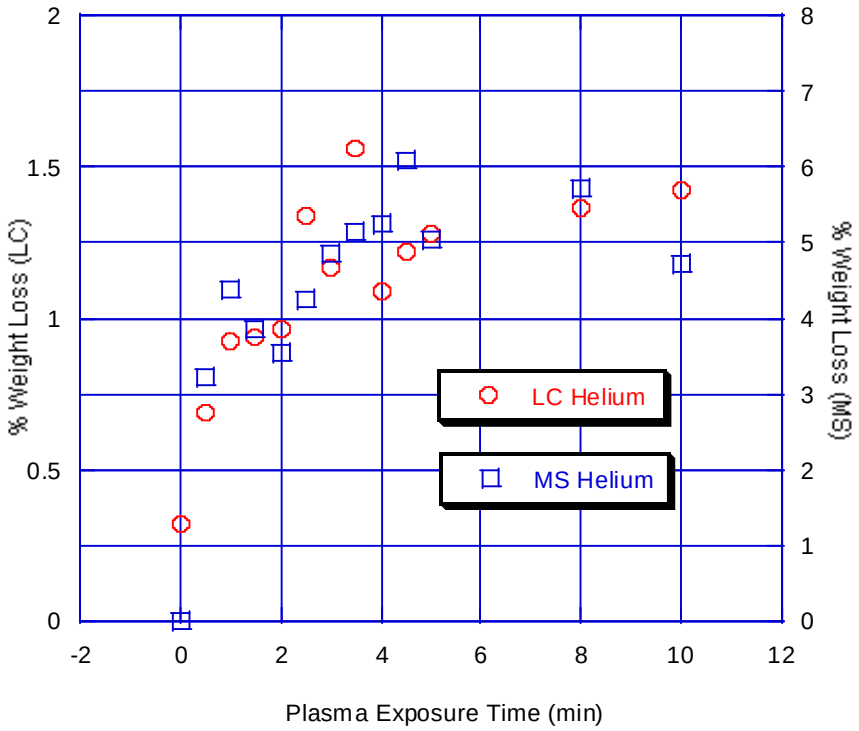

Figure 30 Weight loss comparison between helium plasma-treated LC and MS PVA films

5.2.1.1 Thickness Removal/Depth of Surface Ablation

In addition to weight loss analysis, the thickness removed from each film was also calculated. Calculations were based on initial thickness measurements, the sample weights before and after exposure, as well as the sample size and density. Thickness changes were also calculated from previous research on plasma desizing of PVA coated cotton fabrics [77]. These values were compared to the MS thickness changes. Figure 31 shows a comparison between thickness changes of MonoSol films and previous results of Ref. 77 on sized cotton fabrics.

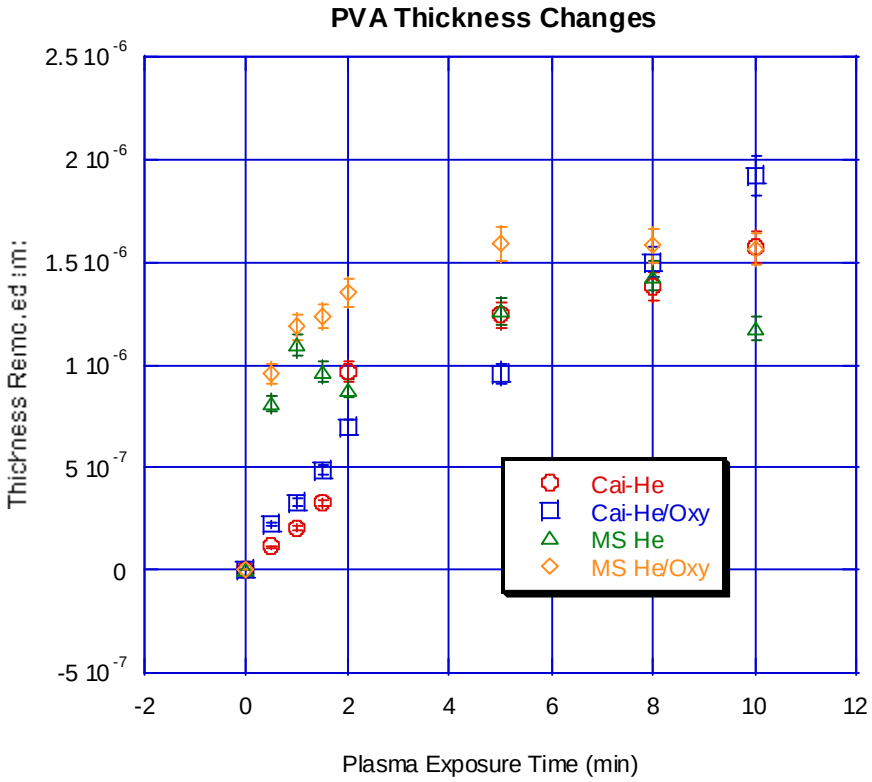

Figure 31 Thickness changes for plasma exposed MonoSol films in comparison to sized cotton fabrics. The 'Cai' markers indicate Ref. 77 results.

The thickness removed from the helium plasma treated MS films increased from 8.1 x 10^{-7}m to 1.2 x 10^{-6} m with increased exposure time. The helium exposed fabrics showed an increase in thickness removal from 1.2 x 10^{-7}m to 1.6 x 10^{-6} m. It is assumed that all the lost weight/depth for the sized fabric samples is from PVA only, and *all* thickness values were calculated for only one side of the given substrate.

The oxygenated-helium exposed samples for both sets had an even greater depth of thickness removal, with up to 1.6 x 10^{-6}m for the MS films and up to 1.9 x 10^{-6} m for the sized fabrics, due to the higher reactive effects of the oxygenated-helium versus pure helium plasma. The MS films exposed to the helium/CF_4 plasma were not used for

comparison since no matching set was available for the sized fabrics, but there was an increase in thickness removal for these films, from 1.3×10^{-6}m to 1.4×10^{-6}m.

Both the MS films and the sized cotton fabrics have similar trends in weight loss and depth of ablation. This is expected since both specimen types were exposed to identical conditions with near identical thicknesses. The thickness changes for the LC films were not used for comparison here because of their large bulk (244 μm). Due to their near identical composition and exposure parameters, as well as the observed weight loss trends for this film set, it is highly probable that a similar pattern of thickness removal would be obtained.

5.2.2 Gel Permeation Chromatography

The PVA weight loss data suggests that the PVA might undergo a significant degree of chain-scission as a result of ion sputtering processes during plasma exposure. To investigate this, and to further understand the plasma-substrate interaction mechanism, gel permeation chromatography was employed. The results for both the number average (Mn) and weight average (Mw) molecular weights of the MS films is shown in Figures 32-33, with additional trial results in Appendix 1.

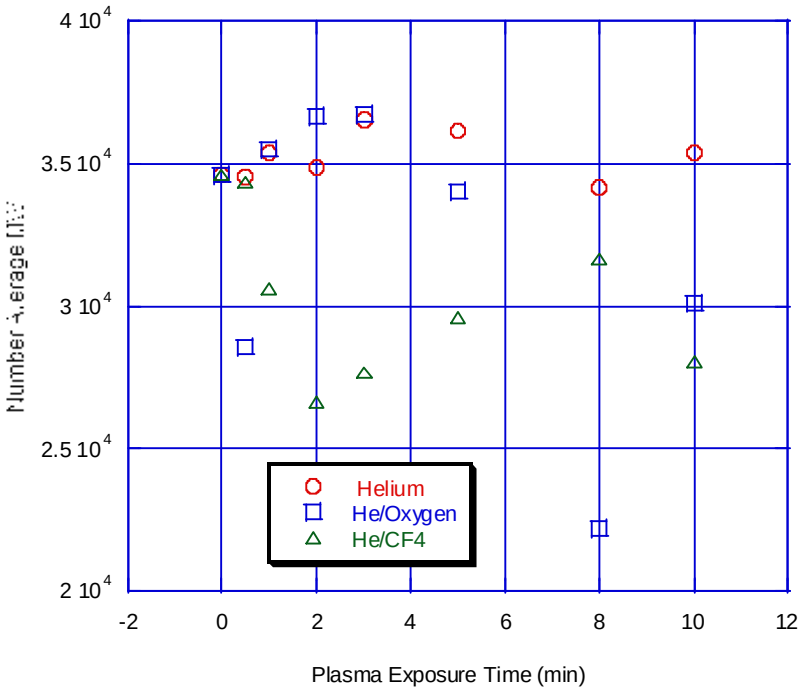

Figure 32 Number average molecular weights of plasma exposed MS films

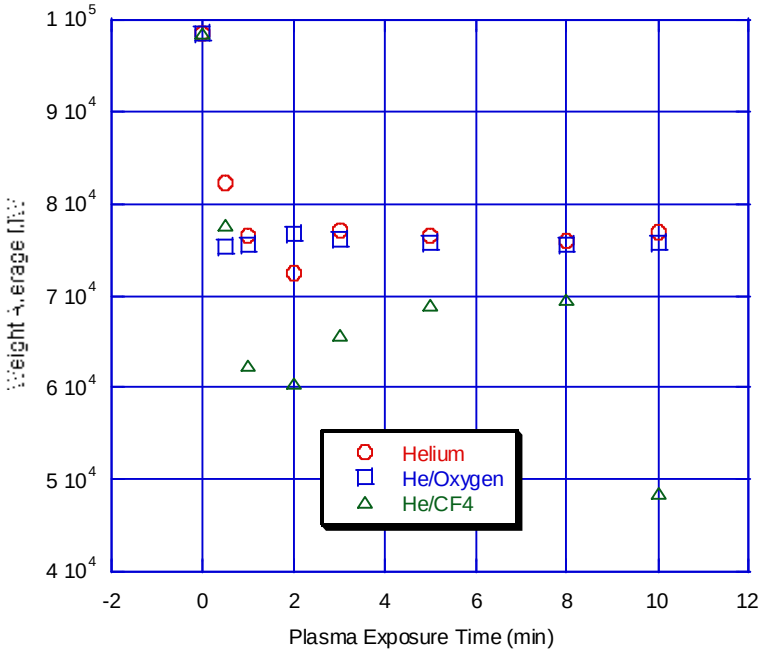

Figure 33 Weight average molecular weight of plasma exposed MS films

For all three trials, Mw decreased with increased exposure time for all gas types, with the most significant decrease resulting from the He/CF_4 treatment. Since Mw is sensitive to changes in high molecular weight species, a drop in these values would indicate that high molecular weight chains are being broken into smaller chains via chain-scission [92]. The clear drop in Mn values for the He/CF_4 samples further supports this conclusion. Although the helium and oxygenated-helium samples showed some increased Mn values, the overall trend still supports chain-scission versus cross-linking. This is confirmed by comparing their polydispersity index values, which are shown in Figure 34. The decrease in PDI values, showing a shift toward a more monodisperse material, correlates well with the Mw values and also supports chain-scission as the dominant mechanism.

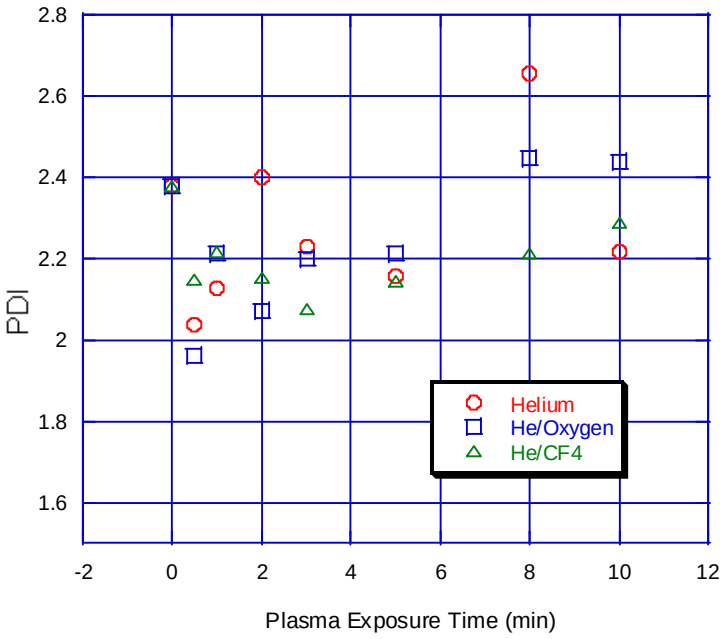

Figure 34 PDI values of plasma exposed MS films

When comparing the elution times shown in Figures 35 and 36, a notable shift is seen for the plasma-exposed films. By evaluating the early elution times, which correlate to high molecular weight species, one can see a shift to the right (i.e. higher elution times), indicating a decrease in the molecular weight chains that are eluting. The same trend is seen, although not as clearly, at the opposite end of the elution curve. Here the higher elution times also shift to the right indicating an increase in lower molecular weight species. These elution times are not as dramatic as the start times, but one can see that the majority of treated samples end at higher elution times than the control, once again indicating a higher content of lower molecular weight species.

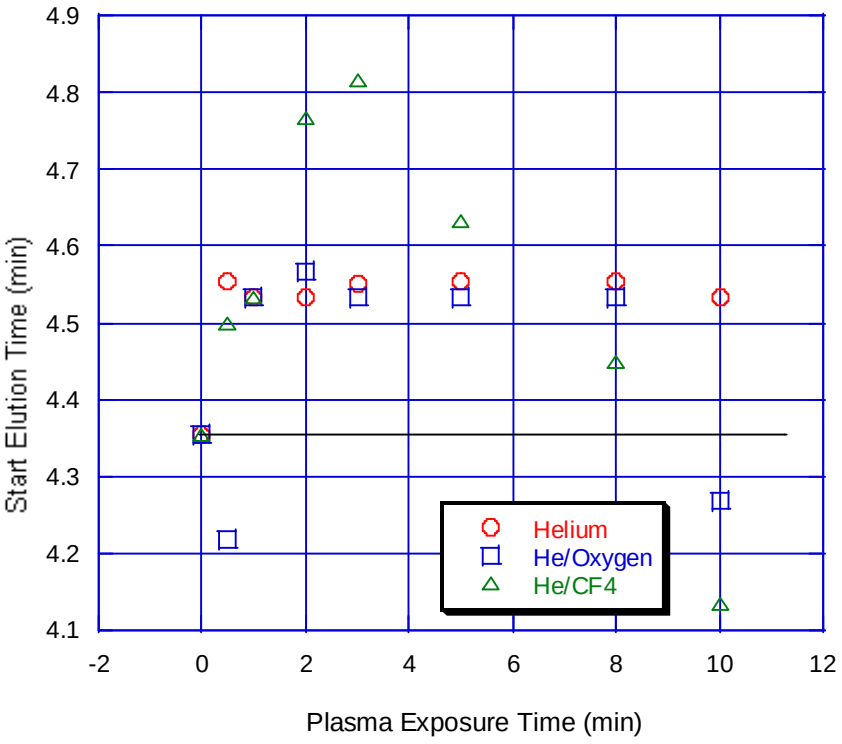

Figure 35 Comparison of start elution time for plasma treated MS films

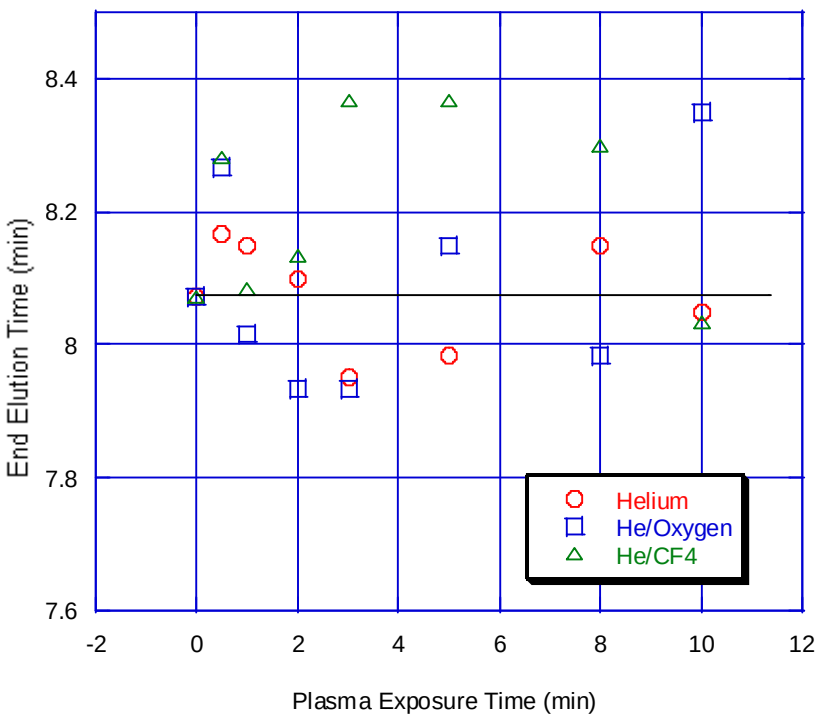

Figure 36 Comparison of end elution time for plasma treated MS films

Although this shift towards low molecular weight is encouraging for desizing, it is in contrast to other plasma treated films. This is due to the fact that there does not appear to be any notable cross-linking occurring. It has been noted in previous studies, however, that unlike other polymers, PVA does not undergo cross-linking from high-energy irradiation, unless treated in solution [93].

5.2.3 Solubility

Following the exposure time effects on weight loss and molecular weight, the relative solubility of the treated films was examined using a swelling agent as in Study 1. Films were weighed before and after soaking in methanol for 20 hours. Unlike the PET, however, these films lost weight and showed signs of solubilization. Their percent weight

change, i.e. weight loss, was then correlated to their relative solubility. These samples were then dried at ambient conditions for 24 hours and weighed again to determine their degree of swelling based on solvent retention, which could then be correlated more accurately with the results from Study 1.

The solubility of these films is a crucial factor for desizing, since the solubility of the PVA is directly related to its ease and degree of removal [91]. Based on the known chain-scission mechanism resulting from plasma exposure, and the well-documented surface functionalization capability of plasma treatment, the degree of solubility of the PVA films should be notably increased [55].

According to the MS results shown in Figures 37-38, there is a distinctive increase in the relative solubility for all treated samples, which is further influenced by the exposure time and gas species used. As exposure time is increased, or oxygen or CF_4 are incorporated into the helium seed gas, there begins to be an increase in the percent of dissolved material. Due to the extended time and increased sputtering activity of the mixed gases, more chain-scission occurs. The lower molecular weight chains then result in a higher degree of solubility. This is maximized by the addition of CF_4 in spite of possible surface fluorination. This can be explained by the reactivity and dissociation of CF_4.

Unlike higher fluorocarbons, such as C_3F_6 and C_2F_4, the CF_4 is more easily dissociated, and results in a relatively high density of free fluorine. This creates plasma with high reactive fluorine and higher sputtering ability, versus plasma with high fluorination ability [57]. This is illustrated below in the following dissociation reactions of CF_4 versus C_2F_4.

$$CF_4 + e^- \rightarrow CF_3 + F + e^-$$

$$CF_4 + e^- \rightarrow CF_2 + F + F^+ + 2e^-$$

$$CF_4 + e^- \rightarrow CF + F_2 + F^+ + 2e^-$$

$$C_2F_4 + e^- \rightarrow CF_2 + C + F_2 + e^-$$

$$C_2F_4 + e^- \rightarrow CF_3 + F + C + e^-$$

$$C_2F_4 + e^- \rightarrow CF_2 + CF + F + e^-$$

$$C_2F_4 + e^- \rightarrow CF_2 + CF + F^+ + 2e^-$$

As shown above, the CF_4 readily dissociates to form free fluorine, whereas the C_2F_4 dissociates to form lower molecular weight fluorocarbon species. The fluorocarbon species will chemically react to form a fluorinated polymer surface, whereas the free fluorine will physically react with the polymer to form a rougher surface through ablation and chain-scission with minimal fluorination.

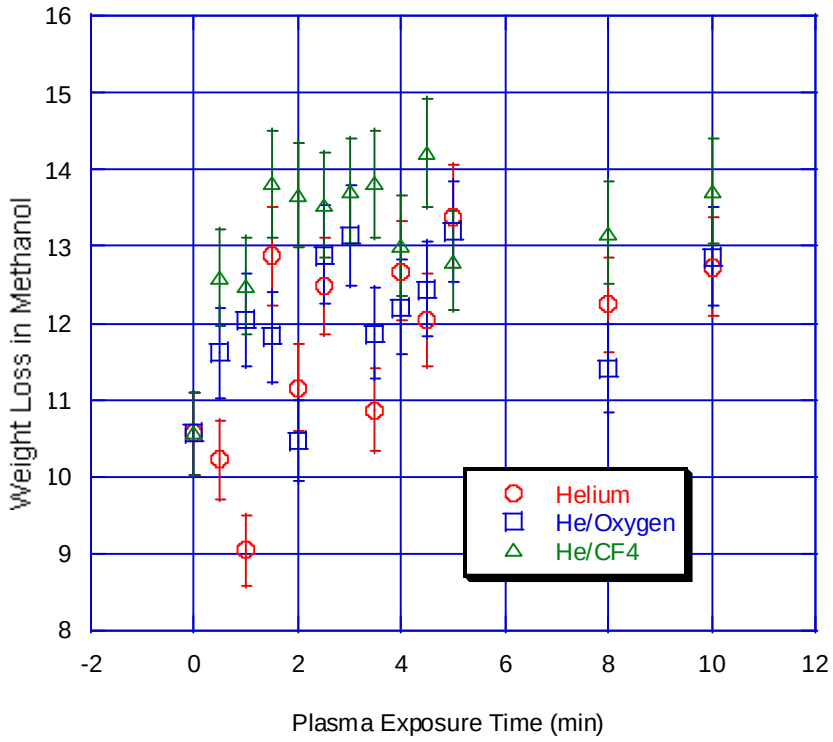

Figure 37 Relative solubility of MS films by weight loss in methanol-Set 1

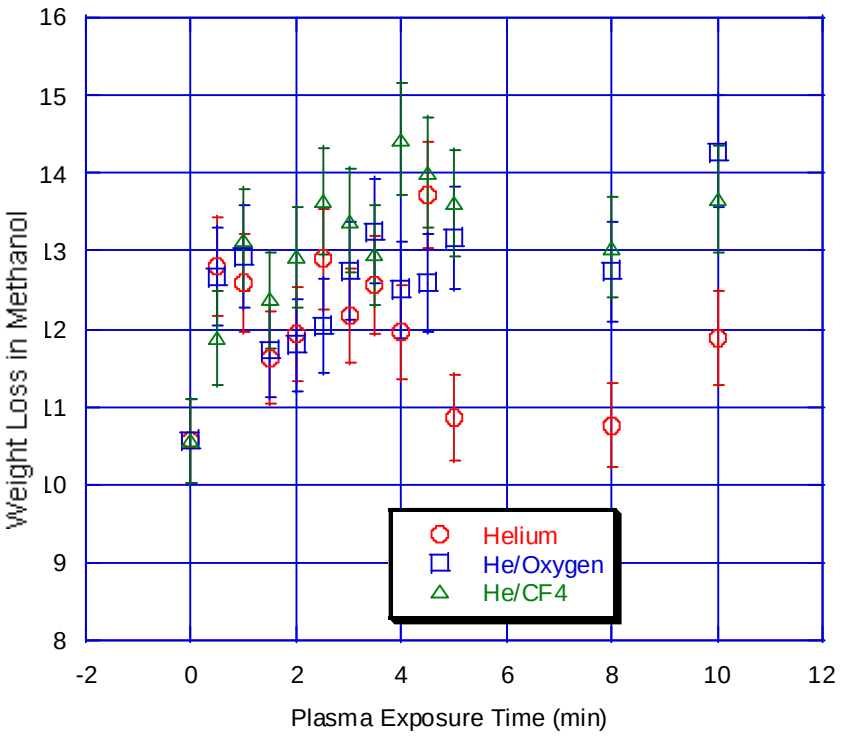

Figure 38 Relative solubility of MS films by weight loss in methanol -Set 2

These results are very encouraging for the desizing processes, but they are very dissimilar to those shown with PET. This goes directly to the composition of the PVA films and to the process of solubilization itself. To understand the effects of plasma on solubility, the act of polymer solvation and dissolution must be fully understood.

The first stage of polymer solvation is swelling of the bulk solid phase, which is a very slow process. In the second stage, the molecules in the swollen polymer phase begin to disentangle and enter into solution, i.e. dissolve. This process is rate controlled by the solvent diffusion rate and is greatly dependent on the degree of crystallinity [92]. In the case of PET, the second stage of solvation was never reached due to the innate hydrophobicity of the polymer itself, in conjunction with the increased percent crystallinity caused by plasma exposure. As for the PVA, the polymer is already highly hydrophilic, and will dissolve more readily than PET. To compare with the PET, the degree of swelling of the PVA was calculated. Results are illustrated in Figure 39.

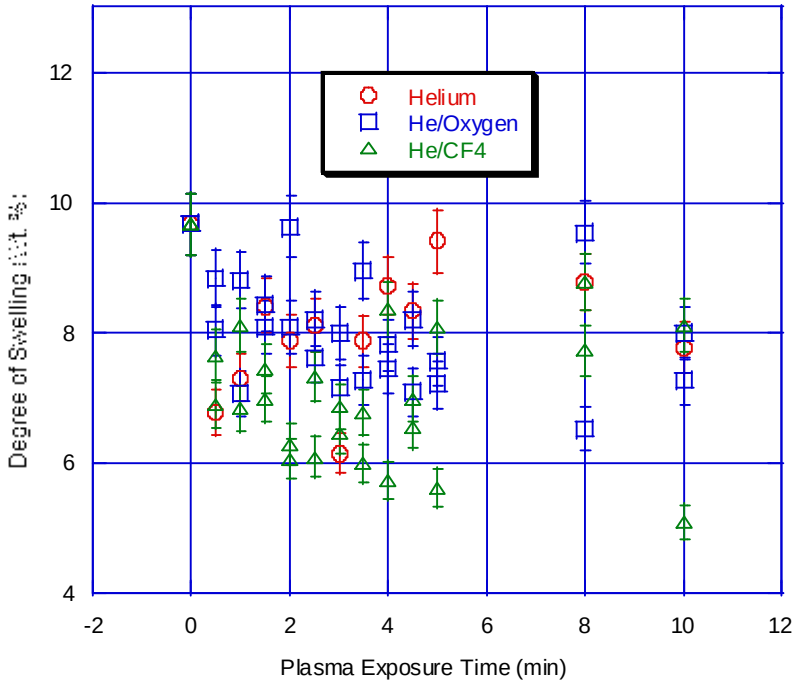

Figure 39 Degree of Swelling for MS PVA films

As observed with the plasma exposed PET samples, there is a decrease in degree of swelling with increased plasma exposure time. Although the PVA samples show an overall increase in solubility (i.e. dissolved material) in methanol, their ability to swell and retain solvent has decreased. This trend is the exact opposite of the relative solubility data. Specifically, the helium/CF_4 samples show the least amount of swelling, followed by the oxygenated-helium, and lastly the helium only samples. It is also noted that the helium/CF_4 and oxygenated-helium samples show a near linear decay. This trend is most likely the result of shorter chains with reduced molecular weights caused by the chain-scission mechanism of sputtering.

With the reduction in molecular weight of the surface chains, there is little swelling and a high degree of dissolution. Since the helium/CF_4 samples had the highest degree of sputtering, it would follow that they would have the highest degree of chain scission, and therefore the lowest degree of swelling. The helium-exposed samples would have a lower degree of chain-scission, which would give its samples the highest degree of swelling of the three exposures.

5.2.4 Differential Scanning Calorimetry

The average change in peak area and melt onset for each set of exposures either decreased or did not significantly change. Due to the low degree of crystallinity and the loosely oriented crystals for these PVA films, no distinct trend could be seen between the untreated and helium plasma exposed samples. There was however, a slight difference when comparing the ΔH values for the samples exposed to oxygenated-helium plasma. As for the helium/CF_4 exposed samples, there was a significant decrease in the percent crystallinity. This data is illustrated in Figure 40.

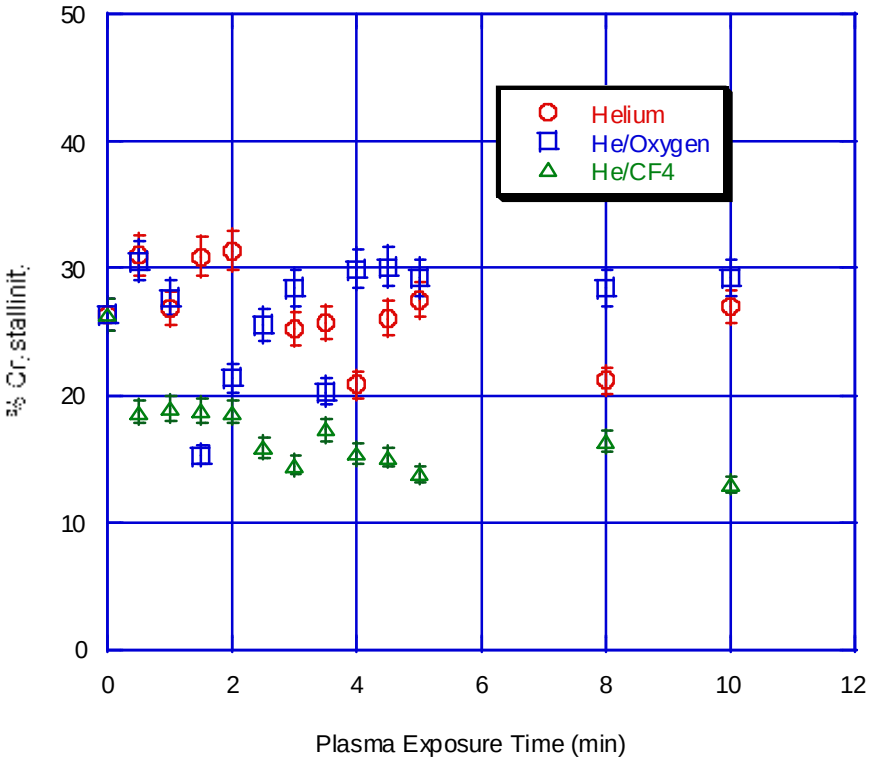

Figure 40 Percent crystallinity values for MS Films

For the MS films, the helium treated samples had higher ΔH values in comparison to those exposed to additional oxygen and CF_4. These lower values once again demonstrate the high reactivity of the oxygen and CF_4 versus the cross-linking nature of the chemically inert helium. With the decrease in ΔH for the oxygen and CF_4 samples, a direct link can be made to a decrease in percent crystallinity. Since the melt temperatures for all three sets stayed constant, it is evident that some crystalline regions have been ablated, thereby shifting the crystalline/amorphous ratio for the plasma exposed films.

Although some selectivity has occurred, it is not as distinctive as the PET. This is due to the higher amorphous content of the PVA films and the loosely bound structure of

the PVA crystals. By including oxygen and CF_4, more amorphous and eventually crystalline material is removed, thereby yielding lower ΔH values by up to 50% in comparison to the helium exposed samples. This decrease in crystalline content cannot only explain the increase in solubility, but the continual sputtering trends observed as well.

5.2.5 X-ray Diffraction

In order to gain a better understanding of the DSC results for both the PVA and the PET, x-ray diffraction of both films was performed. The resulting spectra for the untreated samples are shown below in Figure 41.

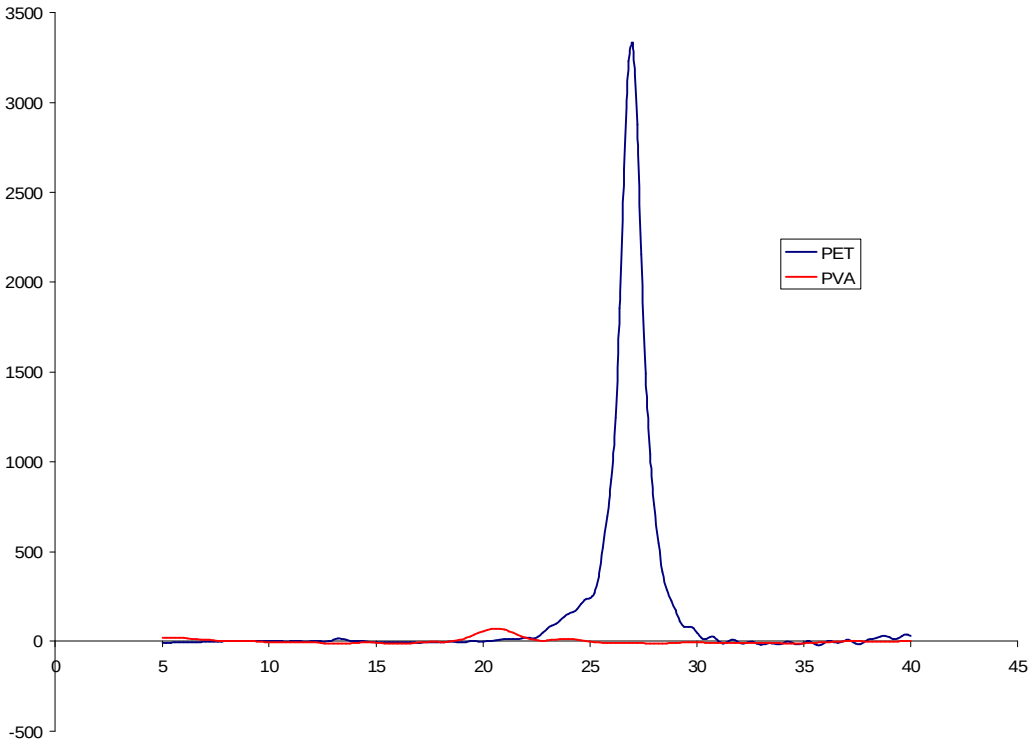

Figure 41: WAXD spectra of PET and MS PVA films

The first, and most notable difference in their spectra is their intensity. The PET film had maximum height reading of 3329; whereas the PVA had a maximum at 93. This much higher intensity reading indicates a well-defined crystal structure for the PET. In addition to the dramatic difference in peak intensity, the width at half height (FWHM) for the PVA film was twice the value recorded for the PET. Specifically, the PVA width was reported as 2.239, whereas the PET had a value of 1.211. This wider width and lower intensity for the PVA reveals smaller crystalline structures, which are poorly developed and randomly oriented [90, 94]. These x-ray results clearly show vastly different crystal structures for the two films. These differences support the DSC data showing selective etching of PET where the crystals remain intact, versus the non-selective sputtering of the PVA where some crystal regions are removed.

5.2.6 Investigation into a Generalized Solubility Model

Experimental results from the PET and PVA plasma exposed films were analyzed to develop a semi-empirical generalized model for solubility. The model encompasses *all* parameters affecting the solubility of the films, including both their physical properties and those imparted by exposure to plasma. When a film/material (A) is treated with plasma (B), the resulting film property would be A_B. For this particular process, A_B will represent the solubility of the treated film.

For the solubility of a polymeric material, the physical factors that must be taken into consideration include the hydrophilicity/hydrophobicity of the polymer, its degree of crystallinity, and its molecular weight. The hydrophilicity of the polymer will determine it's miscibility in a given solvent due to its effect on surface interfacial tension.

The degree of crystallinity will also play a role in the solvation process since swelling occurs in amorphous regions (i.e. the higher the degree of crystallinity, the lower the polymer solubility). Finally, the molecular weight will also play an important role since lower molecular weight chains will dissolve faster and more readily than those with higher molecular weights.

When imparting an external force to the polymer, new mechanisms must also be factored into the equation. For plasma treatment, this includes the chemical etching and physical sputtering parameters discussed in previous sections. This was first shown in Equation 3 from Study 1. Here, our resulting property A_B is the solubility, and is represented by S_r (previously D_S):

$$S_r \propto e^{-(dw)t} \tag{3}$$

By taking Equation 3 and incorporating sputtering from Equation 6 in Study 2, one can develop a combined model, as shown by Equation 7.

$$\begin{aligned} R_{sputter} &\propto \left(\frac{1}{e_t}\right)\left(\frac{m_i}{m_i + m_t}\right)\left(\frac{\Gamma_i}{n_f}\right)\left(\frac{A_t}{A_s}\right) \\ &= C\left(\frac{1}{1+(m_t/m_i)}\right) \end{aligned} \tag{6}$$

$$S_r \propto e^{-(dw)t} + R_{sp} \tag{7}$$

Equation 7 incorporates both etching and physical sputtering effects of the plasma-substrate interaction. This model demonstrates how the gas-substrate kinetics will determine the dominant mechanism. Although etching and sputtering can both occur through plasma exposure, the substrate composition will be the predicting factor for which mechanism dominates. However, partial effects of each mechanism may not be ruled out.

In the case of the PET films, the substrate is comprised of three distinctive regions, which will have corresponding etch rates (n) based on the regional composition. This nonuniformity and highly developed crystal structures within the films allows for etching to dominate as a mechanism. This means that R_{sp} will be negligible and S_r will be dependent on the rates of etching, as shown by Equation 3.

For the PVA films, there is a lower degree of crystallinity, and the crystals present in the film are small and not well defined. This creates a more homogeneous structure in which n is almost 1, causing the etching term to drop out of the equation. This allows for R_{sp} to become the dominant mechanism. For this type of film, S_r will then be dominated by the rate of sputtering for each gas type, as shown by Equation 9.

$$S_r \propto R_{sp(He/HeO/HeCF4)} \tag{9}$$

The next factor for consideration is the hydrophilicity/hydrophobicity property. This term is directly related to the miscibility of the polymer, and is a key predicting factor to how readily a polymer may solvate into solution. This factor will be denoted as K_{hydro}.

In the case of PET, a very hydrophobic film, there is very little dissolution, and the swelling process dominates solvation. The opposite occurs for PVA, since it is a very hydrophilic polymer and will readily dissolve into solution. For plasma-exposed films, the hydrophilicity/hydrophobicity of the substrate surface can be altered by the selection of the feed gas. In other words, oxygen can create –OH groups, which increase hydrophilicity, or fluorine gases can be used to impart hydrophobic fluorine-containing groups. As a result, this factor will always be weighted in significance for any substrate based on its initial hydrophilicity, the type of solvent used, and the exposure to plasma ionic species.

In the case of the very hydrophilic PVA, this parameter may be excluded from the equation since plasma exposure will not dramatically enhance its hydrophilicity. On the other hand, the very hydrophobic PET can be made more hydrophilic through plasma exposure, in which this parameter must be included in the solubility determination.

The second physical factor is the polymer's degree of crystallinity. This factor will be denoted as $(1/K_{cryst})$, and is highly affected by plasma exposure. Unlike K_{hydro} this term is inverted due to its inverse effect on the solubility. In other words, an increase in the degree of crystallinity will directly decrease the solubility of the specimen. Based on well-documented selective etching behavior of plasma causing this increase in percent crystallinity [89], there may be a significant alteration of a polymer's solubility as a result of plasma exposure. This was seen with the PET films in Study 1. It was not, however a significant influence on the PVA films due to differing crystalline content and structure. As with the preceding terms, this parameter may also be excluded depending on the composition of the substrate being tested. If the specimen is almost or entirely

amorphous or crystalline, then this term would not be a participating factor in the solubility equation. Since both the PET and PVA are semi-crystalline, this term will be factored in for both.

The final term to be considered, and one of the most important, is the molecular weight of the substrate. This factor is greatly affected by plasma treatment. During plasma exposure, both chain-scission and cross-linking can occur. The dominating mechanism will depend on the feed gas composition, the exposure time, and the substrate composition. If cross-linking dominates, then swelling will increase, but dissolution will decrease due to the increase in molecular weight. If chain-scission dominates, then dissolution will increase and swelling will decrease. Due to this duality, the following portion of the formula is denoted as:

$$\alpha(1/K_{mw}) \tag{10}$$

where:

$$a = \frac{a_{x-link}}{a_{scission}} \tag{11}$$

and:

$$a_{scisson} = \frac{(MW)_{scission}}{(MW)_0} \tag{12}$$

$$a_{x-link} = \frac{(MW)_{x-link}}{(MW)_{scission}} \tag{13}$$

therefore making:

$$\frac{a_{x-link}}{a_{scission}} = \frac{(MW)_0 (MW)_{x-link}}{(MW)^2_{scission}} \tag{14}$$

Like the crystallinity term, this factor is inversely related to solubility and is therefore denoted by $1/K_{mw}$, showing that a decrease in molecular weight will cause an increase in the solubility. As for α, this term can be calculated from GPC analysis by denoting the start elution time for a sample as $\alpha_{x\text{-}link}$ since it corresponds to the high molecular weight species, and the end elution time as $\alpha_{scission}$ since it corresponds to the low molecular weight species. By taking the ratio of these elution times, shifts to higher or lower molecular weights can be calculated and the cross-linking and chain-scission effects incorporated into the solubility equation.

In contrast to the hydrophilicity and crystallinity terms, this factor is almost entirely dependent on the plasma exposure, and has little dependence on the initial molecular weight of the substrate. This was illustrated by the molecular weight averages obtained for the PVA films. Although GPC was only performed on the PVA samples, it is assumed that the PET also experienced chain-scission based on its weight loss data. It should also be noted that this factor can also be limited by the initial degree of crystallinity.

By combining all the factors that influence the degree of solubility for plasma-exposed films, the generalized model can now be expressed as:

$$S_r \propto e^{-(dw)t} + R_{sp} + K_{hydro} + (1/K_{cryst}) + a(1/K_{mw}) \tag{15}$$

This proposed formula now incorporates all possible mechanisms in plasma-substrate interaction.

Upon completion of this equation, the contact angle, DSC, and molecular weight data acquired for the PET and MS PVA films was entered into the model and evaluated. Figure 42 shows the predicted solubility values for PET calculated from the model, in comparison to the actual values in Figure 43 obtained through testing.

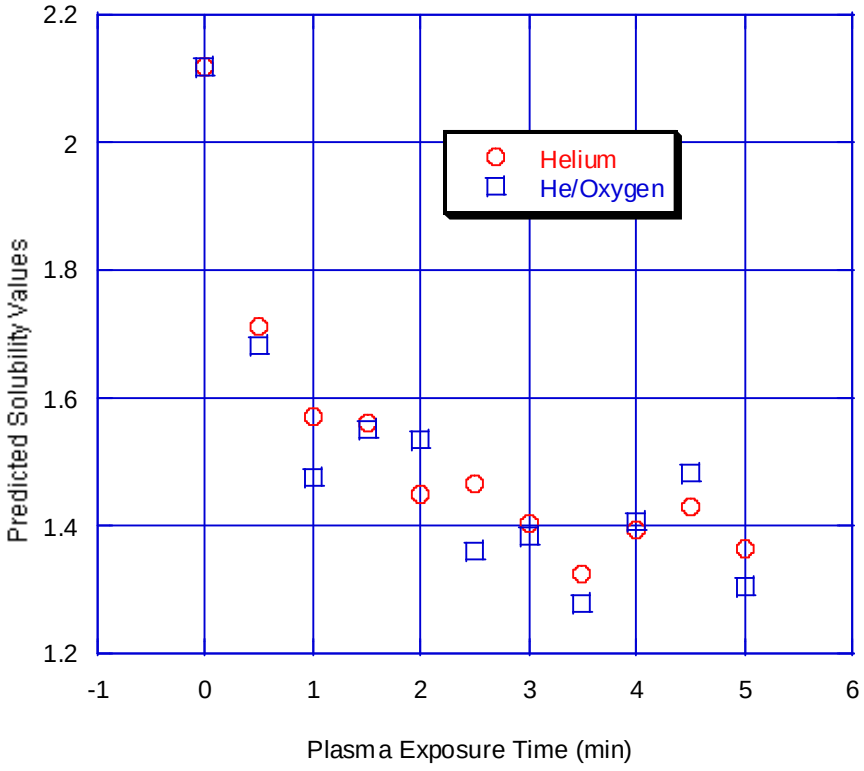

Figure 42 Predicted solubility of plasma exposed PET S/200 films

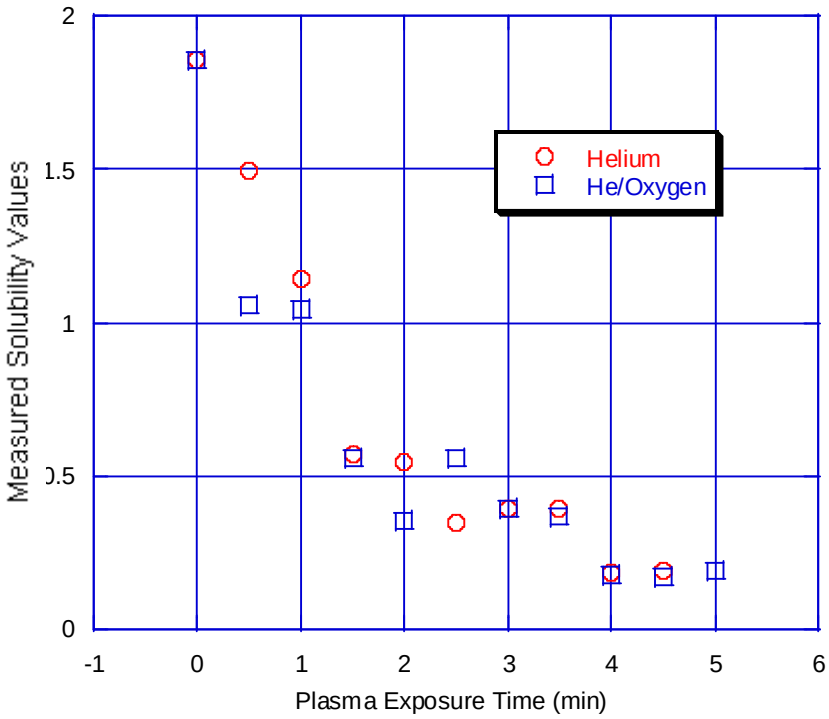

Figure 43 Actual solubility values of plasma exposed PET S/200 films

According to the calculated values, the predicted trend is nearly identical to the actual trend. This shows good agreement between the model and the actual data, where the effect of plasma treatment on the solubility of the PET films is clearly predicted by the model. Although the trends are identical, there is some difference between the actual and calculated values. The model predicted values that were higher than those actually measured. Future work to decouple the gas and substrate effects, and incorporate them into the gas-substrate constant, may reveal closer values to those measured.

To further test the accuracy of the model, the MS film values were calculated. Figures 44-46 show the predicted values for each gas type compared to their actual measured values. Predicted and actual values were on a different scale due to the fact that the proportionality constant is not determined, thus, the predicted values were

multiplied by 3.5 to obtain the same zero-time value to compare the predicted to the experimental trends.

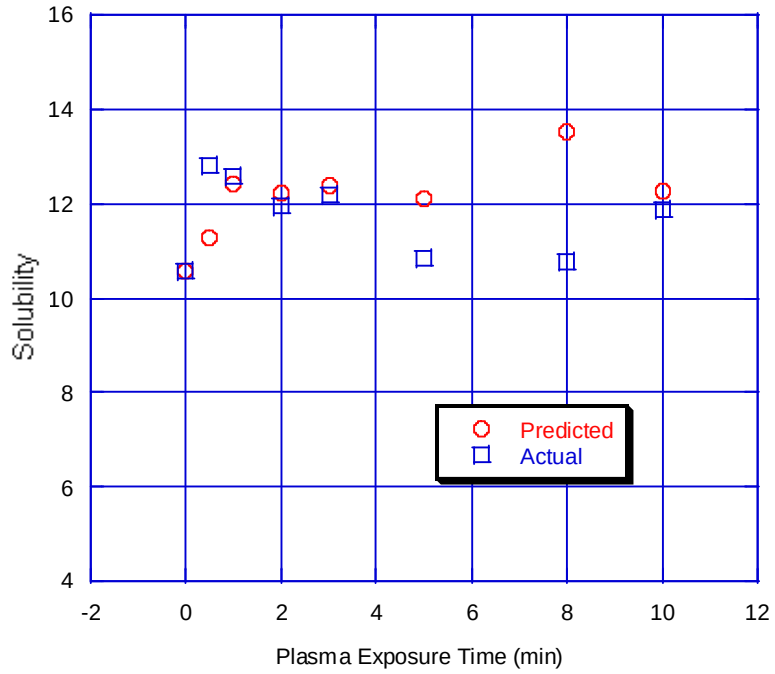

Figure 44 Actual versus predicted solubility values for helium treated MS films

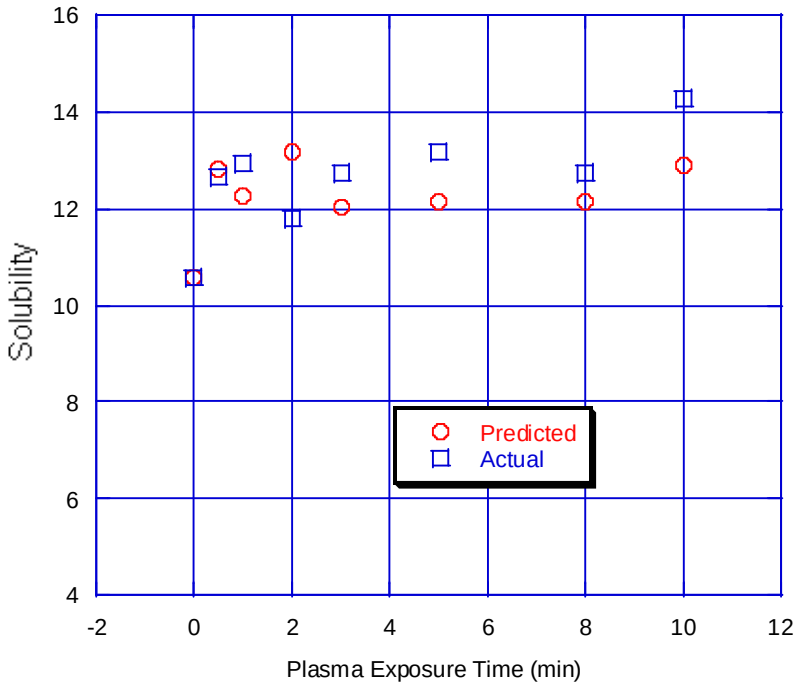

Figure 45 Actual versus predicted solubility values for He/O_2 treated MS films

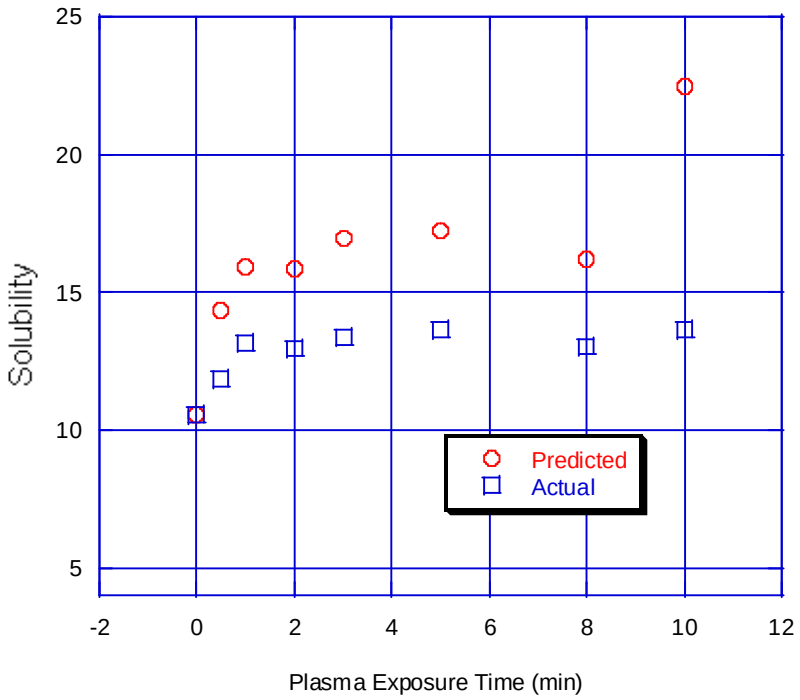

Figure 46 Actual versus predicted solubility values for He/CF_4 treated MS films

The model predicted nearly identical trends to those observed with the measured values. All gas treatments showed a good agreement with the model and further supports its credibility as a solubility prediction tool for a given substrate, solvent, and plasma treatment.

5.3 Study 3: Plasma Aided Graft Copolymerization of PP Nonwoven Fabrics

In conjunction with the PET and PVA studies presented in this work, additional research was conducted on polypropylene nonwoven fabrics to determine plasma induced chemical changes. X-ray Photoelectron Spectroscopy (XPS) from a previous polypropylene study was used to quantify these changes. In this study, the C_{1s} deconvolution for the oxygenated-helium samples revealed a decrease in C-C bonds

caused by chain-scission, and an increase in C-OH,/C=O/CH=O bonds due to functionalization [46].

Based on this knowledge, Study 3 was conducted in order to analyze the effect of plasma initiation for graft copolymerization of bioactive monomers onto fabrics. Due to these plasma generated free radicals and –OH/-OOH sites on polymeric surfaces, graft copolymerization can occur when the plasma treated surface is exposed to a reacting medium [68,4].

5.3.1 Weight Changes and Graft Yield

Fabric weights were measured before plasma treatment and after exposure to GMA to determine the percent graft yield. Based on the plasma exposure time, the GMA solution dwell time, and the concentration of the GMA solution, the graft yield varied from 3.9% to 38%. Figures 47 and 48 illustrate the graft yield dependence on plasma exposure time, and on GMA concentration.

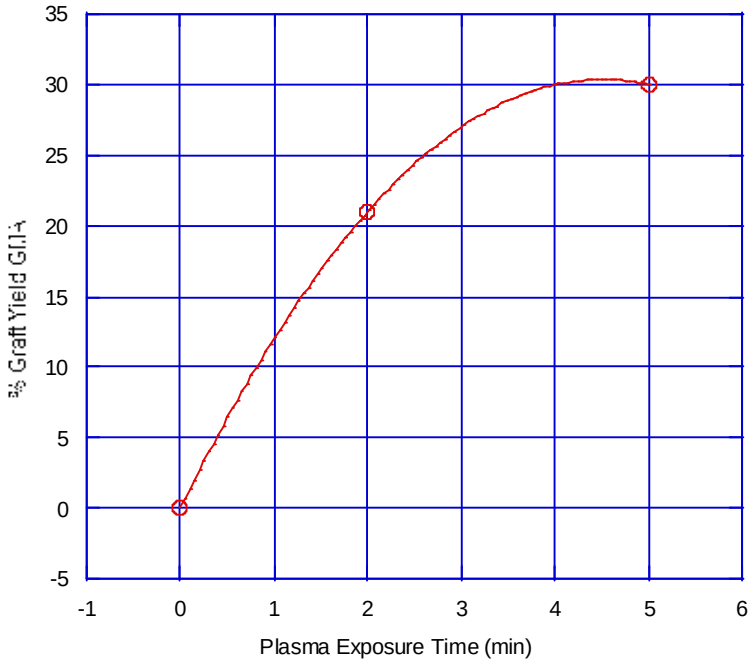

Figure 47 Dependence on plasma exposure time for graft yield of GMA on PP nonwoven

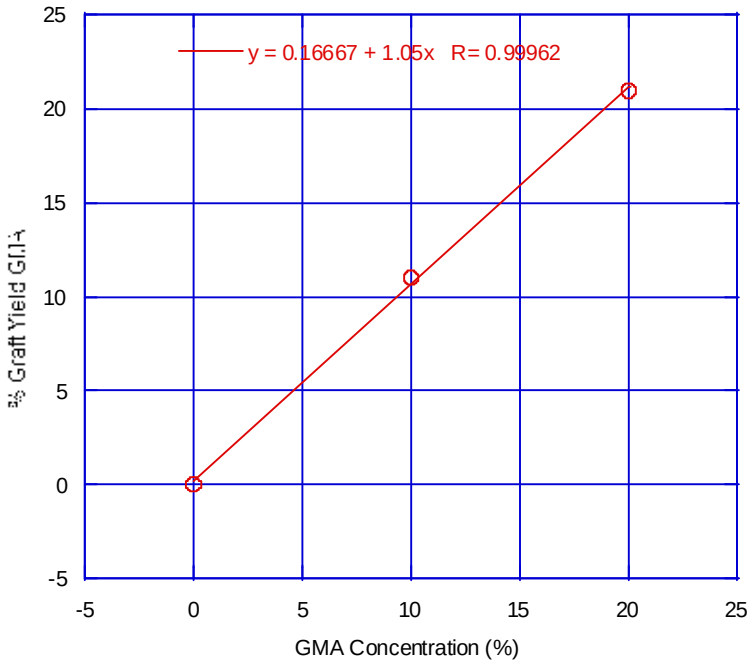

Figure 48 Dependence on GMA solution concentration for graft yield of GMA on PP nonwoven

As seen in Figures 47 and 48, increasing the GMA concentration and the exposure time increases the percent GMA graft yield. This information not only confirms the graft generating ability of the plasma, but also aids in process optimization. Those samples with the highest graft yield were selected for further grafting reactions with β-cyclodextrin and quaternary ammonium chitosan for antimicrobial and insecticidal functionality.

5.3.2 Differential Scanning Calorimetry

Thermal analysis was performed to further confirm the grafting of the PP fabrics. This included differential scanning calorimetry (DSC) and thermal gravimetric analysis (TGA). The DSC profiles of untreated and grafted PP fabrics are shown in Table 4.

Table 4 DSC results for grafted PP nonwoven samples

Sample	He/O_2 Plasma exposure time (min)	Melting Temperature °C	ΔH_f joule/gm	Crystallinity* %
PP control	2	158.84	90.131	60.5
Sample 24 PP/8.7% GMA	2	158.85	83.97	56.4
Sample 12 PP/18.08% GMA	2	159.32	80.67	54.14
Sample 19 PP/20.6% GMA/ 1%CD	2	159.36	75.930	50.96
Sample 18 PP/38% GMA/7.2% CD	2	159.27	68.413	45.9
Sample 10 PP/29.7% GMA/2.6% quaternary chitosan	5	159.80	73.248	49.16
Sample 31 PP/5% MA acid	2	158.86	88.139	59.2

$$\%\ ^{*}\text{crystanility} = \frac{\triangle H_f \times 100}{\triangle H_{cryst}} \qquad \triangle H_{cryst} = 149 \text{ joule/gm}$$

The control PP fabric is characterized by a broad and large endothermic transition starting beyond 155°C, with a peak temperature of 158.84°C. The grafted samples show a slight increase in melting point, and a decrease in both the melt endotherm and the crystallization exotherm. Specifically, the 8.7% GMA grafted fabric has a crystallinity of 56.4% (based on $\Delta H_{endotherm}$), and the 18.08% GMA grafted fabric has a crystallinity of 54.14%. Both are at least 4% lower than the 60.5% crystallinity calculated for the control fabric. Figure 48 further illustrates the effect of crystallinity on graft yield. It is clear from the graph that ΔH varies linearly with percent of grafted GMA, specifically an increase in the percentage of grafted GMA decreases ΔH.

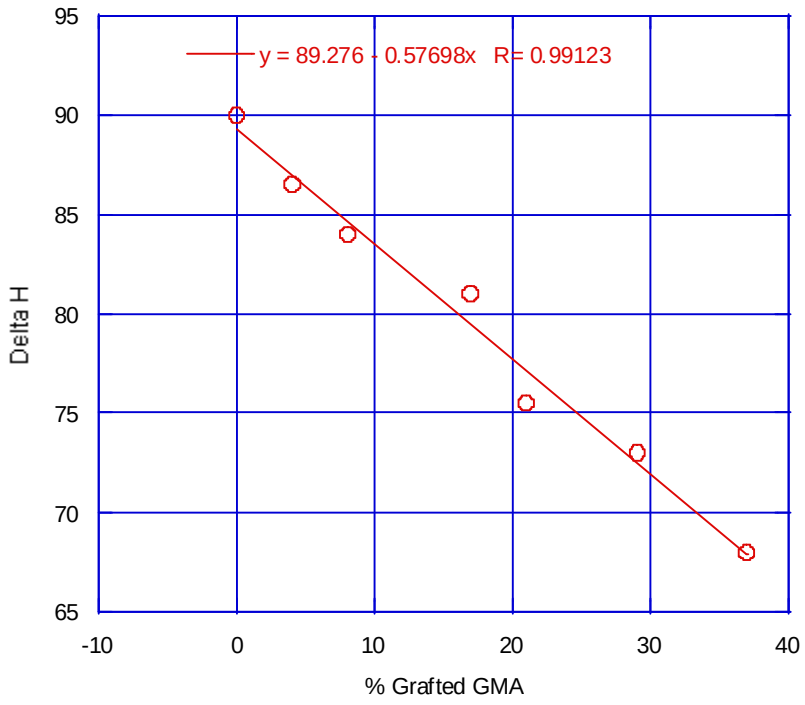

Figure 49 ΔH versus % grafted GMA on nonwoven PP fabrics

In addition to the crystallinity decrease for the PP/GMA fabrics, the multi-grafted fabrics containing either cyclodextrin or chitosan dropped even further. The crystallinity for the PP/GMA/CD sample decreased to 50.96%, and the PP/GMA/chitosan sample dropped to 49.16%. All values are consistent with the percent graft yield.

5.3.3 Thermal Gravimetric Analysis

The increased thermal stability of PP graft fibers is confirmed by thermogravimetric analysis (TGA). The decomposition temperatures of the PP control and grafted fabrics are shown in Table 5, and the weight % curves are illustrated in Figure 50.

Table 5 TGA results for grafted PP nonwoven Fabrics

PP Control		Sample 12 PP/18.1% GMA		Sample 18 PP/38%GMA/7.2%CD		Sample 10 PP/29.7% GMA/ 2.6% quat chitosan	
Temp. (ºC)	Residual wt. (%)	Temp. (ºC)	Residual wt. (%)	Temp. (ºC)	Residual wt. (%)	Temp. (ºC)	Residual wt. (%)
300.9	97.83	300.94	98.09	300.85	97.98	300.42	98.85
324.97	94.83	325.01	96.67	325.08	97.92	325.06	94.62
350.09	88.12	350.11	93.42	350.06	88.86	350.02	96.43
400.02	47.55	401.16	72.08	401.47	55.44	400.74	98.93
425.04	6.87	425.05	43.41	424.83	25.03	425.03	81.38
450	-0.38	449.43	8.01	450.15	5.30	448.19	61.83
499.10	-0.69	500.99	0.51	500.4	3.43	500.78	3.58

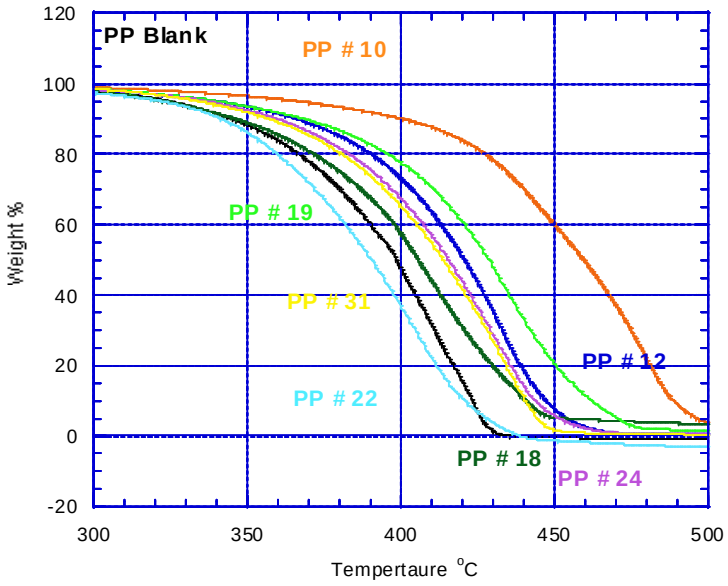

Figure 50 Percent residual weight curves for grafted PP nonwoven fabrics

From the above data, it is apparent that plasma graft copolymerization of the fabric greatly increases the decomposition temperature. Thus, by grafting GMA onto PP, the decomposition temperature is shifted from 433 to 467°C. Further grafting of chitosan reveals an even higher decomposition temperature of 500°C, which correlates well with the additional grafted material.

In contrast to the PP/GMA/chitosan samples, the PP/GMA/CD fabrics show a lowering effect on the decomposition temperature to near 450°C (compared to PP/GMA at 467°C). This temperature correlates to the decomposition temperature of saccharides, and confirms grafting of the β-cyclodextrin compounds. By comparing the residual weights at approximately 400°C, the effect of grafting can also be noted. At this temperature, there is 47.55% remaining from the control, 98% for sample 10 containing

chitosan, 72.08% for sample 12 with GMA only, and 55.44% for sample 18 containing cyclodextrin.

5.3.4 Fourier Transform Infrared Spectroscopy (FTIR)

The infrared spectra of the plasma grafted PP fabrics were obtained and are compared below in Figures 51 and 52. Additional spectra can be found in Appendix 2. The spectrum for PP/10.5% GMA (Sample 13) shows additional absorbance bands as compared to the PP control. These bands can be attributed to the ester carbonyl group of GMA found at 1729.81 cm^{-1}, and the epoxide group of GMA found at 1255.81 cm^{-1}, with a shoulder and increase of the absorbance bands at 900 and 841 cm^{-1}. The stretching and increased peak intensity at 1151.5 cm^{-1} further confirms grafting with the formation of the –C-O-C- ether linkage of the grafted GMA.

In contrast, the grafting of the quaternary chitosan in Sample 10 shows characteristic bands of the quaternary chitosan itself, but with lower absorbance, at 1641 and 1480 cm^{-1} for the methyl group, and 1030 cm^{-1}. The lower absorbance is due to its lower concentration. FTIR spectra were also useful in confirming the grafting of the cyclodextrin onto the PP/GMA fabric. This is illustrated by a significant decrease in the epoxide peak of Sample 18, and the appearance of intense absorbance bands at 1080 and 1030 cm^{-1}, which are characteristic absorbance bands of the cyclodextrin itself. There was also an additional absorbance band at 3348.7cm^{-1}, indicating the –OH group of the β-cyclodextrin.

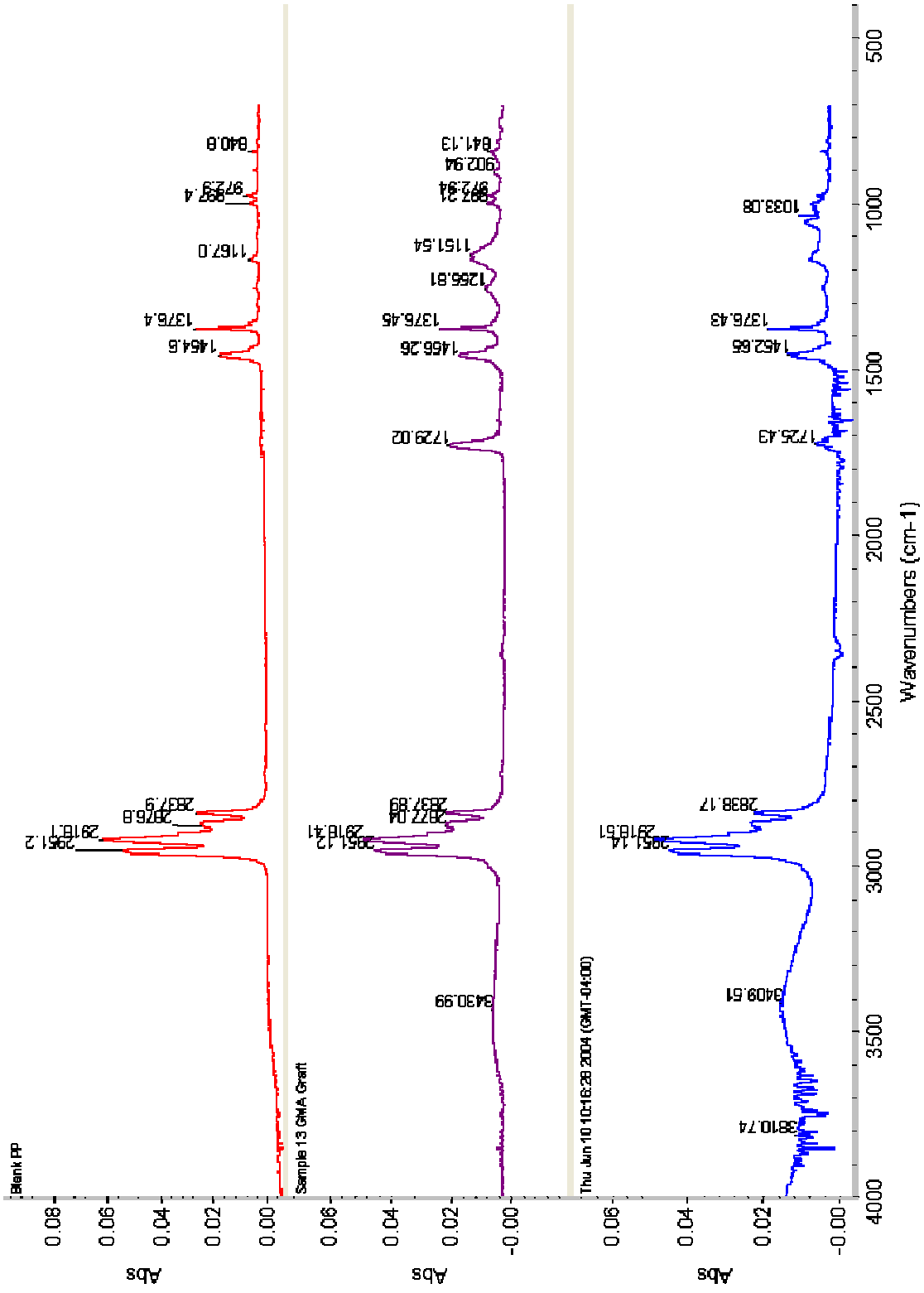

Figure 51 Infrared Spectra of untreated PP nonwoven (top), PP/10.5% GMA (middle), and PP/29.7% GMA/2.6% quaternary chitosan (bottom)

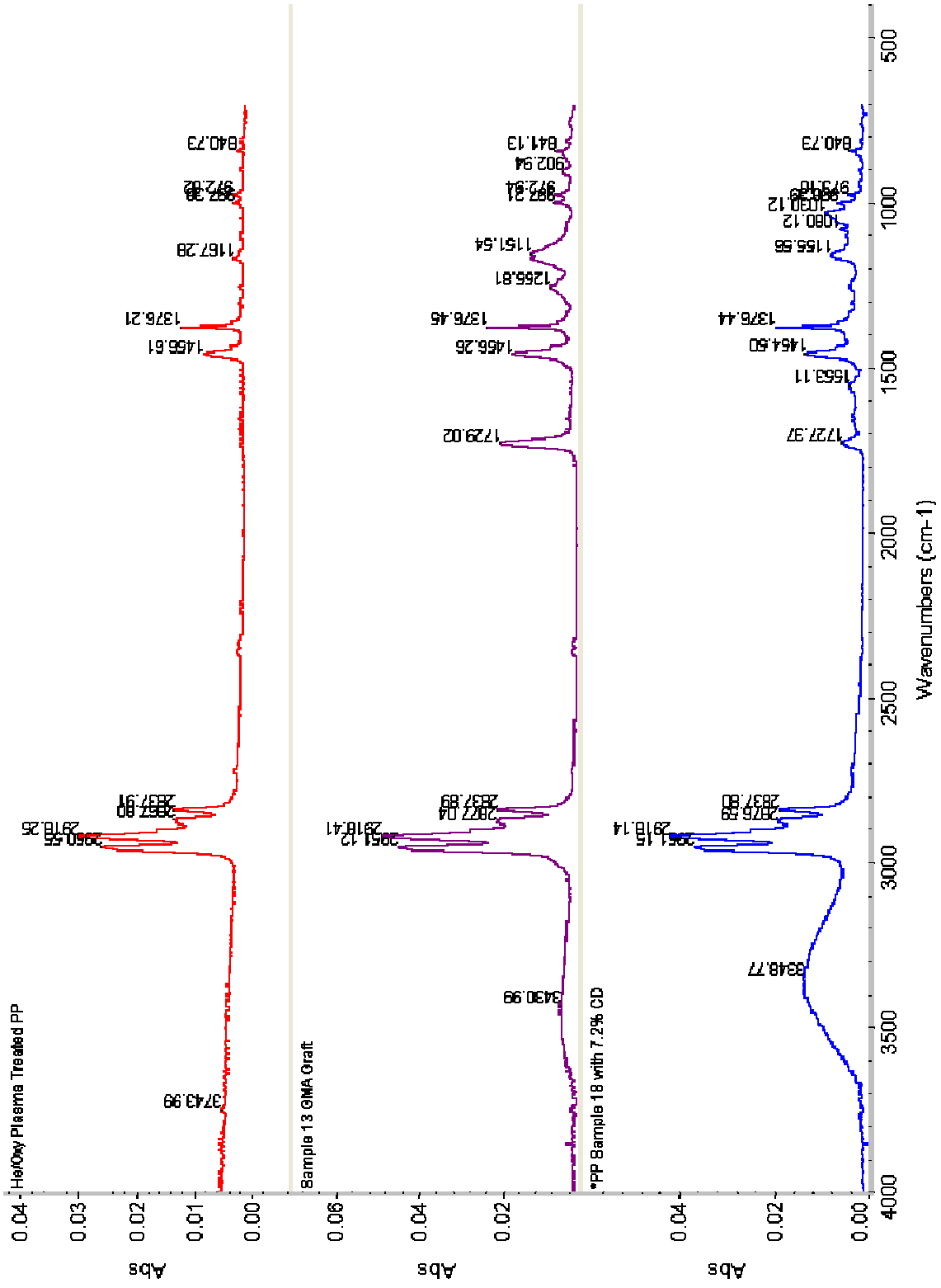

Figure 52 Infrared Spectra of PP nonwoven with 2 min. plasma exposure (top), PP/10.5% GMA (middle), and PP/38% GMA/7.2% β-CD (bottom)

5.3.5 Scanning Electron Microscopy

SEM was conducted to view the extent of grafting on the PP fabrics. Figure 53 shows the SEM micrograph of sample 12, which contains 18.08% grafted GMA. Figure 54 shows sample 10 with 29.7% GMA/ 2.6% quaternary ammonium chitosan, and Figure 55 shows sample 18 with 38% GMA/7.2% β-cyclodextrin.

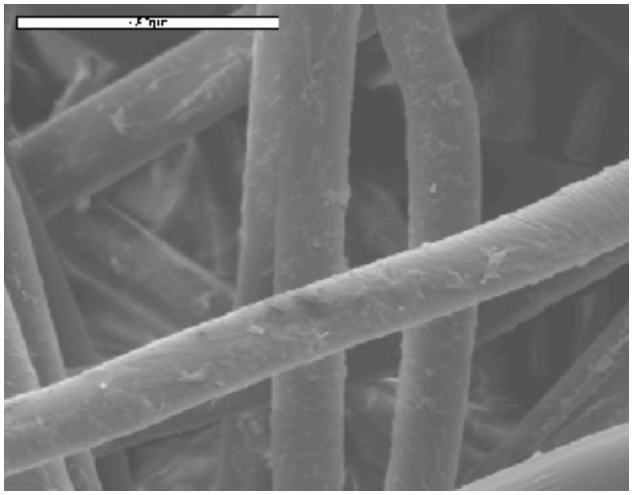

Figure 53 SEM micrograph of PP/GMA Sample 12

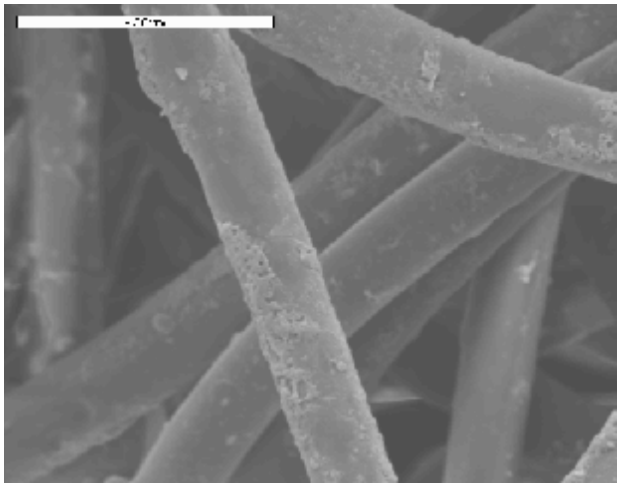

Figure 54 SEM micrograph of PP/GMA/Chitosan Sample 10

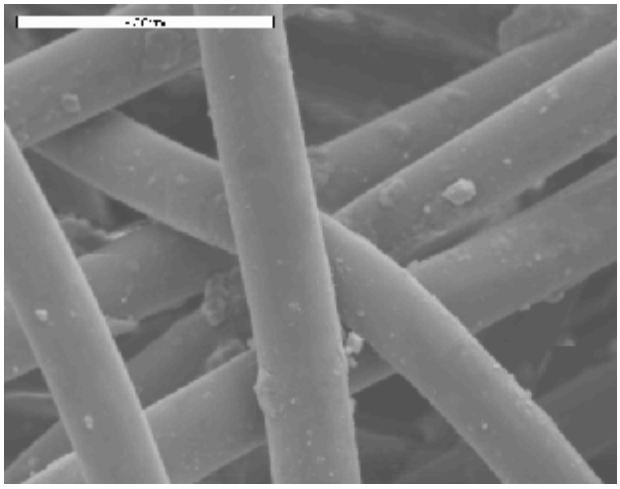

Figure 55 SEM micrograph of PP/GMA/β-CD Sample 18

The particulate matter covering the PP nonwoven fibers in the resulting micrographs confirm grafting of GMA and additional chitosan and cyclodextrin compounds. EDXA analysis of these same samples has shown the additional content of nitrogen on Sample 10, clearly from the quaternary chitosan.

5.3.6 Antimicrobial Assay

Following the plasma grafting study, additional testing was performed to determine the antimicrobial and insecticidal capabilities of the grafted fabrics. Figure 56 shows 2-hour antimicrobial testing on the grafted PP fabrics using Lactobacillus Planterum bacteria [95]. The test indicates that the highest effect is from sample #10, with 2.6% quaternary ammonium chitosan and sample # 19, with 1% cyclodextrin. The log reduction of 1.00 means 90% kill of the bacteria. Other samples included in the study are the control (FC), samples #12, 21 and 23, all of which contain no antimicrobial agent, and sample # 18 which has high concentration of β–cyclodextrin. It is clear that chitosan

has the highest effect followed by low-percentage β–cyclodextrin. Nearly identical results were obtained using various other bacterium, including both gram positive and gram negative species. All antimicrobial testing confirms the viability of this process for antimicrobial finishing. USDA ARS Food Science at N.C. State USDA facilities has completed a comprehensive antimicrobial study. This assay, however, along with the insect repellent testing is outside the scope of this dissertation.

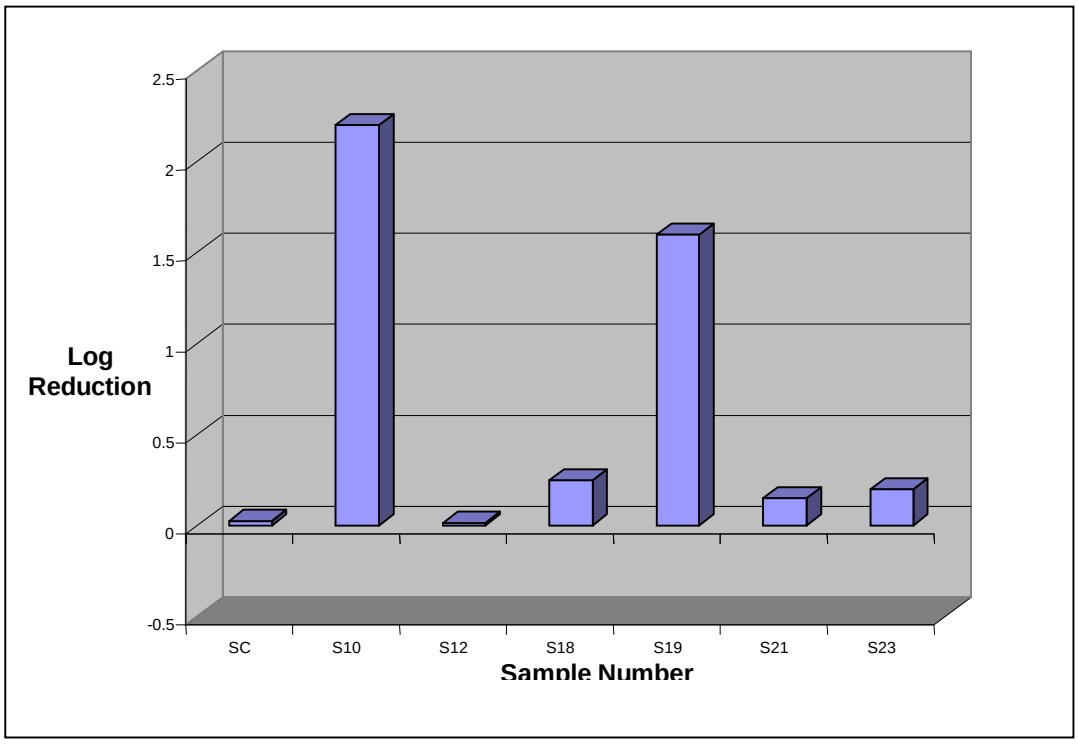

Figure 56 Antimicrobial testing of grafted PP fabrics using Lacto Lactobacillus Planterum bacteria

V. CONCLUSIONS

In Study 1, the effects of gas type and exposure time were established for PET films. Weight change observations revealed a steady weight loss with increasing

exposure time due to continuous etching effects. As a result of closed chamber geometry, etching continued until saturation, then shifts to re-deposition of previously etched film material. The weight loss results demonstrate viability of competing etching and re-deposition mechanisms. The effect of the plasma gas type also showed a marked difference in the weight loss. With the addition of 1% oxygen to the helium feed gas, more material was etched from the films.

Percent crystallinity, shown by DSC, increased as a result of selective amorphous etching. A model was developed, which relates degree of solubility to the total rate of etching and number of phases on the surface. The model correlated well with the experimental results, showing that the degree of solubility will decrease following an exponential decay law, which is directly affected by the substrate and plasma composition.

Following the results of Study 1, the methodology was then applied to finishing applications, starting with desizing of PVA in Study 2. Weight loss curves showed a similar trend as observed with the PET, but with a continual surface ablation, suggesting a dominance of physical sputtering versus etching. The effect of the plasma gas type also followed the previously noted trend for PET. With the inclusion of a stronger etchant species, the percent weight loss was increased.

Solubility tests correlated well with the weight loss data. As oxygen or CF_4 were incorporated into the feed gas, there was a notable increase in the solubility of the PVA due to chain-scission. GPC confirmed chain-scission through a decrease in average molecular weight with increasing exposure time and the addition of oxygen or CF_4. An investigation into developing a generalized solubility model was conducted based on the

PVA and PET data. This model incorporated a set of interaction mechanisms at the plasma-substrate interface. Calculated values from this model showed good agreement with measured values for both PET and PVA.

The second finishing application studied in this work is antimicrobial finishing using plasma-aided grafting. Nonwoven PP fabrics were plasma treated and graft copolymerized with antimicrobial and insecticidal agents. Weight change data have shown successful grafting of GMA onto the nonwoven fabrics. Thermal analysis and FTIR correlated well with the grafting of GMA, chitosan, and cyclodextrin compounds. Further testing on the samples revealed viable antimicrobial finishing.

In conclusion, through the basic understanding of plasma-substrate interactions it is possible to create new processing methods and finishing applications. This was clearly demonstrated through the plasma aided desizing of PVA in Study 2, and in the plasma graft copolymerization of PP nonwovens in Study 3.

VI. FUTURE WORK

Through the above studies, a great deal of insight was gained into understanding the plasma-substrate interaction of polymeric materials. The initial steps for incorporating this knowledge into viable finishing processes have also been achieved. Additional testing is necessary, however, for process optimization. Future testing may include a series of plasma treatments on various organic polymer films to further our understanding of the physics and chemistry involved in plasma modification. This knowledge will allow for more processing possibilities.

VIII. REFERENCES

1. Tyrone L. Vigo, *Textile Processing and Properties: Dyeing, Finishing, and Performance,* Elsevier, Amsterdam (1994).

2. Tomiji Wakida and Seiji Tokino, "Surface modification of fiber and polymeric materials by discharge treatment and its application to textile processing," *Indian Journal of Fibre and Textile Research*, **21**, 69 (1996).

3. Fabio Garbassi, Marco Morra, and Ernesto Occhiello, *Polymer Surfaces: From Physics to Technology,* John Wiley and Sons Ltd., Chichester, UK (1998).

4. Joseph Jagur-Grodzinski, *Heterogenous Modification of Polymers: Matrix and Surface Reactions,* John Wiley and Sons Ltd., Chichester, UK (1997).

5. Charles Tomasino, *Chemistry and Technology of Fabric Preparation and Finishing,* Dept. of Textile Eng., Chem., and Sci., North Carolina State Univ. (1992).

6. Peter Carty and M.S. Byrne, *The Chemical and Mechanical Finishing of Textile Materials,* Newcastle upon Tyne Polytechnic Products Ltd., (1987).

7. J.T. Marsh, *Self-Smoothing Fabrics,* Chapman and Hall Ltd., London (1962).

8. Howard L. Needles, *Textile Fibers, Dyes, Finishes, and Processes: A Concise Guide*, Noyes Publications, New Jersey, 1986.

9. John W. Lyons, *The Chemistry and Uses of Fire Retardants,* Wiley Interscience, New York (1970).

10. Manachen Lewin and Eli M. Pearce, Ed., *Handbook of Fiber Chemistry,* Marcel Dekker, New York, 1998.

11. A.R. Horrocks, "Flame Retardant Finishing of Textiles," *Rev. Prog. Coloration* **16**, 62 (1986).

12. Robert. W. Little, *Flame-Proofing Textile Fabrics,* Reinhold Publishing Corp., New York (1947).

13. Prasad Modak, *The Textile Industry and the Environment,* UNEP, France (1993).

14. T. H. Ferrigno, "Fundamental principles of formulating coatings for fabrics," *J. Coated Fabrics,* **17**, 265 (1988).

15. M. Grayson, Ed., *Kirk-Othmer Encyclopedia of Chemical Technology*, Vol. 6, 3rd Ed., Wiley-Interscience, New York, 1979.

16. G. Nelson, "Microencapsulation in textile coloration and finishing," *Rev. Prog. Color. Rel. Topics*, **21**(1), 72 (1991).

17. Chi-Ming Chan, *Polymer Surface Modification and Characterization*, Hanser/Gardner Publications, Inc., New York (1994).

18. Yves De Pyudt, Patrick Betrand, Yvan Novis, Roland Cuadano, Gusty Feyder, and Pierre Lutgen, "Surface analyses of corona-treated PET," *British Polym. J.*, **21**, 141 (1989).

19. James F. Carly and P. Thomas Kitze, "Corona-discharge treatment of polymeric films, II: Chemical Studies," *Polym. Eng. and Sci.*, **20**(5),330 (1980).

20. K. Pochner, W. Neff, and R. Lebert, "Atmospheric pressure gas discharges for surface treatment," *Surface and Coatings Technology*, **74-75**, 394 (1995).

21. P.A.F. Herbert and E. Bourdin, *J. Coated Fabrics*, **28**, 170 (1999).

22. W.J. Feast and H.S. Munro, Ed., "New generation atmospheric pressure plasma technology for industrial on-line processing," *Polymer Surfaces and Interfaces*, John Wiley and Sons Ltd., Chichester, UK (1987).

23. Walter H. Waddell, Larry R. Evans, James G. Gilick, and Derek Shuttleworth, "Polymer Surface Modification," *Rubber Chem. and Technol.*, **65**, 687 (1992).

24. Elsa Reichmanis, Curtis W. Frank, and James H. O'Donnell, *Irradiation of Polymeric Materials: Processes, Mechanisms, and Applications*, American Chem. Soc., Washington D.C. (1993).

25. P.F.A. Buijsen, *Electron Beam Induced Cationic Polymerization with Omium Salts*, Delft University Press, The Netherlands, 1996.

26. V. Stannett, W.K. Walsh, E. Bittencourt, R. Liepins, and J.R. Surles, "Chemical modification of fibers and fabrics with high-energy radiation," *J. App. Polym. Sci.: App. Polym. Symp.*, **31**, 201 (1977).

27. Roger L. Clough and Shalaby W. Shalaby, Eds., *Irradiation of Polymers: Fundamentals and Technological Applications*, American Chemical Society, Washington, D.C., 1996.

28. Sung-Chul Park, Seok-kuen Koh, and Kook D. Pae, "Effects of surface modification by Ar^+ irradiation on wettability of surfaces of PET films," *Polym. Eng. and Sci.*, **38**(7), 1185 (1998).

29. T. Venkatesan, W.L. Brown, C.A. Murray, K.J. Marcantonio, and B.J. Wilkens, "Dynamics of ion beam modification of polymer films,"*Polym. Eng. and Sci.*, **23**(17), 931 (1983).

30. Stephen M. Rossnagel, Jerome J. Cuomo, and William D. Westwood, Ed., *Handbook of Plasma Processing Technology,* Noyes Publishing, New York (1990).

31. Michael A Lieberman, and Allan J. Lichtenber, *Principles of Plasma Discharges and Materials Processing,* John Wiley & Sons, Inc., New York (1994).

32. J. Reece Roth, *Industrial Plasma Engineering, Vol. 1 Principles,* IOP Pub. Ltd., Bristol (1995).

33. Brian N. Chapman, *Glow Discharge Processes: Sputtering and Plasma Etching,* John Wiley and Sons, Inc., New York (1980).

34. Yuri P. Raizer, Mikhail N. Shneider, and Nikolai A. Yatsenko, *Radio-Frequency Capacitive Discharges*, CRC Press Inc., Boca Raton, 1995.

35. J. T. Gudmundsson and M. A. Lieberman, "Magnetic induction and plasma impedance in a cylindrical inductive discharge," *Plasma Sources Sci. Technol.*, **6**, 540 (1997).

36. Valery Godyak, "Plasma phenomena in inductive discharges," *Plasma Phys. Control. Fusion,* **45**, A399 (2003).

37. George J. Collins, Colorado State University, EE 576, Course notes (2004).

38. R.J. Shul and S. J. Pearton, Eds., *Handbook of Advanced Plasma Processing Techniques,* Springer-Verlag Berlin Hidelberg, Germany, 2000.

39. Tomiji Wakida, Seiji Tokino, Shouhua Niu, and Haruo Kawamura, "Surface characteristics of wool and PET fabrics and film treated with low-temperature plasma under atmospheric pressure," *Textile Res. J.*, **63**(8), 433 (1993).

40. J. Ryu, T. Wakida, and T. Takagishi, "Effect of corona discharge on the surface of wool and its application to printing," *Textile Res. J.*, **61**(10), 595 (1991).

41. N. Carneiro, A.P. Souto, E. Silva, A. Marimba, B. Tena, H. Ferreira, and V. Magalhaes, "Dyeability of corona-treated farics," *Color. Technol.*, **117**, 298 (2001).

42. S. Kanazawa, M. Kogoma, T. Moriwaki, and S. Okazaki, "Stable glow plasma at atmospheric pressure," *J. Phys.D: Appl. Phys.*, **21**(5), 838 (1988).

43. S. Kanazawa, M. Kogoma, T. Moriwaki, and S. Okazaki, "The mechanism of the stabilization of glow plasma at atmospheric pressure," *J. Phys.D: Appl. Phys.*, **23**(8), 1125 (1990).

44. G. Placinta, F. Arefi-Khonsari, M. Gheorghui, J. Amouroux, and G. Popa, "Surface properties and the stability of PET films treated in plasmas of helium-oxygen mixtures," *J. App. Polym. Sci.*, **66**, 1367 (1997).

45. H. Ngo, S. Vojita, J.Rohner, O. Hankins, and M. Bourham, 25th IEEE-ICOPS, Paper 3B03, IEEE Cat.#98CH36221, 178 (1998).

46. M.G. McCord, Y.J. Hwang, P.J. Hauser, Y. Qiu, J.J. Cuomo, O.E. Hankins, M.A. Bourham, and L. K. Canup, "Modification of nylon an polypropylene fabrics with atmospheric pressure plasmas," *Textile Res. J.*, **72**(6), 491 (2002).

47. X.J. Dai and L. Kviz, *CSIRO Textile and Fiber Technology*, Textile Institute 81st World Conference, Melbourne, Australia, April 2001.

48. M.J. Shenton and G.C. Stevens, "Surface modification of polymer surfaces: atmospheric plasma versus vacuum plasma treatments," *J. Phys.D: Appl. Phys.*, **34**, 2761 (2001).

49. Jaeyoung Park, I. Henins, H.W. Herrmann, G.S. Selwyn, and R.F. Hicks, "Discharge phenomena of an atmospheric pressure radio-frequency capacitive plasma source," *J. App. Phys.*, **89**(1), 20 (2001).

50. M.J. Shenton, G.C. Stevens, N. P. Wright, and X. Duan,"Chemical-surface modification of polymers using atmospheric pressure nonequilibrium plasmas and comparisons with vacuum plasmas," *J. Polym. Sci.: Part A: Chemistry*, **40**, 95 (2001).

51. Witold Rakowski, M. Okoneiwski, K. Bartos, and J. Zawadzki, "Plasma treatment of textiles-potential applications and future prospects," *Melliand Textilberichte [English Edition]*, 301 (April 1982).

52. Dennis M. Manos and Daniel L. Flamm, Ed., *Plasma Etching: An Introduction*, Academic Press, Inc., San Diego, 1989.

53. Yoo Won Jong, National University of Singapore, EE3401 "Silicone Processing Technology," Course notes (2004).

54. Chunxiang Zhu, National University of Singapore, EE5516 "Plasma Processes and Interconnects," Course notes (2004).

55. A. M. Wrobel, M. Kryszewski, W. Rakowski, M. Okoneiwski, and Z. Kubaki, "Effect of plasma treatment on surface structure and properties of polyester fabric," *Polymer*, **19**, 908 (1978).

56. K. L. Mittal, Ed., *Polymer Surface Modification: Relevance to Adhesion*, VSP BV, The Netherlands, 1996.

57. R. d'Agostino, F. Cramarossa, and S. De Benedicts, *Plasma Chem. And Plasma Proc.*, **2**(3), 213 (1982).

58. Daniel L. Flamm, "Frequency effects in plasma etching," *J. Vac. Sci. Technol.*, **A4**(3), May/June, 729 (1986).

59. Yoon Hwang, Suzanne Matthews, Marian McCord, and Mohamed Bourham, "Study of organic polymer film treated by helium generated atmospheric pressure plasma," *J. Electrochem. Soc.*, **151**(7), C495-C501 (2004).

60. B. Gupta, J. Hilborn, CH. Hollenstein, C.J.G. Plummer, R. Houriet, and N. Xanthopoulos, "Surface modification of polyester films by RF plasma," *J. App. Polym. Sci.*, **78**, 1083 (2000).

61. Ben D. Beake, John S.G. Ling, and Graham J. Leggett, "Scanning force microscopy investigation of PET modified by argon plasma treatment," *J. Mater. Chem.*, **8**(8),1735 (1998).

62. M.R. Padhye, N.V. Bhat, and P.K. Mittal, "Electron microscopical study of plasma-etched polymers," *Textile Res. J.*, **46**, 502 (1976).

63. T. Okuno, T. Yasuda, and H. Yasuda, "Effect of crystallinity of PET and nylon 66 fibers on plasma etching and dyeability characteristics," *Textile Res. J*, **62**(8), 474 (1992).

64. M.B. Olde Riekerink, J.G.A. Terlingen, G.H.M. Engbers, and J. Feijen, "Selective etching of semicrystalline polymers: CF_4 gas plasma treatment of poly(ethylene)," *Langmuir*, **15**(14), 4847 (1999).

65. N. Inagaki, *Plasma Surface Modification and Plasma Polymerization*, Technomic Pub. Co., Inc., Lancaster, Pennsylvania (1996).

66. Masayuki Kuzuya, Akihiro Noguchi, Masanao Ishikawa, Atsuo Koide, Kazuhiko Sawada, Akiko Ito, and Nahoko Noda, "Electron spin resonance study of free-radical formation and its decay of plasma-irradiated poly(methacrylic acid) and its esters," *J. Phys. Chem.*, **95**, 2398 (1991).

67. Jie Rong Chen, "Free-radicals of fibers treated with low temperature plasma," *J. App. Polym. Sci.*, **42**, 2035 (1991).

68. C.I. Simionescu and F. Denes, "The use of plasma-chemistry in the field of synthesis and modification of the natural macromolecular compounds," *Cellulose Chem. Technol.*, **14**, 285 (1980).

69. Christofor I. Simionescu, Ferencz Denes, Mihaela M. Macoveanu, and Ioan Negulescu, "Surface modification and grafting of natural and synthetic fibers and fabrics under cold plasma conditions," *Makromol. Chem. Suppl.*, **8**, 17 (1984).

70. Zubaidi and Toshihiro Hirotsu, "Graft polymerization of hydrophilic monomers onto textile fibers treated by glow discharge plasmas," *J. App. Polym. Sci.*, **61**, 1579 (1996).

71. Liashun Shi, "Investigation of Surface Modification and Reaction Kinetics of PET in RF CF_4-CH_4," *J. Polym. Eng.*, **19**(6), 445 (1999).

72. S. Meiners, J.G.H. Salge, E. Prinz, and F. Forster, "Surface modification of polymeric material by transient gas discharges at atmospheric pressure," *Surface and Coatings Technol.*, **98**, 1121 (1998).

73. D. Briggs, D.G. Rance, C.R. Kendall, and A.R. Blythe, Surface modification of PET by electrical discharge treatment," *Polymer*, **21**, 895 (1980).

74. Tomiji Wakida, Haruo Kawamura, Jin Cherl Song, Tokuju Goto, and Toru Takagishi, "Surface free energy of PET and nylon 6 films treated with low temperature plasma," *Sen-I Gakkaishi*, **43**(7), 384 (1986).

75. H. Yasuda, Ashok K. Sharma, and Takeshi Yasuda, "Effect of orientation and mobility of polymer molecules on contact angle," *J. Polym. Sci.: Polym. Phys. Ed.*, **19**, 1285 (1981).

76. Ziasheng Cai, Yiping Qiu, and Chuyang Zhang, "Effect of atmospheric plasma treatment on desizing of PVA on cotton," *Textile Res. J.*, 73(8), 670 (2003).

77. Ziasheng Cai, Yoon Joon Hwang, Yoon-cheol Park, Chuyang Zhang, Marian McCord, and Yiping Qiu, "Preliminary investigation of atmospheric pressure plasma-aided desizing for cotton fabrics," *AATCC Review*, **2**(12), 18 (2002).

78. S.S. Block, Encyclopedia of Microbiology, **4**(87), Academic Press (1992).

79. T. Chau, K. Kao, G. Blank, and F. Madrid, "Microwave plasmas for low-temperature dry sterilization," *Biomaterials*, **17**(13), 1273 (1996).

80. Michel Moisan, Jean Barbeau, Marie-Charlotte Crevier, Jacques Pelletier, Nicolas Philip, and Bachir Saoudi, "Plasma sterilization. Methods and mechanisms," *Pure App. Chem.*, **74**(3), 349 (2002).

81. "Plasmas put the hurt on microbes," *Science News*, **153**(23), 364 (1998).

82. T. Ramachandran, K. Rajendrakumar, and R. Rajendran, *IE (1) Journal*, **84**, 42 (2004).

83. *Food Tech.*, **53**(4), 54 (1999).

84. Y. Wang, E.B. Somers, S. Manolache, F.S. Denes, and A.C.L. Wong, *FRI Newsletter*, **15**(4), 2 (2003).

85. Allan P. Gray, "Polymer crystallinity determinations by DSC," *Thermochemica*, **1**, 563 (1970).

86. Kenneth C. Cole, Abdellah Ajji, and Eric Pellerin, "New insights into the development of ordered structure in PET.1.Results from external reflection infrared spectroscopy," *Macromolecules*, **35**(3), 770 (2002).

87. D.C. Prevorsek, "Structure of semi-crystalline fibers from interpretation of anelastic effects," *J. Poly. Sci.*, **C32**, 343 (1971).

88. D.C. Prevorsek, G.A. Tirpak, P.J. Harget, and A.C. Reimschuessel, "Effects of thermal contraction on structure and properties of PET fibers," *J. Macromol. Sci.-Phys.*, **B9**, 733 (1974).

89. Suzanne Matthews, Yoon Hwang, Marian McCord, Mohamed Bourham, "Investigation into the etching mechanism of PET films treated in helium and oxygenated-helium atmospheric plasma," *J. Appl. Polym. Sci.*, **94**(**6**), 2383 (2004).

90. J.G. Pritchard, *Poly(vinyl) Alcohol; Basic Properties and Uses*, Gordon and Breach, London, 1970.

91. Betty Lucy Lopez O., Amanda Ines Mejia G., and Ligia Sierra G., "Biodegradability of Poly(Vinyl Alcohol)," *Polym. Eng. and Sci.*, **39**(8), 1346 (1999).

92. W. Yau, J. Kirkland, and D. Bly, *Modern size-exclusion liquid chromatography: practice of gel permeation and gel filtration chromatography*, Wiley Interscience, New York, 1979.

93. J. Pacansky and S. Schnieder, "Electron beam chemistry in solid films of Poly(vinyl alcohol); Exposures under vacuum and N_2 at atmospheric pressure; Irradiation monitored by using Infrared Spectroscopy," *J. Phys. Chem.*, **94**, 3166(1990).

94. Leroy E. Alexander, *X-Ray Diffraction Methods in Polymer Science,* John Wiley and Sons, Inc., New York, 1969.

95. D.M. Wafa and F. Breidt USDA ARS Food Science, North Carolina State University, 2004.

APPENDICES

Appendix A

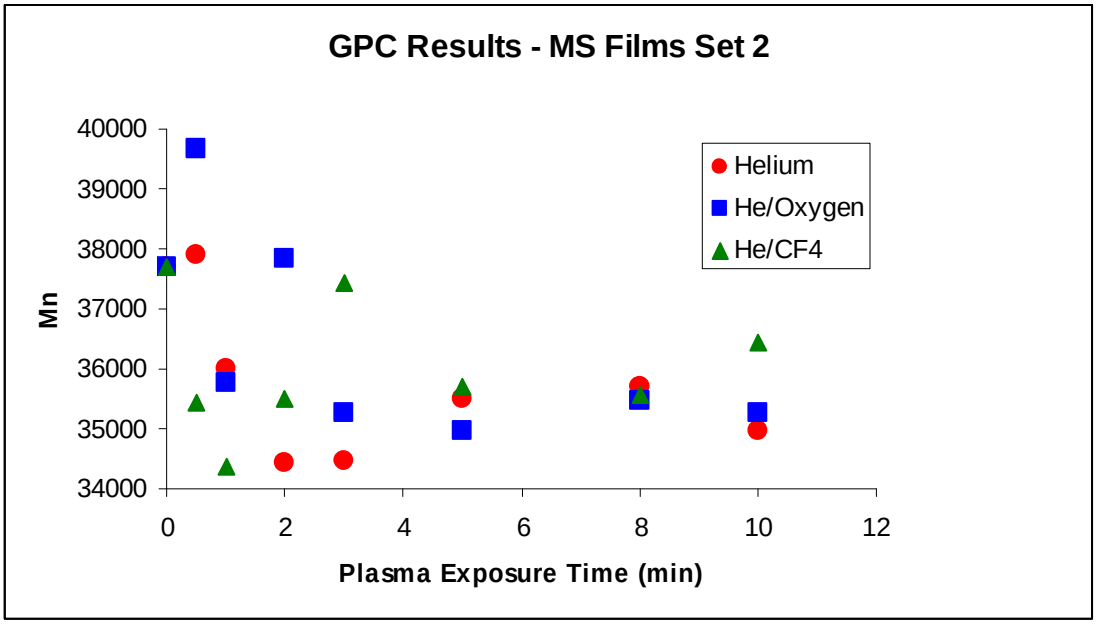
GPC Results - MS Films Set 2
Mn
40000
39000
38000
37000
36000
35000
34000
0
2
4
6
8
10
12
Plasma Exposure Time (min)
Helium
He/Oxygen
He/CF4

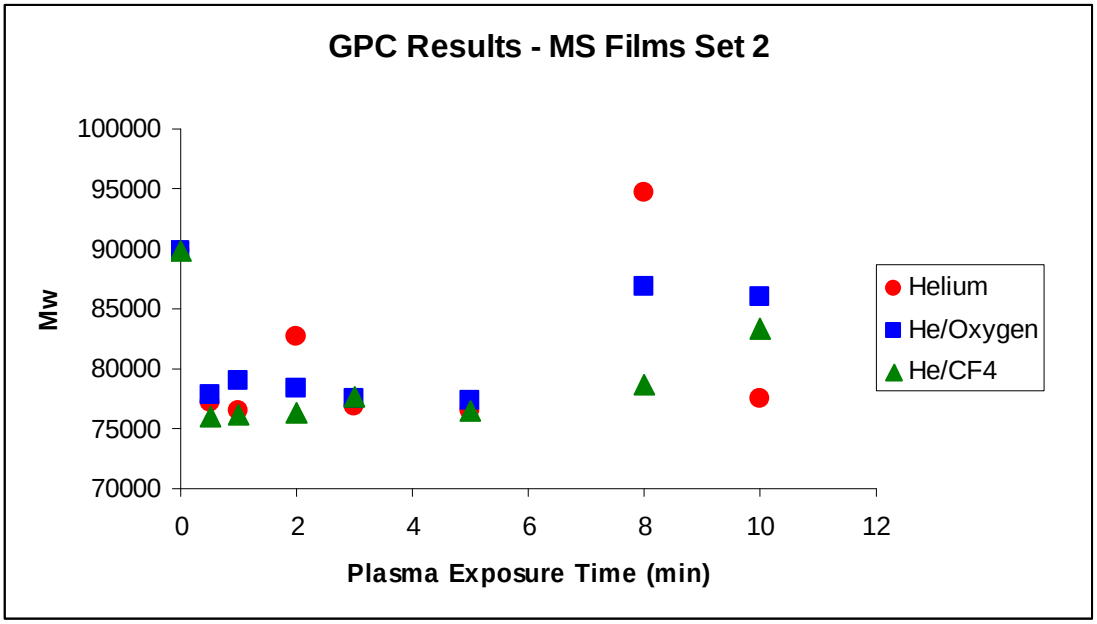
GPC Results - MS Films Set 2
Mw
100000
95000
90000
85000
80000
75000
70000
0
2
4
6
8
10
12
Plasma Exposure Time (min)
Helium
He/Oxygen
He/CF4

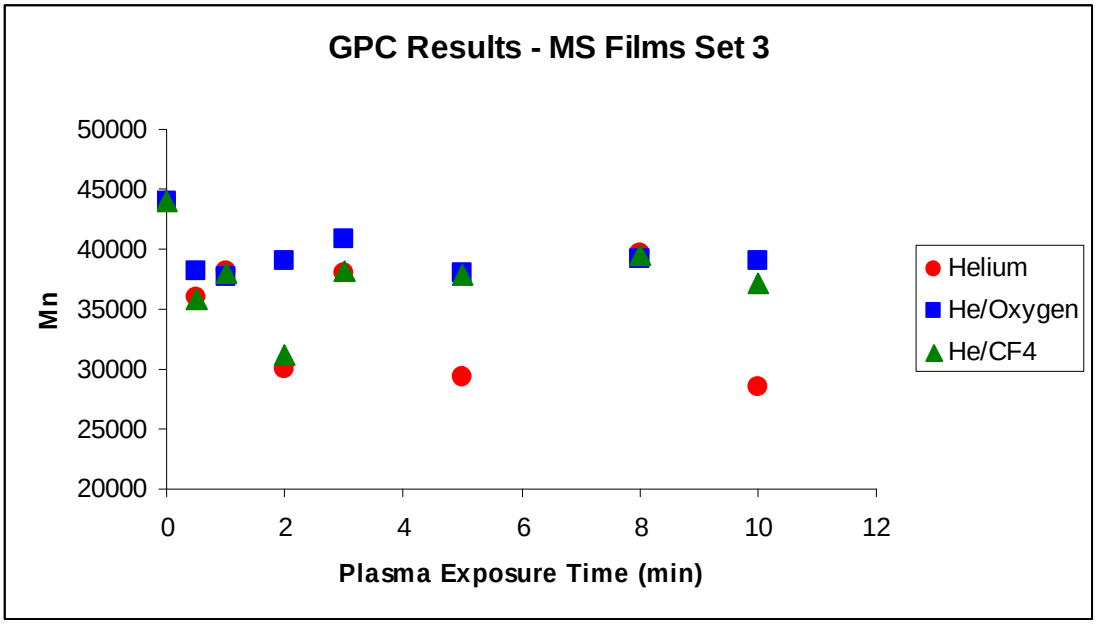
GPC Results - MS Films Set 3
Mn
50000
45000
40000
35000
30000
25000
20000
0
2
4
6
8
10
12
Plasma Exposure Time (min)
Helium
He/Oxygen
He/CF4

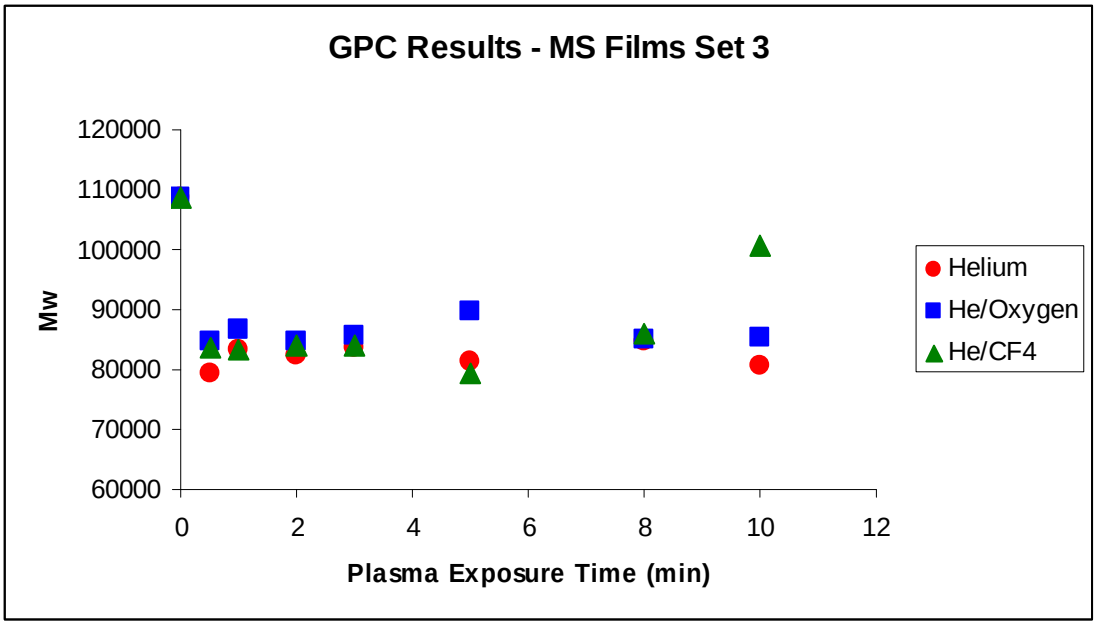
GPC Results - MS Films Set 3
Mw
120000
110000
100000
90000
80000
70000
60000
0
2
4
6
8
10
12
Plasma Exposure Time (min)
Helium
He/Oxygen
He/CF4

Appendix B

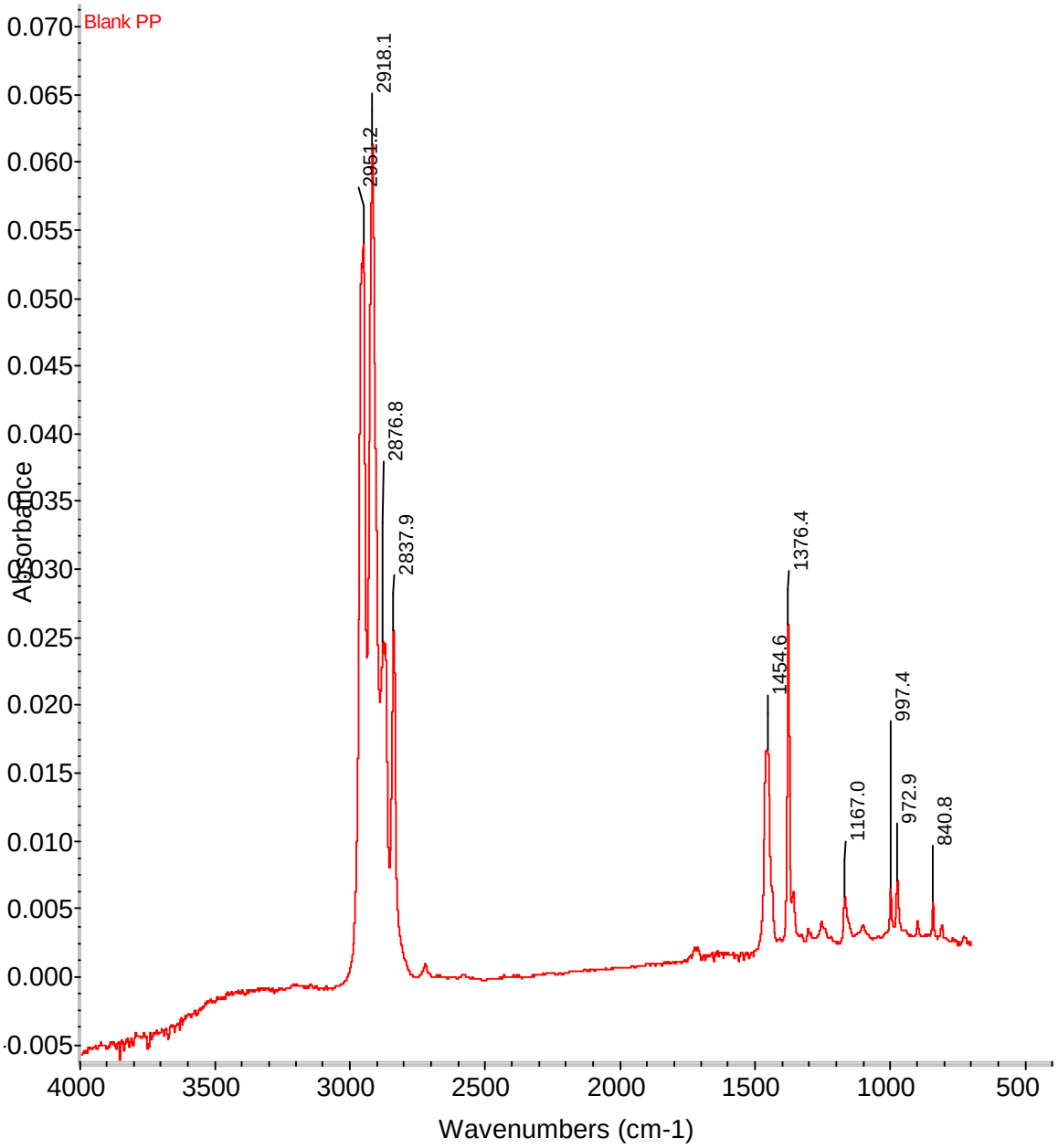

Untreated PP

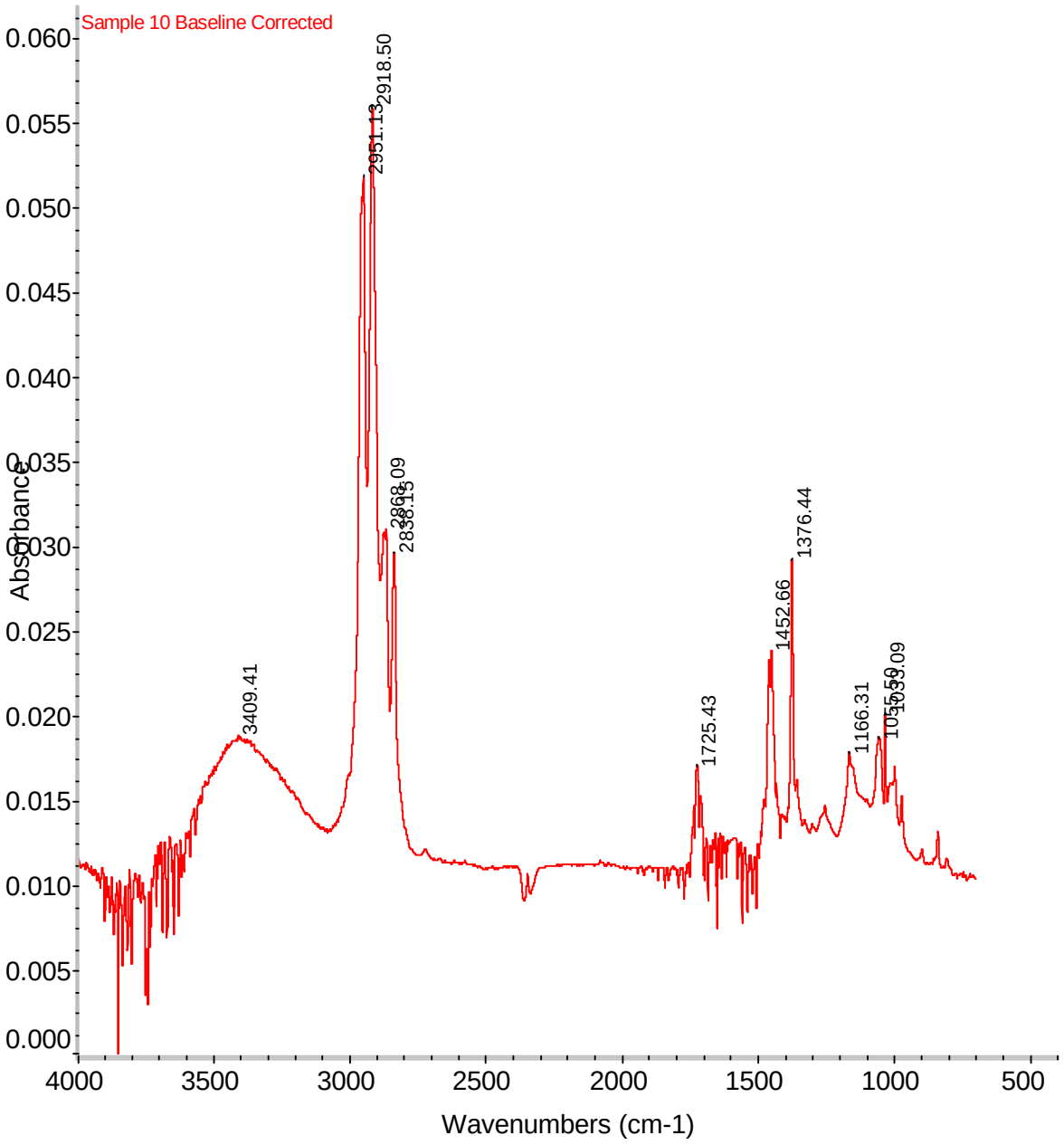
Sample 10 Baseline Corrected
Absorbance
Wavenumbers (cm-1)
0.060
0.055
0.050
0.045
0.040
0.035
0.030
0.025
0.020
0.015
0.010
0.005
0.000
4000
3500
3000
2500
2000
1500
1000
500
3409.41
2951.13
2918.50
2868.09
2838.15
1725.43
1452.66
1376.44
1166.31
1055.50
1039.09

Sample 10

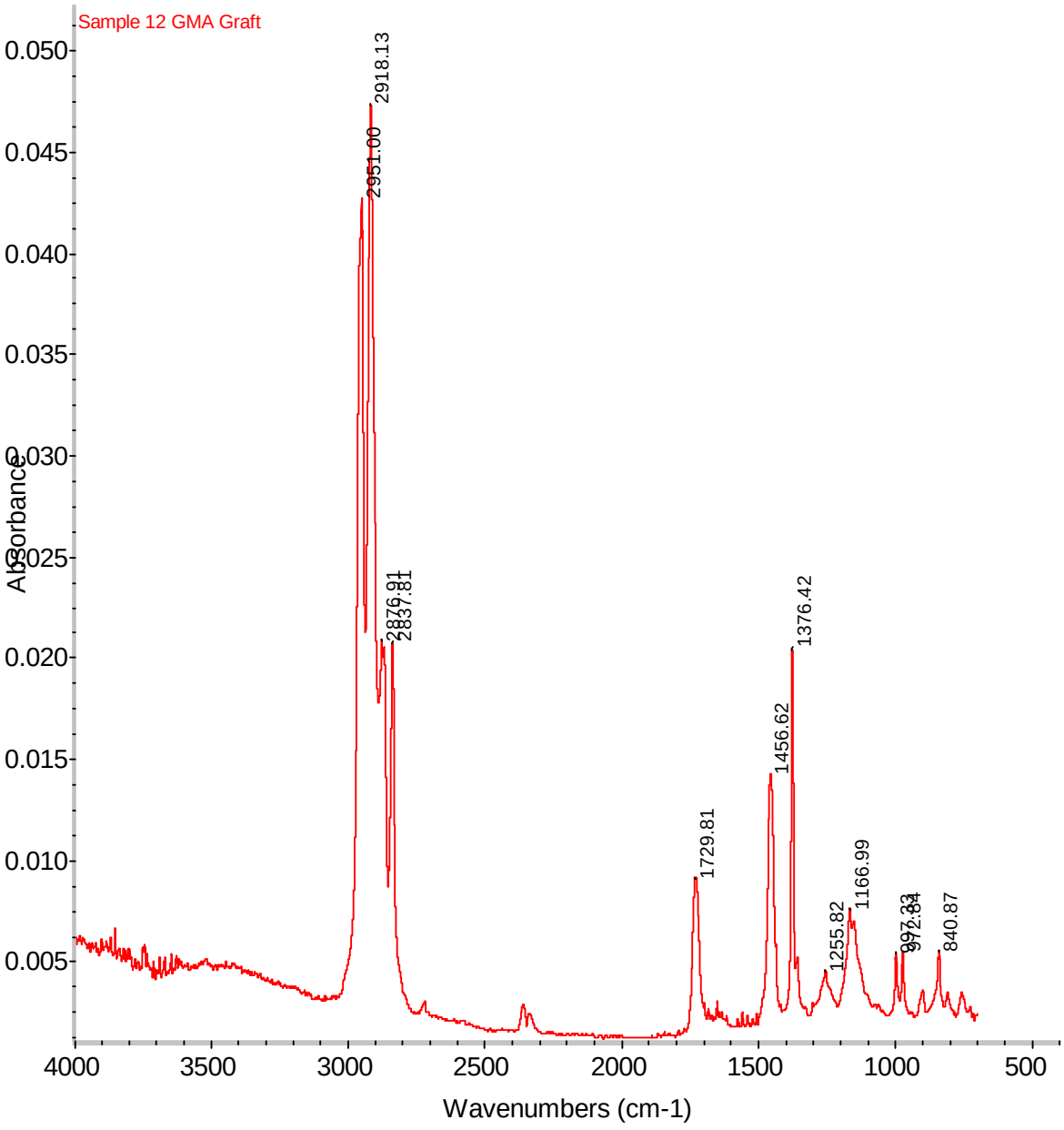
Sample 12 GMA Graft
Absorbance
0.050
0.045
0.040
0.035
0.030
0.025
0.020
0.015
0.010
0.005
2918.13
2951.00
2876.91
2837.81
1729.81
1456.62
1376.42
1255.82
1166.99
997.33
972.84
840.87
4000
3500
3000
2500
2000
1500
1000
500
Wavenumbers (cm-1)

Sample 12

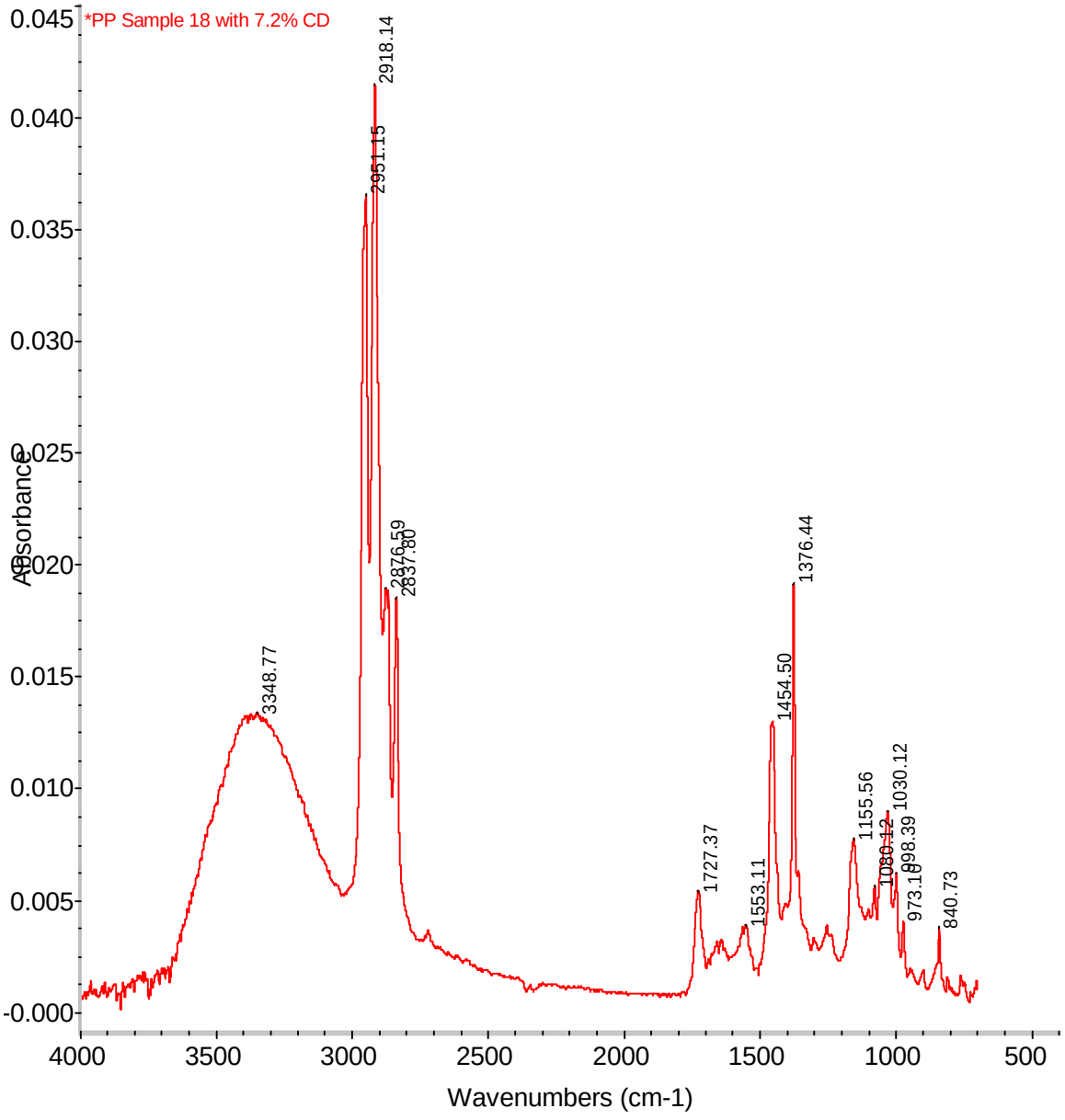
*PP Sample 18 with 7.2% CD
Absorbance
Wavenumbers (cm-1)
0.045
0.040
0.035
0.030
0.025
0.020
0.015
0.010
0.005
-0.000
4000
3500
3000
2500
2000
1500
1000
500
2918.14
2951.15
2876.59
2837.80
3348.77
1727.37
1553.11
1454.50
1376.44
1155.56
1080.12
1030.12
998.39
973.18
840.73

Sample 18

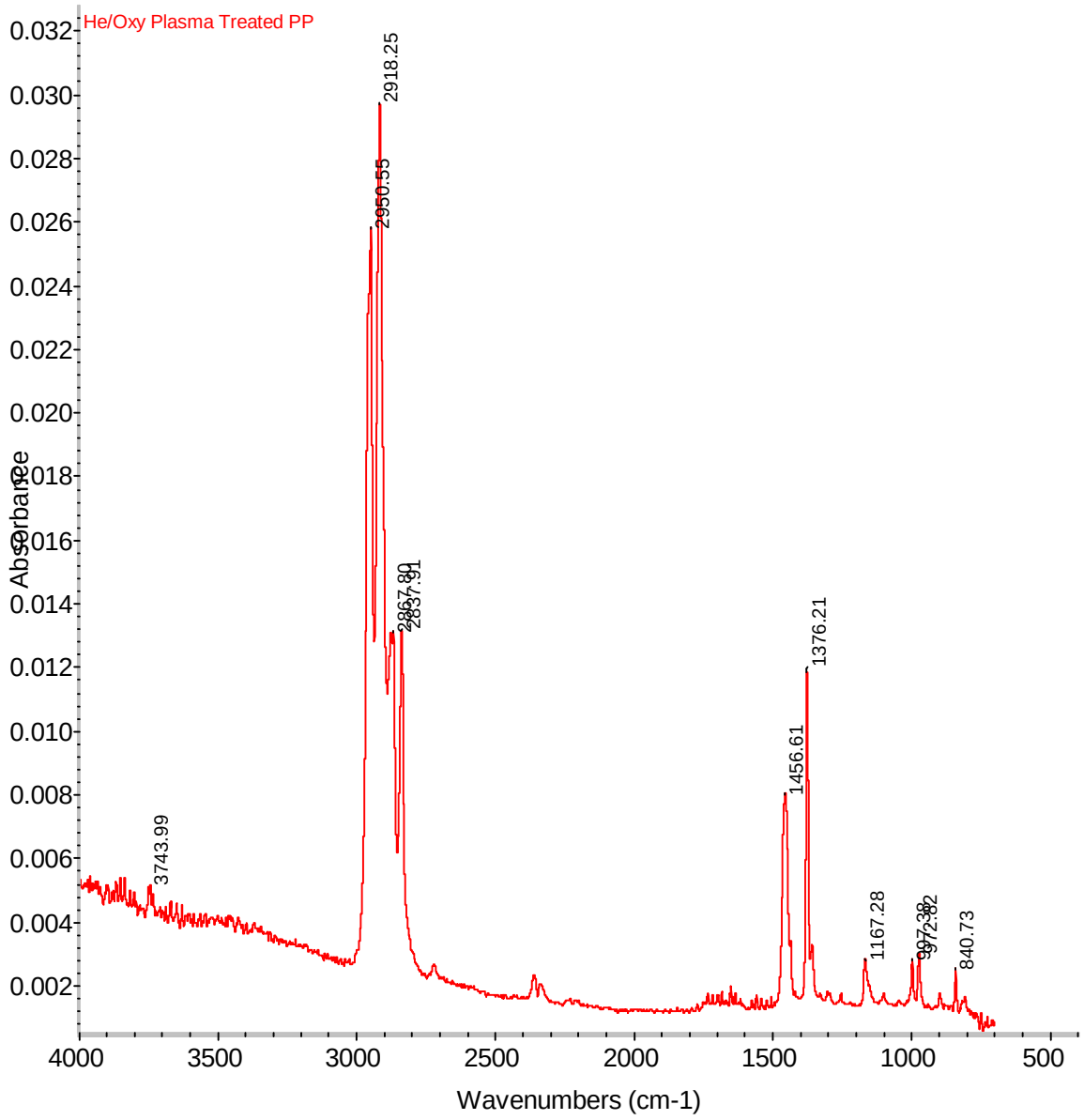

He/Oxygen treated PP

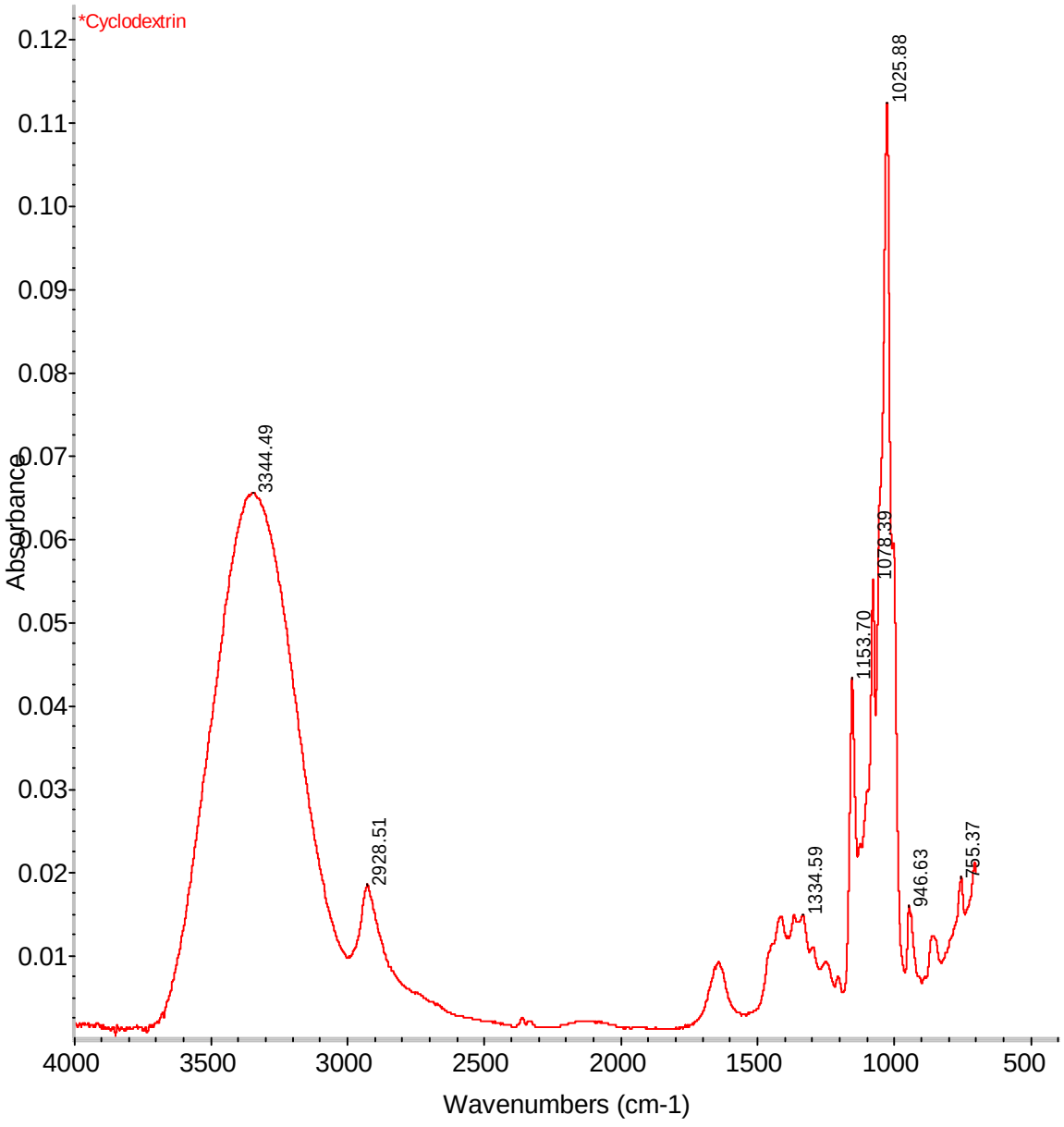

b - **Cyclodextrin**

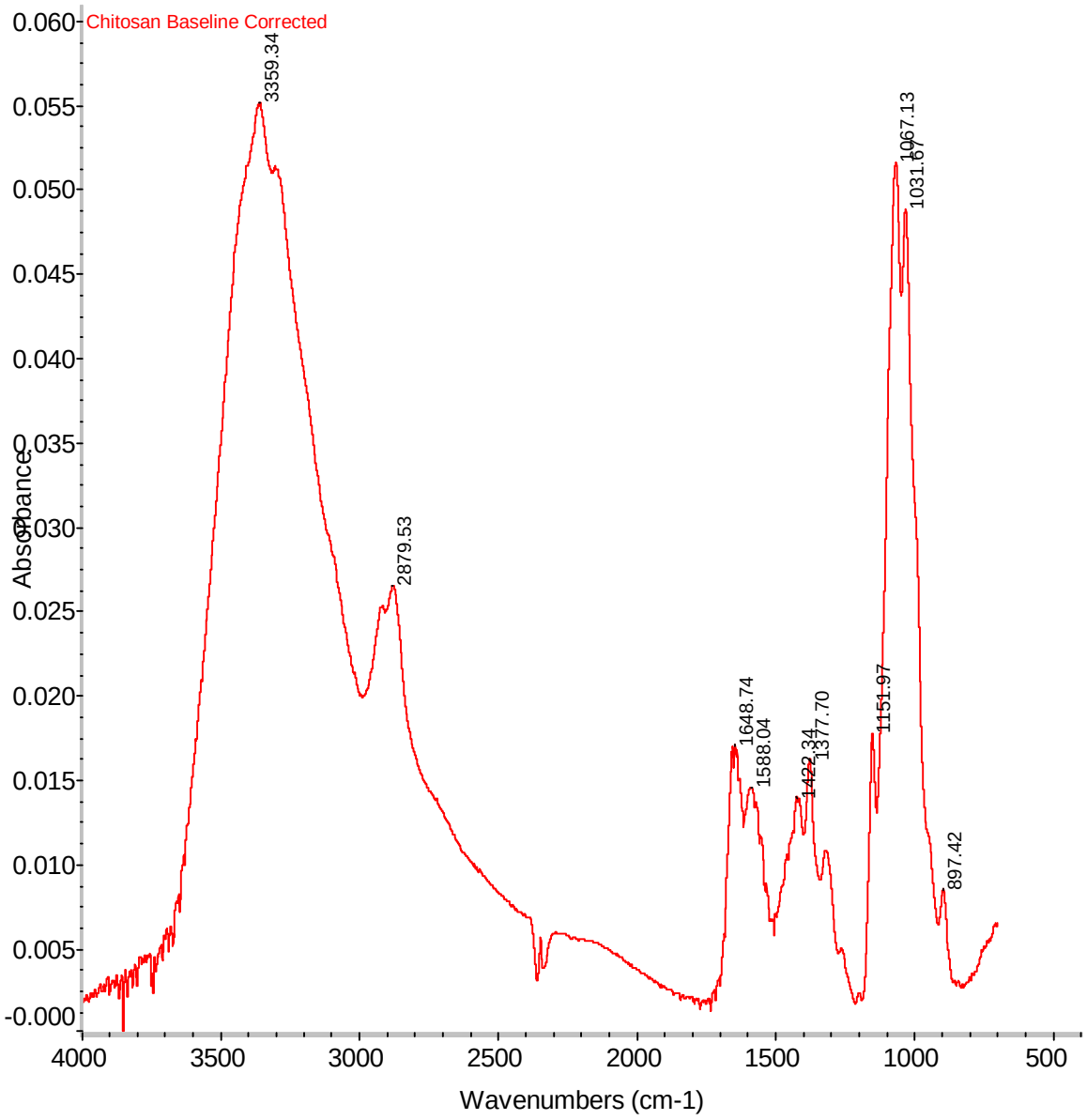

Quaternary Chitosan